



**Department of AERONAUTICS and ASTRONAUTICS
STANFORD UNIVERSITY**

Report to
NASA Ames Research Center
NCC2-304

*AMES
GRAD
N24-CR
233345
1498*

**COMPRESSION BEHAVIOR
OF DELAMINATED COMPOSITE PLATES**

Scott O. Peck and George S. Springer
Department of Aeronautics and Astronautics
Stanford University, Stanford, California 94305

(NASA-CR-184816) COMPRESSION BEHAVIOR OF
DELAMINATED COMPOSITE PLATES (Stanford
Univ.) 149 p CSCL 11D

N89-29492

Unclas
G3/24 0233345

October 1989

Report to
NASA Ames Research Center
NCC2-304

COMPRESSION BEHAVIOR
OF DELAMINATED COMPOSITE PLATES

Scott O. Peck and George S. Springer
Department of Aeronautics and Astronautics
Stanford University, Stanford, California 94305

October 1989

Abstract

The response of delaminated composite plates to compressive in-plane loads was investigated. The delaminated region may be either circular or elliptical, and may be located between any two plies of the laminate. For elliptical delaminations, the axes of the ellipse may be arbitrarily oriented with respect to the applied loads. A model was developed that describes the stresses, strains, and deformation of the sublaminates created by the delamination. The mathematical model is based on a two dimensional nonlinear plate theory that includes the effects of transverse shear deformation. The model takes into account thermal and moisture induced strains, transverse pressures acting on the sublaminates, and contact between the sublaminates and plate. The solution technique used is the Ritz method. A computationally efficient computer implementation of the model was developed. The code can be used to predict the nonlinear load-strain behavior of the sublaminates including the buckling load, postbuckling behavior, and the onset of delamination growth. The accuracy of the code was evaluated by comparing the model results to benchmark analytical solutions.

A series of experiments was conducted on Fiberite T300/976 graphite/epoxy laminates bonded to an aluminum honeycomb core forming a sandwich panel. Either circles or ellipses made from Teflon film were embedded in the laminates, simulating the presence of a delamination. Each specimen was loaded in compression and the strain history of the sublaminates was recorded far into the postbuckling regime. The extent of delamination growth was evaluated by C-scan examination of each specimen. The experimental data were compared to code predictions. The code was found to describe the data with reasonable accuracy.

A sensitivity study examined the relative importance of various material properties, the delamination dimensions, the contact model, the transverse pressure differential, the critical strain energy release rate, and the relative growth direction on the buckling load, the postbuckling behavior, and the growth load of the sublaminates.

Table of Contents

Abstract	i
Table of Contents	ii
List of Figures	v
List of Symbols	ix
Chapter 1. Introduction	1
Chapter 2. Problem Statement	3
Chapter 3. Delamination Analysis	6
3.1 Approach	6
3.2 Coordinate Systems	7
3.3 Constitutive Relations	7
3.4 Displacements, Strains, and Stresses in the Plate	10
3.5 Strain-Displacement Relations for the Sublamine	14
3.6 Displacements, Strains, and Stresses in the Sublamine	16
3.7 Total Potential Energy	21
3.8 Applied Load versus Deformation of the Sublamine	27
3.9 Buckling Condition	29
3.10 Growth Criterion	30
Chapter 4. Implementation	33
4.1 Introduction	33
4.2 Total Potential Energy	35
4.3 Nonlinear Load-Strain Behavior	35
4.4 Buckling Load	36
4.5 Growth Load	37
4.6 Code	37
Chapter 5. Analytical Verification	39
5.1 Introduction	39
5.2 Buckling of Circular and Elliptical Plates Without Delaminations	40
5.3 Large Deflections of Circular Plates Without Delaminations	42

5.4	Change in Total Potential Energy of a Plate Without Delamination .	43
5.5	Buckling of Elliptical Sublaminates in Plates Containing Delaminations	45
5.6	Summary	47
Chapter 6.	Experimental Procedure	49
6.1	Specimen Design and Fabrication	49
6.2	Nondestructive Inspection	51
6.3	Instrumentation	52
6.4	Testing to Failure	54
Chapter 7.	Comparison of Experimental and Model Results	55
7.1	Introduction	55
7.2	Experimental Measurements and Material Properties	56
7.3	Circular Delaminations in Unidirectional Laminated Plates	59
7.4	Circular Delaminations in Cross Ply Laminated Plates	59
7.5	Elliptical Delaminations in Cross Ply Laminated Plates	62
7.6	Buckling and Growth Loads	65
Chapter 8.	Sample Problem and Discussion	69
8.1	Introduction	69
8.2	Sample Problem Description	69
8.3	Geometry Effects	71
8.4	Contact Model Effects	74
8.5	Transverse Pressure Effects	77
8.6	Growth Model Effects	77
8.7	Summary and Recommendations	80
Chapter 9.	Concluding Remarks	81
References	83
Appendices	89
A.	Engineering Constants for Isotropic and Orthotropic Materials	89
B.	Integration of the Plate Strain Expressions	92
C.	Basic Assumptions of Nonlinear Plate Theory	94

D. Contact Model Foundation Modulus	101
E. Parallel Axes Theorem for Unsymmetric Laminates	103
F. Strain Energy Release of an Elliptical Sublaminates	106
G. DELAM Sample Input/Output	107
H. Total Potential Energy Change in an Isotropic Plate	125
I. Ultrasonic Nondestructive Examination	129
J. Uncertainty Analyses	131

List of Figures

Figure 2-1	Plate geometries investigated and the division of the plate into two parts as a result of the delamination.	4
Figure 2-2	Illustration of the in-plane loads acting on a plate containing an elliptical delamination.	5
Figure 3-1	Cartesian coordinate systems: x_1, x_2, x_3 for the plate, x_1, x_2, x_3 for the sublamine, and xyz for the material coordinates of each ply. θ is the angle between the plate and sublamine systems, and ϕ is the angle between the plate and ply systems.	8
Figure 3-2	In-plane load resultants N_1 , N_2 , and N_6 in the plate coordinate system.	12
Figure 3-3	Illustration of the clamped boundary at the sublamine edge.	18
Figure 3-4	Definition of the tangent t and normal n coordinates along the sublamine boundary.	19
Figure 3-5	Possible pressure difference acting across the sublamine thickness.	23
Figure 3-6	Contact between the sublamine and plate.	24
Figure 3-7	Detached elastic foundation model of contact force.	25
Figure 3-8	Illustration of the actual load-strain behavior and the calculated linear buckling load.	30
Figure 3-9	Definition of the growth parameter $\frac{da}{db}$	32
Figure 5-1	Buckling coefficients of clamped and simply supported circular aluminum plates subjected to uniform edge compression ($a = 1.0$ in.).	41
Figure 5-2	Buckling coefficients of clamped and simply supported elliptical aluminum plates subjected to uniform edge compression ($a = 1.0$ in., $h = 0.01$ in.).	41
Figure 5-3	Center deflection of a circular aluminum plate subjected to a uniform load ($a = 1.0$ in., $h = 0.01$ in.).	44
Figure 5-4	Change in total potential energy of a clamped, circular aluminum plate subjected to a uniform load ($a = 1.0$ in., $h = 0.01$ in.).	44
Figure 5-5	Normalized critical buckling strain. Aluminum sublamine on an aluminum base plate (Table 5-1) ($b = 0.5$ in., $h = 0.03$ in.).	47

- Figure 5-6** Normalized critical buckling strain. Unidirectional type A sublamine on an isotropic base plate (Table 5-1) ($b = 0.5$ in., $h = 0.03$ in.). 48
- Figure 5-7** Normalized critical buckling strain. Unidirectional type B sublamine on an isotropic base plate (Table 5-1) ($b = 0.5$ in., $h = 0.03$ in.). 48
- Figure 6-1** Sandwich construction test specimen containing a teflon disk in one facesheet. 50
- Figure 6-2** Specimen strain gauge locations and orientations. 53
- Figure 7-1** Typical sublamine gauge 1 load-strain response. 57
- Figure 7-2** Typical sublamine peripheral gauge 5, 6, 7, 8 load-strain responses. 57
- Figure 7-3** Load versus strain for a $[0_{16}H0_{16}]$ T300/976 laminate under uniaxial compression. Circular delaminations implanted at 2 (Specimen 4-1), 4 (Specimen 4-2), 6 (Specimen 4-3), and 8 (Specimen 4-4) plies from the outer surface. Strain gauge 1 was located on the surface at the center of the sublamine (see also Tables 6-1 and 6-2 and Figures 6-1 and 6-2). 60
- Figure 7-4** Load versus strain for a $[0_{16}H0_{16}]$ T300/976 laminate under uniaxial compression. Circular delaminations implanted at 2 (Specimen 4-1), 4 (Specimen 4-2), 6 (Specimen 4-3), and 8 (Specimen 4-4) plies from the outer surface. Strain gauges 5, 6, 7, and 8 were located around the periphery of the sublamine (see also Tables 6-1 and 6-2 and Figures 6-1 and 6-2). 61
- Figure 7-5** Load versus strain for a $[(0_2/90_2/0_2/90_2)_sH(0_2/90_2/0_2/90_2)_s]$ T300/976 laminate under uniaxial compression. Circular delaminations implanted at 3 (Specimen 5-1), 4 (Specimen 5-2), 5 (Specimen 5-3), and 8 (Specimen 5-4) plies from the outer surface. Strain gauge 1 was located on the surface at the center of the sublamine (see also Tables 6-1 and 6-2 and Figures 6-1 and 6-2). 63
- Figure 7-6** Load versus strain for a $[(0_2/90_2/0_2/90_2)_sH(0_2/90_2/0_2/90_2)_s]$ T300/976 laminate under uniaxial compression. Circular delaminations implanted at 3 (Specimen 5-1), 4 (Specimen 5-2), 5 (Specimen 5-3), and 8 (Specimen 5-4) plies from the outer surface. Strain gauges 5, 6, 7, and 8 were located around the periphery of the sublamine (see also Tables 6-1 and 6-2 and Figures 6-1 and 6-2). 64
- Figure 7-7** Load versus strain for a $[(0_2/90_2/0_2/90_2)_sH(0_2/90_2/0_2/90_2)_s]$ T300/976 laminate under uniaxial compression. 2.0 in. by 1.5 in. elliptical delaminations implanted 4 plies from the outer surface (all specimens). 0° (Specimen 6-1), 30° (Specimen 6-2), 60° (Specimen 6-3), and 90° (Specimen 6-4) orientations of the ellipses with respect to the load. Strain gauge 1 was located on the surface at the center

- of the sublamine (see also Tables 6-1 and 6-2 and Figures 6-1 and 6-2). 66
- Figure 7-8** Load versus strain for a $[(0_2/90_2/0_2/90_2)_s H(0_2/90_2/0_2/90_2)_s]$ T300/976 laminate under uniaxial compression. 2.0 in. by 1.5 in. elliptical delaminations implanted 4 plies from the outer surface (all specimens). 0° (Specimen 6-1), 30° (Specimen 6-2), 60° (Specimen 6-3), and 90° (Specimen 6-4) orientations of the ellipses with respect to the load. Strain gauges 5, 6, 7, and 8 were located around the periphery of the sublamine (see also Tables 6-1 and 6-2 and Figures 6-1 and 6-2). 67
- Figure 7-9** Measured versus predicted buckling loads. Error bars are plus and minus three standard deviations (see Tables J-1 and J-3). . . . 68
- Figure 7-10** Measured versus predicted growth loads. Error bars are plus and minus three standard deviations (see Tables J-1 and J-3). . . . 68
- Figure 8-1** Sample problem description. Input variables are given in Table 8-1. Material properties are given in Table 7-1. 71
- Figure 8-2** Effect of changing ply thickness on the compressive load-strain response of the sample problem described in Figure 8-1. Results calculated by the DELAM code. 73
- Figure 8-3** Effect of changing ply thickness on the buckling and growth loads of the sample problem described in Figure 8-1. Results calculated by the DELAM code. 73
- Figure 8-4** Effect of changing the semi-minor axis "b" of the ellipse on the compressive load-strain response of the sample problem described in Figure 8-1. Results calculated by the DELAM code. 75
- Figure 8-5** Effect of changing the semi-minor axis "b" of the ellipse on the buckling and growth loads of the sample problem described in Figure 8-1. Results calculated by the DELAM code. 75
- Figure 8-6** Effect of changing the contact law foundation modulus K on the compressive load-strain response of the sample problem described in Figure 8-1. Results calculated by the DELAM code. 76
- Figure 8-7** Effect of changing the contact law foundation modulus K on the buckling and growth loads of the sample problem described in Figure 8-1. Results calculated by the DELAM code. 76
- Figure 8-8** Effect of changing the transverse pressure ΔP on the compressive load-strain response of the sample problem described in Figure 8-1. Results calculated by the DELAM code. 78
- Figure 8-9** Effect of changing the transverse pressure ΔP on the buckling and growth loads of the sample problem described in Figure 8-1. Results calculated by the DELAM code. 78

- Figure 8-10** Effect of changing the growth model parameter $\frac{da}{db}$ on the compressive load-strain response of the sample problem described in Figure 8-1. Results calculated by the DELAM code. 79
- Figure 8-11** Effect of changing the critical strain energy release rate G_c on the growth loads of the sample problem described in Figure 8-1. Results calculated by the DELAM code. 79
- Figure C-1** Order of magnitude estimates for displacements and derivatives. 95
- Figure D-1** Uniform pressure load acting on a semi-infinite plate. 102
- Figure E-1** Laminate thickness direction coordinate systems located at the plate midsurface (x_3) and an arbitrary distance d from the plate midsurface (x'_3). 105
- Figure J-1** Load versus strain from each gauge 3 of Experiment Series 5. . 132
- Figure J-2** Uncertainty analysis of Experiment 6-2 prediction. Load versus strain for the sixteen different combinations of input variables. . . . 136

List of Symbols

a	major axis of the ellipse
a_{ij}	plate inverse stiffnesses
b	minor axis of the ellipse
Δc	change in moisture concentration
c_i	plate displacement coefficients
d	distance between parallel axes
e_{ij}	linear strain parameters
f	forces acting on the sublamine surface
h	generic plate thickness
h^{pl}	thickness of the plate
h^{sl}	thickness of the sublamine
k	buckling coefficient
k_d	number of plies in the sublamine
k_p	number of plies in the plate
l_f	characteristic length for foundation modulus estimate
m_i	generic Ritz coefficient
m	shorthand $\sin\theta$
n	shorthand $\cos\theta$
n	subscript indicating normal direction
n_p, n_q, n_r, n_s, n_t	number of coordinate functions
p_j, q_j, r_j, s_j, t_j	Ritz coefficients to be determined
$\hat{p}_j, \hat{q}_j, \hat{r}_j, \hat{s}_j, \hat{t}_j$	Ritz coefficients that have been determined
q_o	transverse pressure
s_2, s_4	perturbation solution functions

t	subscript indicating transverse direction
t_i	thickness of each ply
tr	matrix transpose
u_i	displacements
${}^o u_i^{pl}$	plate midplane displacements
${}^o u_i^{sl}$	sublamine midplane displacements
\hat{u}_i^{sl}	sublamine midplane displacements due to bending
w_o	transverse displacement of the plate center
w_1, w_3	perturbation solution functions
x, y, z	coordinate system for each ply
x_1, x_2, x_3	body coordinate system for the delamination
x_1', x_2', x_3'	body coordinate system for the plate
A	surface area of the sublamine
$A_{ij}, B_{ij}, D_{ij}, E_{ij},$ F_{ij}, G_{ij}, H_{ij}	plate stiffnesses
C_{ijkl}	linear elastic moduli
C_{ij}	linear elastic moduli in contracted notation
D	plate bending stiffness
E_f	Young's modulus of the foundation
E_x	ply longitudinal Young's modulus
E_y	ply transverse Young's modulus
G	strain energy release rate
G_c	critical strain energy release rate of the material
G_{xy}	in-plane ply shear modulus
G_{xz}	out-of-plane ply shear modulus
G_{yz}	out-of-plane ply shear modulus

K	foundation modulus of the plate
L	characteristic plate length
N	applied mechanical load
N_b^l	linear buckling load
N_b	actual buckling load
N_g	growth load
N_i^{plT}	thermal load resultants for the plate
$N_i^{slT}, M_i^{slT}, P_i^{slT}$	thermal load resultants for the sublamine
ΔP	surface pressure differential acting on the sublamine
Q_{ij}	plane stress reduced ply stiffnesses
T	current temperature
T_r	reference temperature
V	volume of the sublamine
α_i	thermal coefficient of linear expansion
β_i	moisture coefficient of linear expansion
δ_{ij}	Kronecker delta
ϵ_{ij}	strain components
ϵ_i	strain components in contracted notation
${}^o\epsilon_i^{pl}$	plate midplane strain components
${}^o\epsilon_i^{sl}$	sublamine midplane strain components
${}^o\epsilon_i^{plT}$	plate thermal midplane strain components
ϵ_{cr}	critical buckling strain
ϵ_n	normalized critical buckling strain
ϕ_i	angles from the plate to the ply coordinate systems
${}^p\phi_j, {}^q\phi_j, {}^r\phi_j, {}^s\phi_j, {}^t\phi_j$	coordinate functions of x_1, x_2
γ_i	load descriptors

ψ_i^{pl}	plate rotations
$\psi_i^{sl}, \xi_i^{sl}, \eta_i^{sl}$	sublamine rotation functions
$\hat{\psi}_i^{sl}$	sublamine rotations at the boundary
${}^o\kappa_i^{sl}, {}^2\kappa_i^{sl}$	sublamine midplane curvatures
ν_{xy}	ply major Poisson's ratio
ν_{yx}	ply minor Poisson's ratio
π	pi
θ	angle from the plate to the delamination coordinate system
ρ_o	mass density in reference configuration
ρ_c	mass density in current configuration
σ_{ij}	stress components
σ_i	stress components in contracted notation
σ_{ij}^C	Cauchy stress components
σ_{ij}^{P-K}	second Piola-Kirchhoff stress components
σ_d	experimental data uncertainty estimate
σ_N	model prediction uncertainty estimate
ω_{ij}	linear rotation parameters
Π^{pl}	total potential energy of the plate
Π^{sl}	total potential energy of the sublamine

Chapter 1

Introduction

Fiber-reinforced organic matrix composite materials may contain delaminations introduced, for example, by manufacturing defects or impact damage. When subjected to compressive in-plane loads, the delaminated region may first buckle and then grow in size. Either of these occurrences may significantly limit the usefulness of the composite plate. Therefore, to utilize the many inherent advantages of composite materials, the behavior of delaminations must be fully understood. This investigation addresses this problem, and specifically seeks to establish a model which predicts the buckling and postbuckling growth behavior of delaminations in composite plates subjected to in-plane compressive and shear loads.

Owing to the significance of the problem, several investigators have proposed models describing the behavior of delaminated plates under compressive loading. The buckling and growth of through-width delaminations in plate strips have been analyzed by Chai et al. [1], Yin et al. [2], Simites et al. [3], Gillespie and Pipes [4], Wang et al. [5,6], Sallam and Simites [7], Williams et al. [8], El-Senussi and Webber [9], Vizzini and Lagace [10], Yin [11], and Kardomateas [12]. The buckling and growth of circular delaminations in isotropic plates under radial loads have been investigated by Bottega and Maewal [13], Yin and Fei [14], and Bruno [15].

In addition to these simple geometries, the behavior of plates containing rec-

tangular delaminations have been analyzed by Konishi [16] and Jones et al. [17], while plates containing elliptical delaminations have been investigated by Konishi [16], Chai and Babcock [18], Kassapoglou [19], Shivakumar and Whitcomb [20], and Whitcomb [21, 22]. In all but one of these analyses, the major axes of the rectangle or ellipse were assumed to be aligned with the direction of the compressive load. The one exception is the analysis of Shivakumar and Whitcomb [20], which assumed an arbitrary orientation for an elliptical delamination with respect to the applied load. However, Shivakumar and Whitcomb calculated only buckling loads and did not consider postbuckling deformation or growth.

It appears that no model exists for predicting the buckling, postbuckling behavior, and growth of: (a) circular delaminations or elliptical delaminations with axes arbitrarily oriented with respect to the applied in-plane loads, and (b) delaminations located between any two plies of the composite plate. Therefore, the primary goal of this investigation was to develop a model capable of addressing this more general problem of delamination in a composite plate.

In developing the model, an additional objective was to make the model readily useable in engineering practice. Substantial effort was made to keep the analysis simple and straightforward, to develop a computer implementation of the model that was computationally efficient, and to incorporate a user-friendly interface for the program so that meaningful results could readily be obtained.

Finally, to firmly establish the credibility of the model, a series of experiments on graphite-epoxy face sheeted aluminum honeycomb sandwich panels containing embedded delaminations was conducted. Strain histories were measured far into the postbuckling regime, and the data were compared to the analytical results, verifying the validity of the model.

Chapter 2

Problem Statement

Consider a multilayer laminated composite plate. The plate may be a "solid" laminate or a "sandwich" laminate consisting of two face sheets bonded to a honeycomb core (Figure 2-1). In either case, the plate must be symmetrically laminated with respect to its midplane. Each layer, or ply, in the plate may be made from a different material. Each material may be isotropic or orthotropic, the latter including continuous fiber reinforced composites. Each material must behave in a linearly elastic manner. A delamination exists between two adjacent plies in the plate (or face sheet) interior. The delamination may occur between any two plies, dividing the plate locally into two parts. The delamination may also be at the face sheet-honeycomb interface. Note that while the plate is symmetric, the two parts on either side of the delamination will, in general, be unsymmetric. The delamination is small with respect to the plate planar dimensions but large with respect to the thickness of the plate. The delamination is either circular or elliptical. The ellipse may have an arbitrary orientation with respect to the plate (Figure 2-2).

In-plane tensile, compressive, and shear loads may act on the plate. The response of the plate to the applied loads is assumed to be initially unaffected by the behavior of the sublaminate formed by the delamination. The plate response to the applied loads determines the displacement boundary conditions for the sub-

laminates. Under the action of the applied loads, the delaminated sublaminates may buckle and subsequently grow in area. Given the plate material properties and the delamination geometry, the problem is to find: (a) the load-strain behavior of the sublaminates, (b) the load applied to the plate at which the sublaminates buckle, and (c) the load applied to the plate which causes an onset of delamination growth.

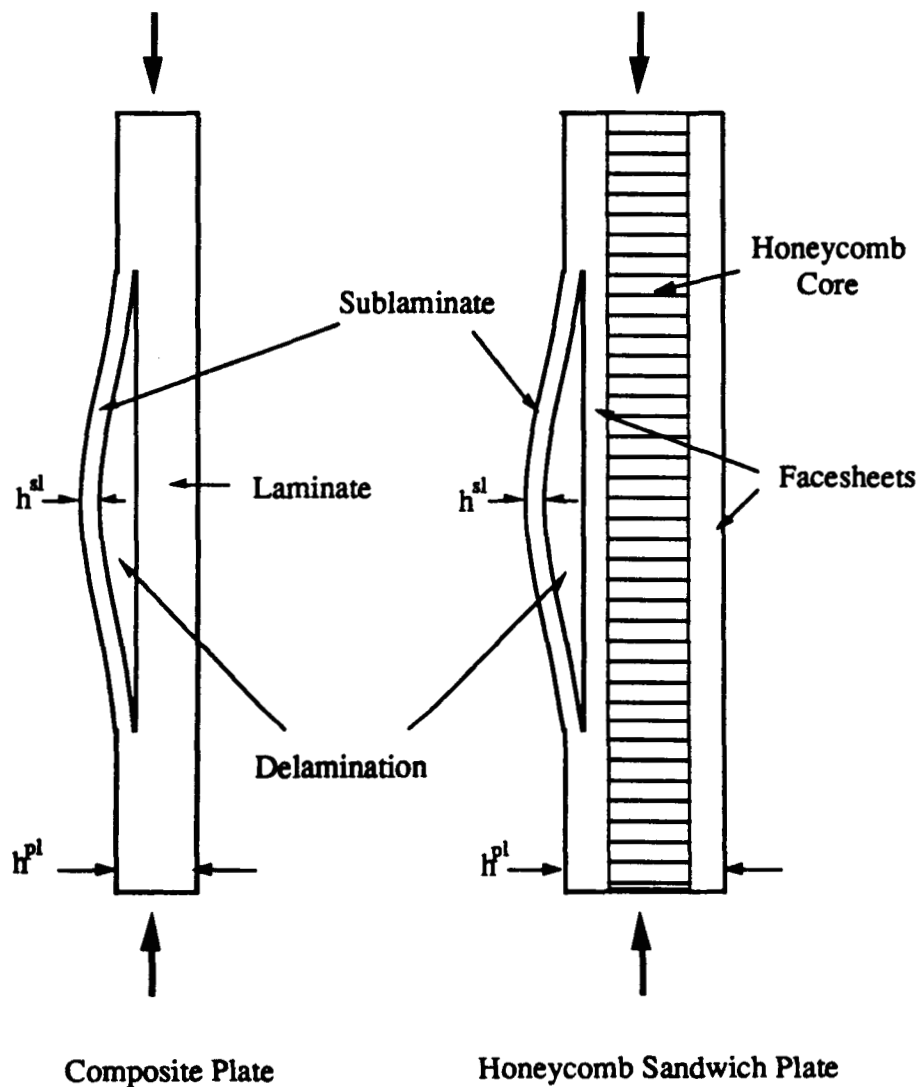


Figure 2-1 Plate geometries investigated and the division of the plate into two parts as a result of the delamination.

Chapter 3

Delamination Analysis

§3.1 Approach

The major concepts of the analysis of a delaminated composite plate are presented in this chapter. The analysis proceeds in four major steps. First, the displacements, strains, and stresses in the plate are calculated as though the delamination were not present. Second, the load at which the delaminated sublamine buckles is determined. Third, the displacements, strains, and stresses in the sublamine are determined using the condition that the displacements at the delamination boundary match those of the plate determined in step one. Fourth, the load at which the sublamine grows in size is established. In the first step, the behavior of the plate is calculated directly from laminated plate theory [23]. In the remaining steps, the approximate behavior of the sublamine is determined using energy methods.

The following fundamental assumptions of plate theory are employed in the analysis:

1. The thicknesses of both the plate and the sublamine are small compared to all other dimensions.
2. The thicknesses of both the plate and sublamine are constant.
3. The material behaves in a linearly elastic manner.

4. Each layer is either isotropic or orthotropic.
5. The plate and the sublamine undergo small strains, and the sublamine experiences moderate rotations.
6. The transverse normal stresses are zero in both the plate and the sublamine.
7. Perfect bonding exists between adjacent layers of the composite (except, of course, at the location of the delamination).
8. The transverse displacements and rotations in the plate are zero.

§3.2 Coordinate Systems

Three cartesian coordinate systems are employed in the analysis (Figure 3-1). The coordinate system coincident with the principal material axes of each orthotropic ply is the x, y, z system. The coordinate system coincident with the semi-axes of the delamination ellipse is the x_1, x_2, x_3 system. The coordinate system of the plate is the x_1', x_2', x_3' system. The x, y, z system is the on-axis system, while the other two systems are off-axis systems. The two off-axis systems are related to the on-axis system by rotations about the transverse axes, where these axes are all equivalent ($z = x_3 = x_3'$).

§3.3 Constitutive Relations

The constitutive relations for a linearly elastic material are

$$\sigma_{ij} = C_{ijkl} \epsilon_{kl} \quad i, j = 1, 2, 3 \quad (3.1)$$

where the C_{ijkl} are elastic constants relating the stresses σ_{ij} to the strains ϵ_{kl} . For an orthotropic or isotropic material in the on-axis coordinate system, the constitutive

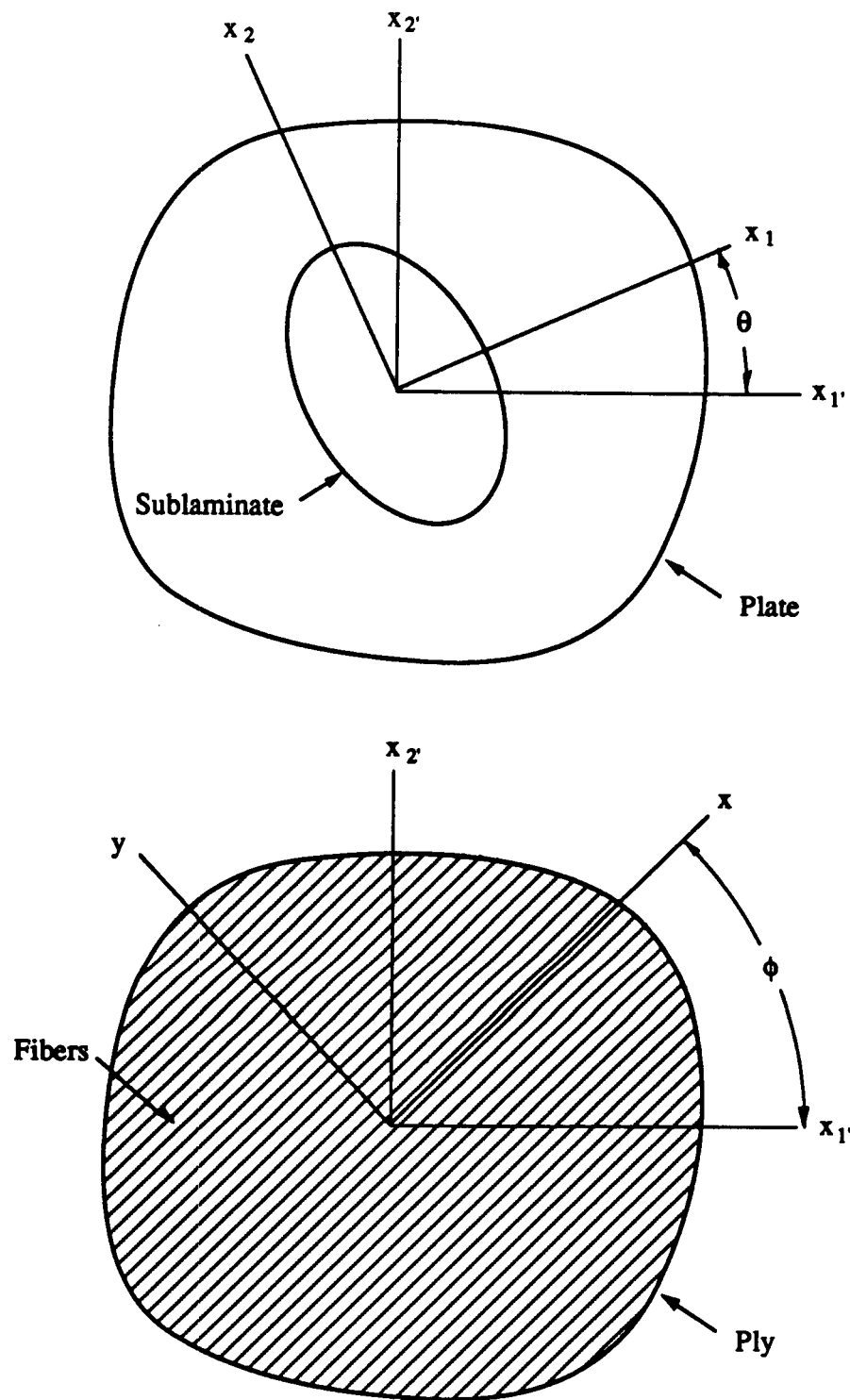


Figure 3-1 Cartesian coordinate systems: x_1, x_2, x_3 for the plate, x_1, x_2, x_3 for the sublamine, and x, y, z for the material coordinates of each ply. θ is the angle between the plate and sublamine systems, and ϕ is the angle between the plate and ply systems.

relations are

$$\begin{pmatrix} \sigma_{xx} \\ \sigma_{yy} \\ \sigma_{zz} \\ \sigma_{yz} \\ \sigma_{zx} \\ \sigma_{xy} \end{pmatrix} = \begin{pmatrix} C_{xxxx} & C_{xxyy} & C_{xxzz} & 0 & 0 & 0 \\ C_{xxyy} & C_{yyyy} & C_{yyzz} & 0 & 0 & 0 \\ C_{xxzz} & C_{yyzz} & C_{zzzz} & 0 & 0 & 0 \\ 0 & 0 & 0 & C_{yzyz} & 0 & 0 \\ 0 & 0 & 0 & 0 & C_{zxzx} & 0 \\ 0 & 0 & 0 & 0 & 0 & C_{xyxy} \end{pmatrix} \begin{pmatrix} \epsilon_{xx} - \alpha_x \Delta T \\ \epsilon_{yy} - \alpha_y \Delta T \\ \epsilon_{zz} - \alpha_z \Delta T \\ 2\epsilon_{yz} \\ 2\epsilon_{zx} \\ 2\epsilon_{xy} \end{pmatrix} \quad (3.2)$$

where the α_i are the on-axis linear coefficients of thermal expansion. The temperature difference ΔT is defined as

$$\Delta T = T - T_r \quad (3.3)$$

where T is the uniform temperature of the composite and T_r is a reference temperature at which the thermal strain is defined to be zero. A convenient value for T_r is the temperature at which the material "solidifies" during curing.

The effects of moisture absorption by the composite material can be treated in an analogous manner. The strain due to moisture uptake is $\beta_i \Delta c$, where the β_i are the on-axis linear coefficients of moisture-induced expansion and Δc is the relative change in moisture concentration. For simplicity, the analytical development presented here is in terms of thermal strains. However, an equivalent analysis of moisture effects can be made by substituting $\beta_i \Delta c$ for $\alpha_i \Delta T$.

Contracted notation will be used in the rest of the analysis except where noted. For example, in an off-axis x_1 , x_2 , and x_3 coordinate system the stresses, strains, and elastic constants are represented by [24]

$$\begin{array}{llll}
\sigma_{11} \rightarrow \sigma_1 & \epsilon_{11} \rightarrow \epsilon_1 & C_{1111} \rightarrow C_{11} & C_{2323} \rightarrow C_{44} \\
\sigma_{22} \rightarrow \sigma_2 & \epsilon_{22} \rightarrow \epsilon_2 & C_{2222} \rightarrow C_{22} & C_{1313} \rightarrow C_{55} \\
\sigma_{33} \rightarrow \sigma_3 & \epsilon_{33} \rightarrow \epsilon_3 & C_{3333} \rightarrow C_{33} & C_{1212} \rightarrow C_{66} \\
\sigma_{23} \rightarrow \sigma_4 & 2\epsilon_{23} \rightarrow \epsilon_4 & C_{2233} \rightarrow C_{23} & C_{2313} \rightarrow C_{45} \\
\sigma_{13} \rightarrow \sigma_5 & 2\epsilon_{13} \rightarrow \epsilon_5 & C_{1133} \rightarrow C_{13} & C_{2312} \rightarrow C_{46} \\
\sigma_{12} \rightarrow \sigma_6 & 2\epsilon_{12} \rightarrow \epsilon_6 & C_{1122} \rightarrow C_{12} & C_{1312} \rightarrow C_{56}
\end{array} \quad (3.4)$$

Note that ϵ_4 , ϵ_5 , and ϵ_6 are engineering strains.

For a material in plane stress, the constitutive relations (Eq. 3.2) may be conveniently written in an off-axis coordinate system as

$$\begin{pmatrix} \sigma_1 \\ \sigma_2 \\ \sigma_6 \\ \sigma_4 \\ \sigma_5 \end{pmatrix} = \begin{pmatrix} Q_{11} & Q_{12} & Q_{16} & 0 & 0 \\ Q_{12} & Q_{22} & Q_{26} & 0 & 0 \\ Q_{16} & Q_{26} & Q_{66} & 0 & 0 \\ 0 & 0 & 0 & Q_{44} & Q_{45} \\ 0 & 0 & 0 & Q_{45} & Q_{55} \end{pmatrix} \begin{pmatrix} \epsilon_1 - \alpha_1 \Delta T \\ \epsilon_2 - \alpha_2 \Delta T \\ \epsilon_6 - \alpha_6 \Delta T \\ \epsilon_4 \\ \epsilon_5 \end{pmatrix} \quad (3.5)$$

where the Q_{ij} are the plane stress reduced stiffnesses defined as

$$\begin{aligned}
Q_{ij} &= C_{ij} - \frac{C_{i3}C_{j3}}{C_{33}} & i, j &= 1, 2, 6 \\
Q_{ij} &= C_{ij} & i, j &= 4, 5
\end{aligned} \quad (3.6)$$

The stresses and strains have been arranged so as to group the in-plane and out-of-plane components separately. The apparent thermal shear term ($\alpha_6 \Delta T$) appears since the constitutive relations are expressed in an off-axis coordinate system. Expressions for Q_{ij} in terms of engineering constants for isotropic and orthotropic materials are given in Appendix A.

§3.4 Displacements, Strains, and Stresses in the Plate

In the plate coordinate system (x_1', x_2', x_3'), the in-plane total strains in the symmetrically laminated plate (containing no delamination) resulting from uni-

formly applied in-plane load resultants $N_{1'}$, $N_{2'}$, and $N_{6'}$ (Figure 3-2), and a temperature difference ΔT are [23]

$$\begin{pmatrix} \epsilon_{1'}^{pl} \\ \epsilon_{2'}^{pl} \\ \epsilon_{6'}^{pl} \end{pmatrix} = \begin{pmatrix} a_{1'1'} & a_{1'2'} & a_{1'6'} \\ a_{1'2'} & a_{2'2'} & a_{2'6'} \\ a_{1'6'} & a_{2'6'} & a_{6'6'} \end{pmatrix} \begin{pmatrix} N_{1'} + N_{1'}^{plT} \\ N_{2'} + N_{2'}^{plT} \\ N_{6'} + N_{6'}^{plT} \end{pmatrix} \quad (3.7)$$

The matrix elements a_{ij} , which are the inverses of the plate stiffness matrix elements A_{ij} [23], are

$$(a_{i'j'}) = (A_{i'j'})^{-1} = \left(\int_{-\frac{h^{pl}}{2}}^{\frac{h^{pl}}{2}} Q_{i'j'} dx_3 \right)^{-1} \quad i', j' = 1, 2, 6 \quad (3.8)$$

where h^{pl} is the thickness of the plate. The thermal load resultants $N_{1'}^{plT}$, $N_{2'}^{plT}$, and $N_{6'}^{plT}$ are

$$\begin{pmatrix} N_{1'}^{plT} \\ N_{2'}^{plT} \\ N_{6'}^{plT} \end{pmatrix} = \int_{-\frac{h^{pl}}{2}}^{\frac{h^{pl}}{2}} \begin{pmatrix} Q_{1'1'} & Q_{1'2'} & Q_{1'6'} \\ Q_{1'2'} & Q_{2'2'} & Q_{2'6'} \\ Q_{1'6'} & Q_{2'6'} & Q_{6'6'} \end{pmatrix} \begin{pmatrix} \alpha_{1'} \\ \alpha_{2'} \\ \alpha_{6'} \end{pmatrix} \Delta T dx_3 \quad (3.9)$$

In the sublamine coordinate system (x_1, x_2, x_3) , the total strain components are determined by a tensor rotation about the transverse axis x_3 ,

$$\begin{pmatrix} \epsilon_1^{pl} \\ \epsilon_2^{pl} \\ \epsilon_6^{pl} \end{pmatrix} = \begin{pmatrix} m^2 & n^2 & nm \\ n^2 & m^2 & nm \\ -2nm & 2nm & m^2 - n^2 \end{pmatrix} \begin{pmatrix} \epsilon_{1'}^{pl} \\ \epsilon_{2'}^{pl} \\ \epsilon_{6'}^{pl} \end{pmatrix} \quad (3.10)$$

where m and n are $\cos \theta$ and $\sin \theta$, respectively, and θ is the angle between the plate and sublamine coordinate systems (Figure 3-1).

To simplify the buckling and postbuckling analyses, proportional mechanical loading is assumed. Each of the in-plane load resultants may have a unique value, but the relationship of one to another is fixed. In this way, a single load parameter N suffices to characterize the total load on the plate

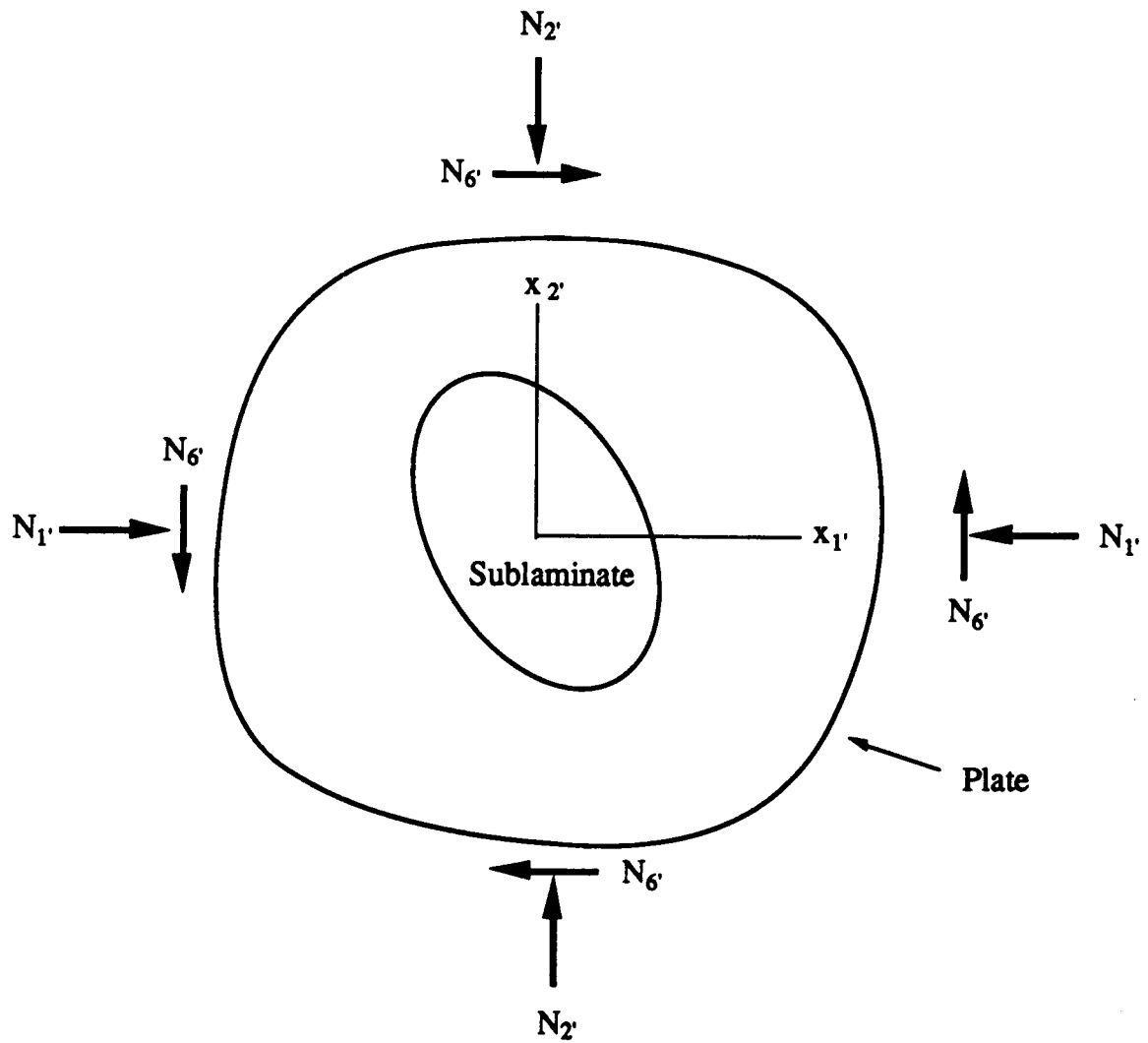


Figure 3-2 In-plane load resultants N_1' , N_2' , and N_6' in the plate coordinate system.

$$\begin{pmatrix} N_{1'} \\ N_{2'} \\ N_{6'} \end{pmatrix} = \begin{pmatrix} \gamma_1 \\ \gamma_2 \\ \gamma_6 \end{pmatrix} N \quad (3.11)$$

with the relative magnitude of each load described by the fractions γ_1 , γ_2 , and γ_6 ($\gamma_1 + \gamma_2 + \gamma_6 = 1$). The resulting total strains in the sublamine coordinate system (x_1, x_2, x_3) may now be expressed as

$$\begin{pmatrix} \epsilon_1^{pl} \\ \epsilon_2^{pl} \\ \epsilon_6^{pl} \end{pmatrix} = \begin{pmatrix} c_1 \\ c_2 \\ c_6 \end{pmatrix} N + \begin{pmatrix} \epsilon_1^{plT} \\ \epsilon_2^{plT} \\ \epsilon_6^{plT} \end{pmatrix} \quad (3.12)$$

where c_1 , c_2 , and c_3 are defined by

$$\begin{pmatrix} c_1 \\ c_2 \\ c_6 \end{pmatrix} = \begin{pmatrix} m^2 & n^2 & nm \\ n^2 & m^2 & nm \\ -2nm & 2nm & m^2 - n^2 \end{pmatrix} \begin{pmatrix} a_{1'1'} & a_{1'2'} & a_{1'6'} \\ a_{1'2'} & a_{2'2'} & a_{2'6'} \\ a_{1'6'} & a_{2'6'} & a_{6'6'} \end{pmatrix} \begin{pmatrix} \gamma_1 \\ \gamma_2 \\ \gamma_6 \end{pmatrix} \quad (3.13)$$

and the thermal strains in the plate by

$$\begin{pmatrix} \epsilon_1^{plT} \\ \epsilon_2^{plT} \\ \epsilon_6^{plT} \end{pmatrix} = \begin{pmatrix} m^2 & n^2 & nm \\ n^2 & m^2 & nm \\ -2nm & 2nm & m^2 - n^2 \end{pmatrix} \begin{pmatrix} a_{1'1'} & a_{1'2'} & a_{1'6'} \\ a_{1'2'} & a_{2'2'} & a_{2'6'} \\ a_{1'6'} & a_{2'6'} & a_{6'6'} \end{pmatrix} \begin{pmatrix} N_{1'}^{plT} \\ N_{2'}^{plT} \\ N_{6'}^{plT} \end{pmatrix} \quad (3.14)$$

Integration of Equation 3.12 (Appendix B) gives the in-plane displacements of the plate

$$\begin{aligned} u_1^{pl} &= (c_1 N + \epsilon_1^{plT})x_1 + \frac{1}{2}(c_6 N + \epsilon_6^{plT})x_2 \\ u_2^{pl} &= \frac{1}{2}(c_6 N + \epsilon_6^{plT})x_1 + (c_2 N + \epsilon_2^{plT})x_2 \end{aligned} \quad (3.15)$$

Equation 3.15 together with Assumption 8 ($u_3^{pl} = 0$) completely describe the displacements in the plate. The displacements at the sublamine boundary must match these displacements. Note again that the displacements and strains are taken to be zero when the temperature is T_r and no mechanical loads act on the plate.

§3.5 Strain-Displacement Relations for the Sublamine

The nonlinear strain-displacement relations used for the sublamine are those proposed by von Karman [25] for the large displacement analysis of plates. Although von Karman discussed the use of these strain-displacement relations only in the context of classical plate theory, it has been shown (Appendix C) that they are appropriate for the moderate rotation, shear deformation theory used here. The strains ϵ_{ij} (reverting to conventional notation for the moment) are related to the displacements by

$$\epsilon_{ij} = \frac{1}{2} \left(\frac{\partial u_i}{\partial x_j} + \frac{\partial u_j}{\partial x_i} + \frac{\partial u_3}{\partial x_i} \frac{\partial u_3}{\partial x_j} \right) \quad (3.16)$$

Using a higher order shear deformation theory [26–29], the sublamine displacements are taken to be cubic functions of the transverse coordinate x_3

$$\begin{aligned} u_1^{sl}(x_1, x_2, x_3) &= {}^0u_1^{sl}(x_1, x_2) + x_3\psi_1^{sl}(x_1, x_2) + x_3^2\xi_1^{sl}(x_1, x_2) + x_3^3\eta_1^{sl}(x_1, x_2) \\ u_2^{sl}(x_1, x_2, x_3) &= {}^0u_2^{sl}(x_1, x_2) + x_3\psi_2^{sl}(x_1, x_2) + x_3^2\xi_2^{sl}(x_1, x_2) + x_3^3\eta_2^{sl}(x_1, x_2) \\ u_3^{sl}(x_1, x_2, x_3) &= {}^0u_3^{sl}(x_1, x_2) \end{aligned} \quad (3.17)$$

where ${}^0u_1^{sl}$, ${}^0u_2^{sl}$, and ${}^0u_3^{sl}$ are the displacements of the sublamine midplane, and ψ_1^{sl} , ψ_2^{sl} , ξ_1^{sl} , ξ_2^{sl} , η_1^{sl} , η_2^{sl} describe rotations of line segments originally perpendicular to the sublamine midplane.

No shear forces act on any of the lateral surfaces of the sublamine. Hence, the shear stress components (returning to contracted notation) on these surfaces are

$$\sigma_4 = \sigma_5 = 0 \quad \text{at} \quad x_3 = \pm \frac{h^{sl}}{2} \quad (3.18)$$

where h^{sl} is the thickness of the sublamine. For a sublamine constructed of isotropic or orthotropic materials, the above condition requires that the corresponding

shear strains on the lateral surfaces also be zero (Eq. 3.2).

$$\epsilon_4 = \epsilon_5 = 0 \quad \text{at} \quad x_3 = \pm \frac{h^{sl}}{2} \quad (3.19)$$

Substituting the displacements (Eq. 3.17) into the strain-displacement relations (Eq. 3.16), differentiating, and applying the four boundary conditions (Eq. 3.19), the relationships between the rotation functions are [30]

$$\begin{aligned} \xi_1^{sl} &= \xi_2^{sl} = 0 \\ \eta_1^{sl} &= -\frac{4}{3(h^{sl})^2} \left(\frac{\partial u_3^{sl}}{\partial x_1} + \psi_1^{sl} \right) \\ \eta_2^{sl} &= -\frac{4}{3(h^{sl})^2} \left(\frac{\partial u_3^{sl}}{\partial x_2} + \psi_2^{sl} \right) \end{aligned} \quad (3.20)$$

Using Eq. 3.20, the displacements (Eq. 3.17) may be rewritten as

$$\begin{aligned} u_1^{sl} &= {}^0u_1^{sl} + x_3 \left\{ \psi_1^{sl} - \frac{4x_3^2}{3(h^{sl})^2} \left(\frac{\partial u_3^{sl}}{\partial x_1} + \psi_1^{sl} \right) \right\} \\ u_2^{sl} &= {}^0u_2^{sl} + x_3 \left\{ \psi_2^{sl} - \frac{4x_3^2}{3(h^{sl})^2} \left(\frac{\partial u_3^{sl}}{\partial x_2} + \psi_2^{sl} \right) \right\} \\ u_3^{sl} &= {}^0u_3^{sl} \end{aligned} \quad (3.21)$$

The displacements are now specified in terms of only five functions: three midplane displacements ${}^0u_1^{sl}$, ${}^0u_2^{sl}$, ${}^0u_3^{sl}$, and two rotation functions ψ_1^{sl} and ψ_2^{sl} . Using the displacements in Eq. 3.21, the nonlinear strains (Eq. 3.16) may be expressed as

$$\begin{aligned} \epsilon_1^{sl} &= {}^0\epsilon_1^{sl} + x_3 {}^0\kappa_1^{sl} + x_3^2 {}^2\kappa_1^{sl} \\ \epsilon_2^{sl} &= {}^0\epsilon_2^{sl} + x_3 {}^0\kappa_2^{sl} + x_3^2 {}^2\kappa_2^{sl} \\ \epsilon_3^{sl} &= 0 \\ \epsilon_4^{sl} &= {}^0\epsilon_4^{sl} + x_3^2 {}^2\kappa_4^{sl} \\ \epsilon_5^{sl} &= {}^0\epsilon_5^{sl} + x_3^2 {}^2\kappa_5^{sl} \\ \epsilon_6^{sl} &= {}^0\epsilon_6^{sl} + x_3 {}^0\kappa_6^{sl} + x_3^2 {}^2\kappa_6^{sl} \end{aligned} \quad (3.22)$$

In these expressions, ${}^0\epsilon_i^{sl}$ are the midplane strains, and ${}^0\kappa_i^{sl}$ and ${}^2\kappa_i^{sl}$ are the midplane curvatures of the sublamine defined by

$$\begin{aligned}
 {}^0\epsilon_1^{sl} &= \frac{\partial {}^0u_1^{sl}}{\partial x_1} + \frac{1}{2} \left(\frac{\partial {}^0u_3^{sl}}{\partial x_1} \right)^2 & {}^0\kappa_1^{sl} &= \frac{\partial \psi_1^{sl}}{\partial x_1} & {}^2\kappa_1^{sl} &= -\frac{4}{3(h^{sl})^2} \left(\frac{\partial^2 {}^0u_3^{sl}}{\partial x_1^2} + \frac{\partial \psi_1^{sl}}{\partial x_1} \right) \\
 {}^0\epsilon_2^{sl} &= \frac{\partial {}^0u_2^{sl}}{\partial x_2} + \frac{1}{2} \left(\frac{\partial {}^0u_3^{sl}}{\partial x_2} \right)^2 & {}^0\kappa_2^{sl} &= \frac{\partial \psi_2^{sl}}{\partial x_2} & {}^2\kappa_2^{sl} &= -\frac{4}{3(h^{sl})^2} \left(\frac{\partial^2 {}^0u_3^{sl}}{\partial x_2^2} + \frac{\partial \psi_2^{sl}}{\partial x_2} \right) \\
 {}^0\epsilon_4^{sl} &= \psi_2^{sl} + \frac{\partial {}^0u_3^{sl}}{\partial x_2} & & & {}^2\kappa_4^{sl} &= -\frac{4}{(h^{sl})^2} \left(\psi_2^{sl} + \frac{\partial {}^0u_3^{sl}}{\partial x_2} \right) \\
 {}^0\epsilon_5^{sl} &= \psi_1^{sl} + \frac{\partial {}^0u_3^{sl}}{\partial x_1} & & & {}^2\kappa_5^{sl} &= -\frac{4}{(h^{sl})^2} \left(\psi_1^{sl} + \frac{\partial {}^0u_3^{sl}}{\partial x_1} \right) \\
 {}^0\epsilon_6^{sl} &= \frac{\partial {}^0u_1^{sl}}{\partial x_2} + \frac{\partial {}^0u_2^{sl}}{\partial x_1} & {}^0\kappa_6^{sl} &= \frac{\partial \psi_1^{sl}}{\partial x_2} + \frac{\partial \psi_2^{sl}}{\partial x_1} & {}^2\kappa_6^{sl} &= -\frac{4}{3(h^{sl})^2} \left(\frac{\partial \psi_1^{sl}}{\partial x_2} + \frac{\partial \psi_2^{sl}}{\partial x_1} \right. \\
 & \quad \left. + \frac{\partial {}^0u_3^{sl}}{\partial x_1} \frac{\partial {}^0u_3^{sl}}{\partial x_2} \right) & & & & \left. + 2 \frac{\partial^2 {}^0u_3^{sl}}{\partial x_1 \partial x_2} \right)
 \end{aligned} \tag{3.23}$$

§3.6 Displacements, Strains, and Stresses in the Sublamine

The displacements in the sublamine are assumed to be a linear combination of two parts: (a) the displacements that would exist in the sublamine in the absence of the delamination, plus (b) the displacements introduced by transverse deformation of the sublamine. The five functions describing the sublamine displacements are

$$\begin{aligned}
 {}^0u_1^{sl} &\cong {}^0u_1^{pl} + \hat{u}_1^{sl} \\
 {}^0u_2^{sl} &\cong {}^0u_2^{pl} + \hat{u}_2^{sl} \\
 {}^0u_3^{sl} &\cong {}^0u_3^{pl} + \hat{u}_3^{sl} = \hat{u}_3^{sl} \\
 \psi_1^{sl} &\cong \psi_1^{pl} + \hat{\psi}_1^{sl} = \hat{\psi}_1^{sl} \\
 \psi_2^{sl} &\cong \psi_2^{pl} + \hat{\psi}_2^{sl} = \hat{\psi}_2^{sl}
 \end{aligned} \tag{3.24}$$

The in-plane displacements in the plate (${}^0u_1^{pl}$, ${}^0u_2^{pl}$) are given in Eq. 3.15. The second equalities in the last three expressions can be written because the transverse displacements and rotations in the plate are assumed to be zero (Assumption 8). The displacements in the sublamine due to out-of-plane deformation (the quantities with the hat) are represented by

$$\begin{aligned}
 {}^0\hat{u}_1^{sl} &= \sum_{j=1}^{n_p} p_j^p \phi_j \\
 {}^0\hat{u}_2^{sl} &= \sum_{j=1}^{n_q} q_j^q \phi_j \\
 {}^0\hat{u}_3^{sl} &= \sum_{j=1}^{n_r} r_j^r \phi_j \\
 \hat{\psi}_1^{sl} &= \sum_{j=1}^{n_s} s_j^s \phi_j \\
 \hat{\psi}_2^{sl} &= \sum_{j=1}^{n_t} t_j^t \phi_j
 \end{aligned} \tag{3.25}$$

where n_p through n_t are the number of terms in each series. The parameters p_j , q_j , r_j , s_j , and t_j are coefficients, while ${}^p\phi_j$, ${}^q\phi_j$, ${}^r\phi_j$, ${}^s\phi_j$, and ${}^t\phi_j$ are functions of the coordinates x_1 and x_2 . Expressions for these coordinate functions must be chosen such that they: (a) satisfy the boundary conditions on the sublamine (discussed below) and (b) are linearly independent, continuous, and complete [30].

One of the fundamental assumptions of this analysis is that the displacements of the sublamine and plate match along the boundary of the sublamine. Along this boundary, the displacements are completely specified, while the force and moment resultants are unspecified. Thus, by definition, the sublamine boundary is a clamped boundary (Figure 3-3). The appropriate clamped boundary conditions are [26, 27]

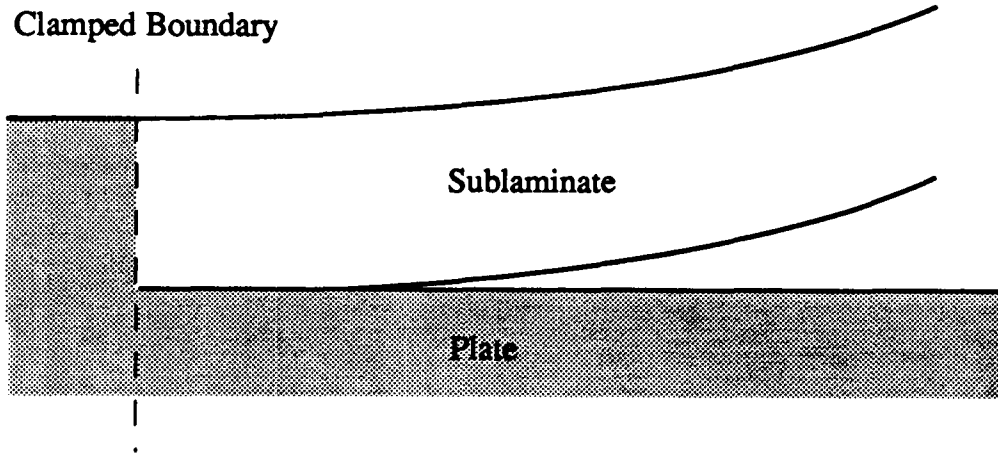


Figure 3-3 Illustration of the clamped boundary at the sublamine edge.

$$\begin{aligned}
 {}^o u_1^{sl} &= {}^o u_1^{pl} & \psi_n^{sl} &= \psi_n^{pl} = 0 \\
 {}^o u_2^{sl} &= {}^o u_2^{pl} & \psi_t^{sl} &= \psi_t^{pl} = 0 \\
 {}^o u_3^{sl} &= {}^o u_3^{pl} = 0 & \frac{\partial {}^o u_3^{sl}}{\partial x_n} &= \frac{\partial {}^o u_3^{pl}}{\partial x_n} = 0
 \end{aligned} \tag{3.26}$$

The subscripts n and t refer to the normal and tangential directions, respectively, to the sublamine boundary (Figure 3-4). Clearly, the first five boundary conditions require that the functions ${}^p\phi_j$, ${}^q\phi_j$, ${}^r\phi_j$, ${}^s\phi_j$, and ${}^t\phi_j$ vanish at every point on the boundary (Eqs. 3.24 and 3.25). The final boundary condition of Eq. 3.26 requires that the derivative of ${}^r\phi_j$ also vanish on the boundary. Accordingly, the following polynomial coordinate functions were chosen

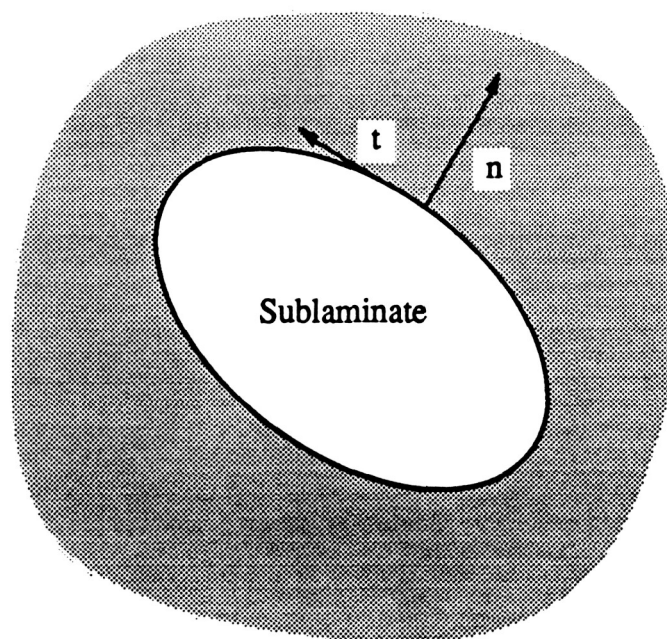


Figure 3-4 Definition of the tangent t and normal n coordinates along the sub-laminate boundary.

$$\begin{aligned}
p_j^p \phi_j &= (1 - \bar{x}_1^2 - \bar{x}_2^2)(p_1 \bar{x}_1 + p_2 \bar{x}_2 + p_3 \bar{x}_1^3 + p_4 \bar{x}_1^2 \bar{x}_2 + p_5 \bar{x}_1 \bar{x}_2^2 + p_6 \bar{x}_2^3 \\
&\quad + p_7 \bar{x}_1^5 + p_8 \bar{x}_1^4 \bar{x}_2 + p_9 \bar{x}_1^3 \bar{x}_2^2 + p_{10} \bar{x}_1^2 \bar{x}_2^3 + p_{11} \bar{x}_1 \bar{x}_2^4 + p_{12} \bar{x}_2^5 \\
&\quad + p_{13} \bar{x}_1^7 + p_{14} \bar{x}_1^6 \bar{x}_2 + p_{15} \bar{x}_1^5 \bar{x}_2^2 + p_{16} \bar{x}_1^4 \bar{x}_2^3 \\
&\quad + p_{17} \bar{x}_1^3 \bar{x}_2^4 + p_{18} \bar{x}_1^2 \bar{x}_2^5 + p_{19} \bar{x}_1 \bar{x}_2^6 + p_{20} \bar{x}_2^7) \\
q_j^q \phi_j &= (1 - \bar{x}_1^2 - \bar{x}_2^2)(q_1 \bar{x}_1 + q_2 \bar{x}_2 + q_3 \bar{x}_1^3 + q_4 \bar{x}_1^2 \bar{x}_2 + q_5 \bar{x}_1 \bar{x}_2^2 + q_6 \bar{x}_2^3 \\
&\quad + q_7 \bar{x}_1^5 + q_8 \bar{x}_1^4 \bar{x}_2 + q_9 \bar{x}_1^3 \bar{x}_2^2 + q_{10} \bar{x}_1^2 \bar{x}_2^3 + q_{11} \bar{x}_1 \bar{x}_2^4 + q_{12} \bar{x}_2^5 \\
&\quad + q_{13} \bar{x}_1^7 + q_{14} \bar{x}_1^6 \bar{x}_2 + q_{15} \bar{x}_1^5 \bar{x}_2^2 + q_{16} \bar{x}_1^4 \bar{x}_2^3 \\
&\quad + q_{17} \bar{x}_1^3 \bar{x}_2^4 + q_{18} \bar{x}_1^2 \bar{x}_2^5 + q_{19} \bar{x}_1 \bar{x}_2^6 + q_{20} \bar{x}_2^7)
\end{aligned} \tag{3.27}$$

$$r_j^r \phi_j = (1 - \bar{x}_1^2 - \bar{x}_2^2)^2 (r_1 + r_2 \bar{x}_1^2 + r_3 \bar{x}_2^2 + r_4 \bar{x}_1 \bar{x}_2)$$

$$s_j^s \phi_j = (1 - \bar{x}_1^2 - \bar{x}_2^2)(s_1 \bar{x}_1 + s_2 \bar{x}_2 + s_3 \bar{x}_1^3 + s_4 \bar{x}_1^2 \bar{x}_2 + s_5 \bar{x}_1 \bar{x}_2^2 + s_6 \bar{x}_2^3)$$

$$t_j^t \phi_j = (1 - \bar{x}_1^2 - \bar{x}_2^2)(t_1 \bar{x}_1 + t_2 \bar{x}_2 + t_3 \bar{x}_1^3 + t_4 \bar{x}_1^2 \bar{x}_2 + t_5 \bar{x}_1 \bar{x}_2^2 + t_6 \bar{x}_2^3)$$

where

$$\begin{aligned}
\bar{x}_1 &= \left(\frac{x_1}{a}\right) \\
\bar{x}_2 &= \left(\frac{x_2}{b}\right)
\end{aligned}$$

These expressions satisfy the boundary conditions for an elliptically-shaped sublamine (semi-axes a and b), and satisfy the condition that the functions be linearly independent, continuous, and complete.

The functions in Eq. 3.27 are similar to those used by previous investigators [16,18,19]. However, previous investigators have omitted various terms from the series. Either the omission of terms from a series or the premature truncation of a series can affect the accuracy of the results. In particular, it is important to retain

1. Crossproduct terms (e.g. $r_4 \bar{x}_1 \bar{x}_2$) for arbitrary delamination orientations;
2. ${}^p\phi_j$ and ${}^q\phi_j$ to at least one order higher than ${}^r\phi_j$ for accurate postbuckling calculation of in-plane strains; and
3. ${}^s\phi_j$ and ${}^t\phi_j$ to the same order as $\frac{\partial u_3}{\partial x_i}$ for accurate representation of transverse shear rotations.

The displacements in the sublaminates (Eq. 3.21) are now specified in terms of the unknown coefficients p_j , q_j , r_j , s_j , and t_j and their associated coordinate functions (Eq. 3.27). The off-axis strains at any point in the sublaminates may be calculated from the midplane strain and curvature definitions (Eq. 3.23) and the strain-displacement relations (Eq. 3.22). Using the strains, the associated off-axis stresses in each ply of the sublaminates may be calculated from the off-axis constitutive relations (Eq. 3.5). On-axis strains and stresses in each ply are obtained by rotating the respective off-axis strains and stresses into the on-axis coordinate system [23].

The displacements, strains, and stresses in the sublaminates are thus specified in terms of the coefficients p_j , q_j , r_j , s_j , and t_j . These coefficients are determined by the Ritz energy method.

§3.7 Total Potential Energy

The total potential energy of the sublaminates Π^{sl} in the absence of body forces is [31]

$$\Pi^{sl} = \int_V \left(\int_0^{\epsilon_i} \sigma_i d\epsilon_i \right) dV - \int_A \left(\int_0^{u_3^{sl}} f du_3 \right) dA \quad i = 1, 2, 4, 5, 6 \quad (3.28)$$

where V is the volume of the sublaminates, A is the lateral surface area of the sublaminates, and f is the force per unit area acting on the surface. The subscript 3 is not included since the transverse normal stress σ_3 is assumed to be zero. Note

that repeated subscripts imply summation. Substituting the constitutive relations (Eq. 3.5) for σ_i yields

$$\Pi^{sl} = \int_V \left(\int_0^{\epsilon_i} Q_{ij}(\epsilon_j - \alpha_j \Delta T) d\epsilon_i \right) dV - \int_A \left(\int_0^{u_3^{sl}} f du_3 \right) dA \quad i, j = 1, 2, 4, 5, 6 \quad (3.29)$$

Integration of Eq. 3.29 with respect to ϵ_i produces

$$\Pi^{sl} = \frac{1}{2} \int_V \epsilon_i Q_{ij} \epsilon_j dV - \int_V \epsilon_i Q_{ij} \alpha_j \Delta T dV - \int_A \left(\int_0^{u_3^{sl}} f du_3 \right) dA \quad i, j = 1, 2, 4, 5, 6 \quad (3.30)$$

Two kinds of surface traction are considered to act on the lateral surfaces of the sublaminates. First, a uniform transverse pressure may exist due to a pressure difference ΔP between the outside and inside surfaces of the sublaminates (Figure 3-5). The pressure on the outside surface is generally atmospheric. On the inside surface the pressure may be subatmospheric due to a partial vacuum that may form as the sublaminates buckle. Second, a force may result from contact between the buckled sublaminates and the plate over portions of the delaminated surface (Figure 3-6) [32]. Where the sublaminates tend to deform toward the plate, contact between the two will occur and a force resisting the sublaminates deformation will arise. This contact is modeled by considering the sublaminates to be resting on a detached elastic foundation (Figure 3-7). The restoring force is taken to vary linearly with the sublaminates transverse displacement u_3^{sl} for positive displacements, and to vanish for negative displacements. Therefore, the force per unit area acting on the sublaminates at a given point is

$$f = \begin{cases} \Delta P - K u_3^{sl} & u_3^{sl} \geq 0 \\ \Delta P & u_3^{sl} < 0 \end{cases} \quad (3.31)$$

The foundation modulus K [33, 34] is estimated from (Appendix D)

$$K \approx \frac{E_f}{l_f} \quad (3.32)$$

where E_f is the elastic modulus of the foundation and l_f is a characteristic length (for example, the sublamine diameter).

Note that the transverse pressure model only makes sense in conjunction with the contact model. Without the contact model, the transverse pressure would simply produce sublamine bending toward the plate.

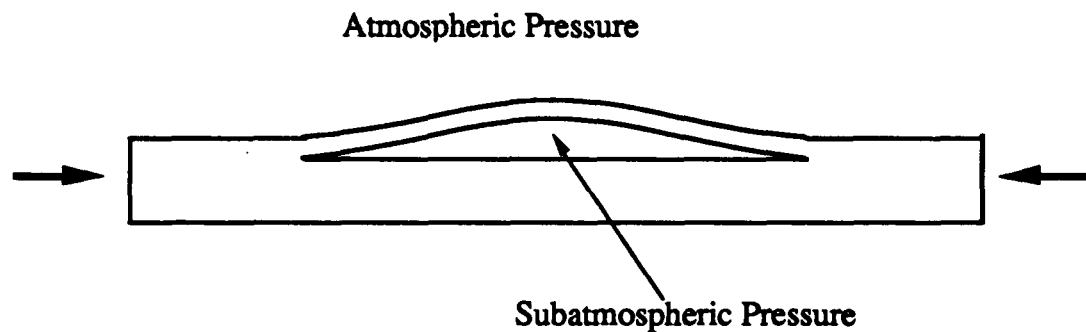
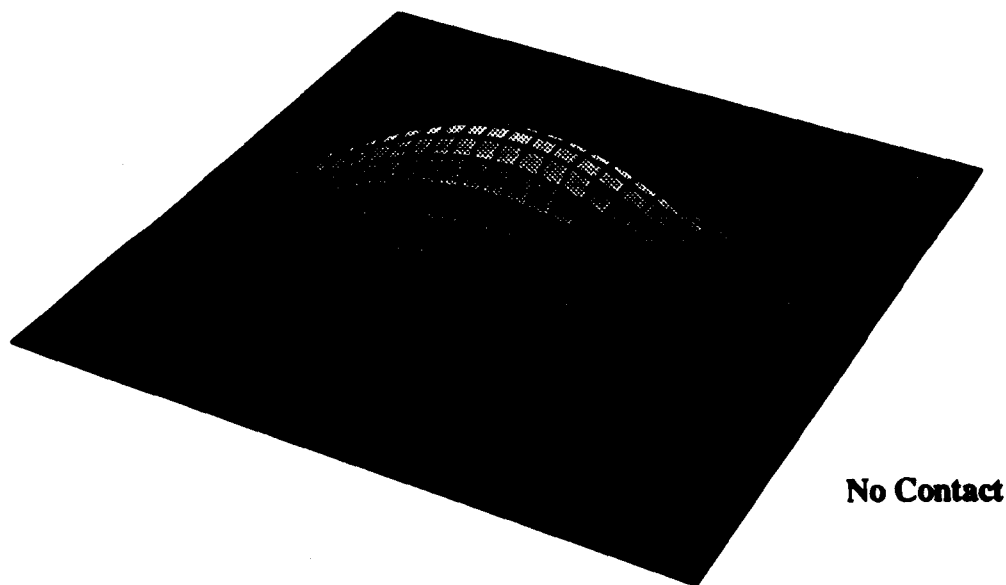
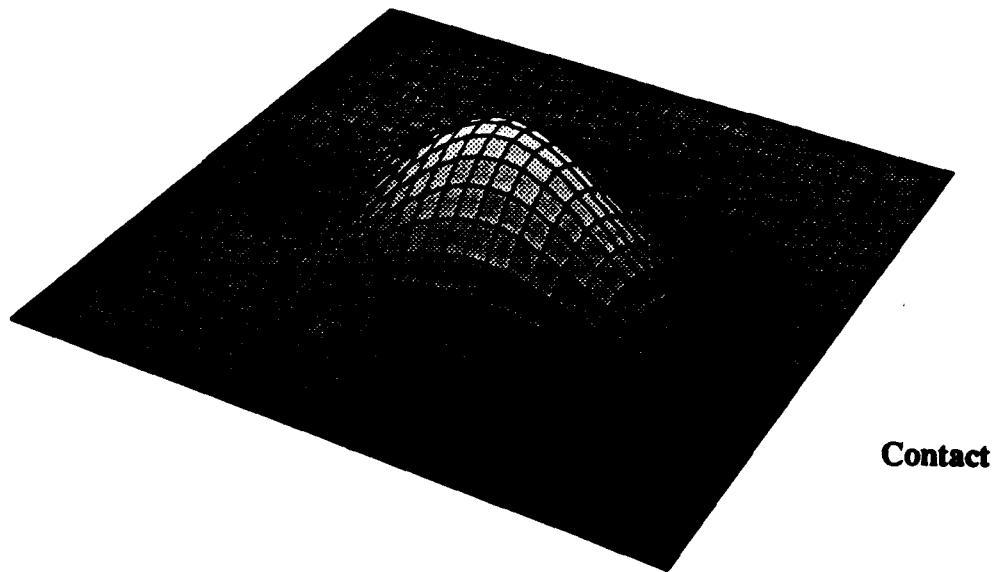


Figure 3-5 Possible pressure difference acting across the sublamine thickness.



~~ORIGINAL PAGE~~
~~BLACK AND WHITE PHOTOGRAPH~~

Figure 3-6 Contact between the sublaminate and plate.

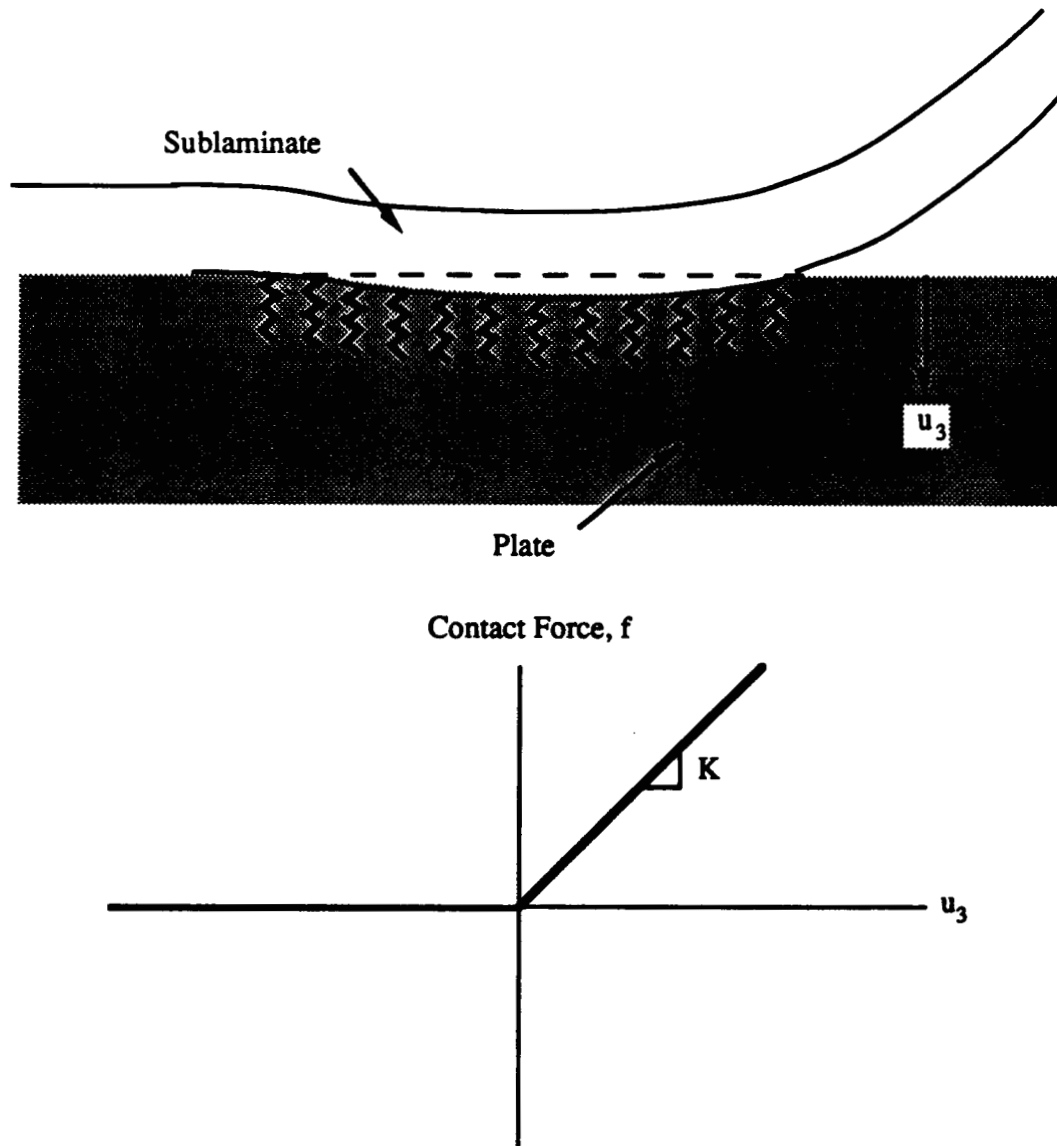


Figure 3-7 Detached elastic foundation model of contact force.

ORIGINAL PAGE
BLACK AND WHITE PHOTOGRAPH

Integration of Eq. 3.30 with respect to the thickness h^{sl} , together with the strain definitions (Eqs. 3.22 and 3.23), results in the following expression for the total potential energy [30]

$$\begin{aligned}
 \Pi^{sl} = & \frac{1}{2} \iint_A \begin{pmatrix} \epsilon_4^{sl} \\ \epsilon_5^{sl} \\ 2\kappa_4^{sl} \\ 2\kappa_5^{sl} \end{pmatrix}^{tr} \begin{pmatrix} A_{44} & A_{45} & D_{44} & D_{45} \\ & A_{55} & D_{45} & D_{55} \\ & sym & F_{44} & F_{45} \\ & & F_{45} & F_{55} \end{pmatrix} \begin{pmatrix} \epsilon_4^{sl} \\ \epsilon_5^{sl} \\ 2\kappa_4^{sl} \\ 2\kappa_5^{sl} \end{pmatrix} dA + \\
 & \frac{1}{2} \iint_A \begin{pmatrix} \epsilon_1^{sl} \\ \epsilon_2^{sl} \\ \epsilon_6^{sl} \\ \kappa_1^{sl} \\ \kappa_2^{sl} \\ \kappa_6^{sl} \\ 2\kappa_1^{sl} \\ 2\kappa_2^{sl} \\ 2\kappa_6^{sl} \end{pmatrix}^{tr} \begin{pmatrix} A_{11} & A_{12} & A_{16} & B_{11} & B_{12} & B_{16} & E_{11} & E_{12} & E_{16} \\ & A_{22} & A_{26} & B_{12} & B_{22} & B_{26} & E_{12} & E_{22} & E_{26} \\ & & A_{66} & B_{16} & B_{26} & B_{66} & E_{16} & E_{26} & E_{66} \\ & & & D_{11} & D_{12} & D_{16} & F_{11} & F_{12} & F_{16} \\ & & & & D_{22} & D_{26} & F_{12} & F_{22} & F_{26} \\ & & & & & D_{66} & F_{16} & F_{26} & F_{66} \\ & & & & & & H_{11} & H_{12} & H_{16} \\ & & & & & & & H_{22} & H_{26} \\ & & & & & & & & H_{66} \end{pmatrix} \begin{pmatrix} \epsilon_1^{sl} \\ \epsilon_2^{sl} \\ \epsilon_6^{sl} \\ \kappa_1^{sl} \\ \kappa_2^{sl} \\ \kappa_6^{sl} \\ 2\kappa_1^{sl} \\ 2\kappa_2^{sl} \\ 2\kappa_6^{sl} \end{pmatrix} dA \\
 & - \iint_A (\epsilon_1^{sl}, \epsilon_2^{sl}, \epsilon_6^{sl}, \kappa_1^{sl}, \kappa_2^{sl}, \kappa_6^{sl}, 2\kappa_1^{sl}, 2\kappa_2^{sl}, 2\kappa_6^{sl}) \begin{pmatrix} N_1^{slT} \\ N_2^{slT} \\ N_6^{slT} \\ M_1^{slT} \\ M_2^{slT} \\ M_6^{slT} \\ P_1^{slT} \\ P_2^{slT} \\ P_6^{slT} \end{pmatrix} dA - \iint_A \left(\int_0^{u_3^{sl}} f du_3 \right) dA
 \end{aligned} \tag{3.33}$$

where tr represents the matrix transpose, and A_{ij} , B_{ij} , D_{ij} , E_{ij} , F_{ij} , H_{ij} are sublamine stiffnesses (Appendix E) defined by

$$\begin{aligned}
 (A_{ij}, B_{ij}, D_{ij}, E_{ij}, F_{ij}, H_{ij}) &= \int_{-\frac{h^s l}{2}}^{\frac{h^s l}{2}} Q_{ij}(1, x_3, x_3^2, x_3^3, x_3^4, x_3^6) dx_3 \quad i, j = 1, 2, 6 \\
 (A_{ij}, D_{ij}, F_{ij}) &= \int_{-\frac{h^s l}{2}}^{\frac{h^s l}{2}} Q_{ij}(1, x_3^2, x_3^4) dx_3 \quad i, j = 4, 5
 \end{aligned} \tag{3.34}$$

The thermal force and moment resultants are

$$(N_i^{s l T}, M_i^{s l T}, P_i^{s l T}) = \int_{-\frac{h^s l}{2}}^{\frac{h^s l}{2}} Q_{ij} \alpha_j \Delta T(1, x_3, x_3^3) dx_3 \quad i, j = 1, 2, 6 \tag{3.35}$$

The specific limits of integration over the area A of the elliptical sublaminates are

$$\int_{-a}^a \int_{-b\sqrt{1-(\frac{x_1}{a})^2}}^{b\sqrt{1-(\frac{x_1}{a})^2}} [\dots] dx_2 dx_1 \tag{3.36}$$

where the ellipse is bounded by $1 - (\frac{x_1}{a})^2 - (\frac{x_2}{b})^2 = 0$, and a and b are the semi-axes in the x_1 and x_2 directions, respectively.

§3.8 Applied Load versus Deformation of the Sublaminates

To establish the relationship between the applied mechanical and thermal loads (N and ΔT) and the sublaminates deformation ($u_1^{s l}$, $u_2^{s l}$, and $u_3^{s l}$), the total potential energy of the sublaminates ($\Pi^{s l}$) is first assembled by substituting the displacement approximations (Eqs. 3.24, 3.25, and 3.27) into the midplane strain and curvature definitions (Eq. 3.23), and then substituting these results into the expressions for the total potential energy (Eq. 3.28). The resulting expression is extremely lengthy and will not be given here. Essentially, the total potential energy of the sublaminates is now expressed as a function of the known geometry (a, b), material properties

$(A_{ij}, \dots, \alpha_i)$, and applied loads $(N, \Delta T)$, and a set of as yet unknown coefficients $(p_j, q_j, r_j, s_j, t_j)$

$$\Pi^{sl} = \Pi^{sl}(a, b; A_{ij}, \dots, \alpha_i; N, \Delta T; p_j, q_j, r_j, s_j, t_j) \quad (3.37)$$

The unknown coefficients are determined by minimizing the total potential energy with respect to the coefficients [30]

$$\frac{\partial \Pi^{sl}}{\partial m_j} = 0 \quad j = 1 \text{ to } 56 \quad (3.38)$$

where m_j is used as a generic unknown coefficient representing p_j, q_j, r_j, s_j , or t_j . The differentiations indicated in Eq. 3.38 result in a system of 56 nonlinear algebraic equations in the unknown coefficients. These are the equilibrium equations. A solution to these equations yields a set of coefficients $(\hat{p}_j, \hat{q}_j, \hat{r}_j, \hat{s}_j, \hat{t}_j)$ corresponding to specified values of the applied loads $(\hat{N}, \hat{\Delta T})$, where the hat indicates a particular set of loads. Knowing the coefficients, the displacements, strains and stresses throughout the sublamine can be determined.

A load-deformation history for the sublamine is mapped out by solving the equilibrium equations over a range of applied loads. However, care must be exercised due to the nonlinearity of the equations. In general, more than one solution exists for a given load. The solution must correspond to a local minimum of the total potential energy, implying that the solution must be physically stable. Furthermore, multiple stable solutions are possible. Therefore, each possible solution $(\hat{p}_j, \hat{q}_j, \hat{r}_j, \hat{s}_j, \hat{t}_j)$ must be tested to determine whether it corresponds to a local minimum of the the total potential energy (stable solution) or a local maximum (unstable solution). The stability test [35] requires that the determinant of the matrix of second partial

derivatives of the the total potential energy be positive definite

$$\left| \frac{\partial^2 \Pi^I(\hat{p}_j, \hat{q}_j, \hat{r}_j, \hat{s}_j, \hat{t}_j)}{\partial m_i \partial m_k} \right| > 0 \quad i, k = 1 \text{ to } 56 \quad (3.39)$$

where m_i is again a generic coefficient. If multiple stable solutions are shown to exist, each with an associated total potential energy, then the solution with the minimum total potential energy of the sublaminates is assumed to be the most likely solution.

§3.9 Buckling Condition

The buckling load is one at which the system changes from one configuration to another, energetically more favorable, configuration. This change occurs at a load for which the determinant of the matrix of second partial derivatives of the potential energy ceases to be positive definite [31, 36]

$$\left| \frac{\partial^2 \Pi^I(\hat{m}_j)}{\partial m_i \partial m_k} \right| = 0 \quad i, k = 1 \text{ to } 56 \quad (3.40)$$

In the equilibrium problem described above, the unknown coefficients are determined for a known load. In the buckling problem, both the load and the coefficients for which Eq. 3.40 applies are desired. Two different approaches have been used to solve the buckling problem. In the linear method, the values of the unknown coefficients are assumed to be zero ($p_j = q_j = r_j = s_j = t_j = 0$) and the buckling load N_b^I satisfying Eq. 3.40 is found. In the equilibrium method, the load N is gradually incremented over a range of values, each time solving the nonlinear equilibrium equations for the unknown coefficients as above. The point at which the displacements change dramatically with increasing load (Figure 3-8) is the buckling load N_b . Since unsymmetric laminates may deform out-of-plane at loads less than the linear buckling load, the equilibrium method is recommended.

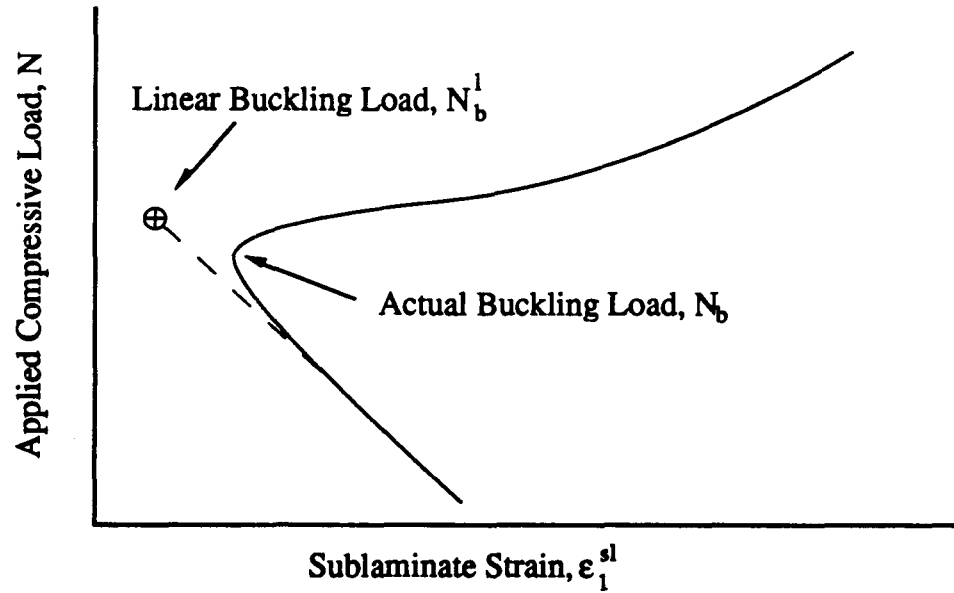


Figure 3-8 Illustration of the actual load-strain behavior and the calculated linear buckling load.

§3.10 Growth Criterion

The strain energy released per unit area by the plate-sublamine system for an increment of sublamine growth is the strain energy release rate G . The delaminated sublamine is assumed to grow for a given load when G exceeds a critical strain energy release rate G_c of the material [37]

$$G \equiv \frac{d(\Pi^{pl} - \Pi^{sl})}{dA} \geq G_c \quad (3.41)$$

where Π^{sl} and Π^{pl} refer to the strain energies of the sublamine and plate, respectively, and A is the surface area of the sublamine. The strain energy released by the plate is the strain energy of that portion of the plate which becomes part of the

new sublaminates after growth (Figure 3-9). Thus, the strain energy of the plate is

$$\begin{aligned} \Pi^{pl} = & \frac{1}{2} \iint_A \begin{pmatrix} \epsilon_1^{pl} \\ \epsilon_2^{pl} \\ \epsilon_6^{pl} \end{pmatrix}^T \begin{pmatrix} A_{11} & A_{12} & A_{16} \\ A_{12} & A_{22} & A_{26} \\ A_{16} & A_{26} & A_{66} \end{pmatrix} \begin{pmatrix} \epsilon_1^{pl} \\ \epsilon_2^{pl} \\ \epsilon_6^{pl} \end{pmatrix} dA \\ & - \iint_A (\epsilon_1^{pl}, \epsilon_2^{pl}, \epsilon_6^{pl}) \begin{pmatrix} N_1^{plT} \\ N_2^{plT} \\ N_6^{plT} \end{pmatrix} dA \end{aligned} \quad (3.42)$$

The stiffnesses A_{ij} and thermal resultants N_i^{plT} are evaluated over the thickness of the sublaminates because the strain energy of the balance of the plate does not change during growth of the sublaminates. Only the sublaminates portion of the plate contributes.

Following Chai and Babcock [18], the total strain energy release is considered during growth of the sublaminates. That is, although the strain energy released during growth of the sublaminates varies along the sublaminates boundary, local variations in the strain energy release are not included here. For an elliptically-shaped sublaminates, Eq. 3.41 may be written (Appendix F)

$$G = \frac{(\frac{\partial \Pi^{pl}}{\partial a} \frac{da}{db} + \frac{\partial \Pi^{pl}}{\partial b}) - (\frac{\partial \Pi^{pl}}{\partial a} \frac{da}{db} + \frac{\partial \Pi^{pl}}{\partial b})}{\pi(b \frac{da}{db} + a)} \geq G_c \quad (3.43)$$

where $A = \pi ab$ is the area of the elliptical delamination. The parameter $\frac{da}{db}$ describes the direction in which the sublaminates grows (Figure 3-9). For example, $\frac{da}{db} = 0$ implies growth in the b direction only, $\frac{da}{db} = \infty$ implies growth in the a direction only, and $\frac{da}{db} = \frac{a}{b}$ implies self-similar growth. The strain energy release rate is evaluated over a range of values of the parameter $\frac{da}{db}$ so that the lowest G can be found. In practice, sublaminates growth is often observed in a direction perpendicular to the applied load. Thus, a suitable choice would be $\frac{da}{db} = 0$ (growth in the b , or x_2 , direction) for a load applied in the x_1 direction.

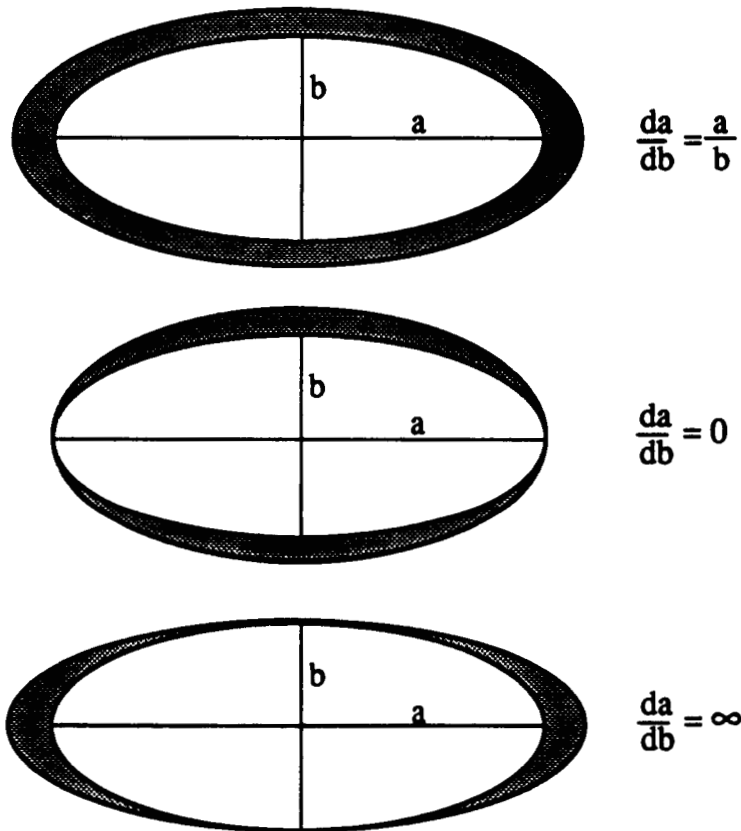
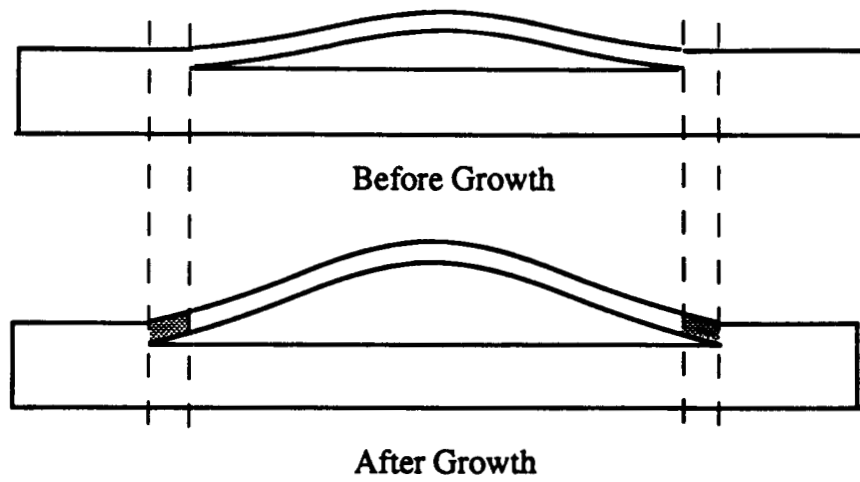


Figure 3-9 Definition of the growth parameter $\frac{da}{db}$.

Chapter 4

Implementation

§4.1 Introduction

The FORTRAN computer code DELAM was developed from the analysis of sublaminates buckling and postbuckling behavior (Chapter 3). The program reads input data describing the delamination and the plate in which it is contained, including: (a) the plate material properties, geometry, and layup; (b) the location, dimensions and orientation of the delamination; and (c) the applied loads. A list of the required input data is given in Table 4-1.

From the input data, derived properties are calculated for subsequent use in the delamination analysis: (a) the on-axis stiffnesses of each ply (Appendix A); (b) the ply on-axis plane stress reduced stiffnesses (Eq. 3.6); (c) the ply off-axis reduced stiffnesses which appear in Eq. 3.5 in both the plate and the sublamine coordinate systems; (d) the laminate stiffnesses for the plate (Eq. 3.8) and the sublamine (Eq. 3.34) from the off-axis reduced stiffnesses; (e) the thermal resultants for the plate (Eq. 3.9) and sublamine (Eq. 3.35) from the off-axis reduced stiffnesses, the thermal coefficients of expansion (as rotated into the off-axis system [24]), and the specified temperature difference; (f) the constants describing the mechanical response of the plate (Eq. 3.13); and (g) the thermal strains (Eq. 3.14).

Table 4-1 Input Parameters Required for the DELAM Computer Code

Plate and sublamine geometry and layup

Number of plies in the plate, k_p Number of plies in the sublamine, k_d Semi-axes of the ellipse, a, b Angle of the sublamine axes with respect to the plate, θ Thickness of each ply, t_i Orientation of each ply, ϕ_i

Material properties for each ply

Longitudinal Young's modulus, E_x Transverse Young's modulus, E_y Longitudinal to transverse Poisson's ratio, ν_{xy} In-plane shear modulus, G_{xy} Out-of-plane shear moduli, G_{xz}, G_{yz} Thermal (or hygro) coefficients of expansion, α_x, α_y (β_x, β_y)

Growth and contact parameters

Critical strain energy release per unit area, G_c Relative growth direction parameter, $\frac{da}{db}$ Contact law foundation modulus, K

Load description

Normal load in the 1 direction, γ_1 Normal load in the 2 direction, γ_2 Shear load in the 1-2 plane, γ_6 Change from reference temperature (or from dry) state, ΔT (or Δc)Transverse pressure load, ΔP

§4.2 Total Potential Energy

The total potential energy of the sublamine is calculated from Eq. 3.33, using the laminate stiffnesses and thermal resultants which have already been determined. The substitutions and integration were performed by the symbolic mathematics program MACSYMA [38], with the exception of the contact model, which was integrated numerically [39]. An expression for the total potential energy was thus established as a function of the known geometry, material properties, applied loads, and a set of unknown coefficients to be determined. The first and second mixed partial derivatives of the total potential energy with respect to the unknown coefficients were determined using MACSYMA. In addition, the partial derivatives of the total potential energy with respect to the major and minor axes of the sublamine ellipse were evaluated using MACSYMA. The expressions for these derivatives were then inserted into the computer code DELAM for use in the load-strain behavior, buckling, and growth calculations.

§4.3 Nonlinear Load-Strain Behavior

The stresses and strains in the sublamine are determined by obtaining solutions to the equilibrium equations (Eq. 3.38) for specified values of the load N . The equilibrium equations are a set of 56 simultaneous algebraic equations nonlinear in the coefficients m_i . These equations are solved for the unknown coefficients m_i by the Newton-Raphson method [39]. Once a solution for a given N is found, the stability of the solution is checked by calculating the determinant of the matrix of second partial derivatives of the total potential strain energy using the values of the coefficients obtained in the solution (Eq. 3.39). A positive determinant indicates that the solution is stable.

The displacements at any point in the sublamine are calculated by substi-

tuting into Eq. 3.24 the solution coefficients and associated coordinate functions (Eqs. 3.25 and 3.27) together with the boundary conditions (Eq. 3.15). The mid-plane strains and curvatures are then determined from Eq. 3.23. The strains at any point in the sublamine are calculated from Eq. 3.22. Finally, the stresses associated with these strains are determined from the constitutive relationship (Eq. 3.5). The load versus strain behavior is determined by repeating the above procedure for different values of the applied load N .

§4.4 Buckling Load

The linear buckling load N_b^l is the load at which the determinant of the matrix of second partial derivatives of the total potential energy equals zero (Eq. 3.40). Using the given geometry and material properties, the elements of the matrix are numerically evaluated for an initial estimate of the buckling load, assuming that the unknown coefficients are equal to zero. The determinant of the matrix is found by decomposing the matrix into lower and upper triangular matrices. The product of the diagonal elements of the upper triangular matrix (LU decomposition [39]) is the value of the determinant. This constitutes a single evaluation of the determinant as a function of N . In general, the determinant is a nonlinear function of the load N , and explicit derivatives of the function with respect to N do not exist. The load at which the determinant is zero is found using the secant method [39].

Alternatively, the buckling load N_b is graphically determined by examining the complete load-strain behavior of the sublamine. The load at which the sublamine behavior begins to markedly deviate from a linear response is defined to be the buckling load.

§4.5 Growth Load

The growth load of the sublaminates is the load at which the strain energy release rate of the plate-sublaminates system exceeds the critical strain energy release rate of the material (Eq. 3.41). A value is assumed for the growth load N_g , and the associated nonlinear equilibrium displacements are determined in the same manner as in Section 4.3 above. For the displacements thus obtained, the derivatives of the total potential energy with respect to the geometry are evaluated and the strain energy release rate G of the system is calculated (Eq. 3.43). This G is a nonlinear function of N . The value of N at which G equals G_c is found using the secant method [39].

§4.6 Code

The computer program DELAM was specifically written to be used for design calculations as well as for research. It has a user friendly interface, and is computationally efficient and fast. For example, the computation of the nonlinear load-strain behavior of a sublaminates over sixteen values of the applied load requires 7 minutes of CPU time on a Sun 3/160 workstation. The input parameters required by the code are given in Table 4-1. The outputs provided by the code are listed in Table 4-2 and illustrated in detail in Chapter 8. Sample input and output of the code are included in Appendix G.

Table 4-2 DELAM Output

Linear buckling load, N_b^l

Actual buckling load, N_b

Growth load, N_g

Stress-strain behavior in the sublamine, $\sigma_{ij}^{sl}(x, y), \epsilon_{ij}^{sl}(x, y)$

Stress-strain behavior in the plate, $\sigma_{ij}^{pl}(x, y), \epsilon_{ij}^{pl}(x, y)$

Chapter 5

Analytical Verification

§5.1 Introduction

Verification of the delamination behavior model consists of three tasks: (a) comparison to known benchmark analytical solutions, (b) comparison to other approximate solutions, and (c) comparison to experimental data. The first two verification tasks are presented here; the experimental procedure and results are presented in Chapters 6 and 7, respectively.

The benchmark problems consider the behavior of circular and elliptical plates without delaminations under various loadings. The computer program DELAM must be able to predict the behavior of simple plates under edge compression and uniform pressure loads. For certain geometries and material properties, closed form analytical solutions exist. These have been chosen as the benchmark problems.

Approximate solutions to the behavior of plates containing elliptical delaminations have been proposed by several investigators [16,18,19,20,21,22]. In general, these solutions pertain to problems more limited than the analysis presented here. Nevertheless, some of the approximate solutions may be compared to the present method for a select set of problems.

§5.2 Buckling of Circular and Elliptical Plates Without Delaminations

Consider the buckling of an isotropic, circular plate subjected to uniform edge compression. The buckling coefficients k , defined as

$$k = N_b \frac{a^2}{D} \quad (5.1)$$

were calculated by DELAM for both clamped and simply supported aluminum plates, where N_b is the critical buckling load and a is the plate radius. The plate bending stiffness D is

$$D = \frac{Eh^3}{12(1 - \nu^2)} \quad (5.2)$$

where E is Young's modulus, h is the plate thickness, and ν is Poisson's ratio. The classical buckling coefficients for clamped and simply supported plates are given by Timoshenko and Gere [33] as 14.68 and 4.20, respectively. The coefficients are independent of the plate radius-to-thickness (aspect) ratio $\frac{a}{h}$ since the solution is based on classical plate theory. The DELAM and classical buckling coefficients are plotted versus the plate thickness ratio in Figure 5-1. The primary difference between classical plate theory and the present method is the inclusion of transverse shear deformation in DELAM. At large thickness ratios, the predictions are identical; at thickness ratios of less than 20, the effects of shear deformation become apparent as the DELAM buckling coefficient drops significantly below the classical value.

Consider next the buckling of an isotropic elliptical plate under uniform edge compression. The buckling coefficients k for clamped and simply supported plates were calculated by DELAM for an aluminum plate over a range of ellipticities ($\frac{a}{b}$) from one to five. The present results are compared with an approximate solution developed by Voinovsky-Krieger [40] in Figure 5-2. As Voinovsky-Krieger did not

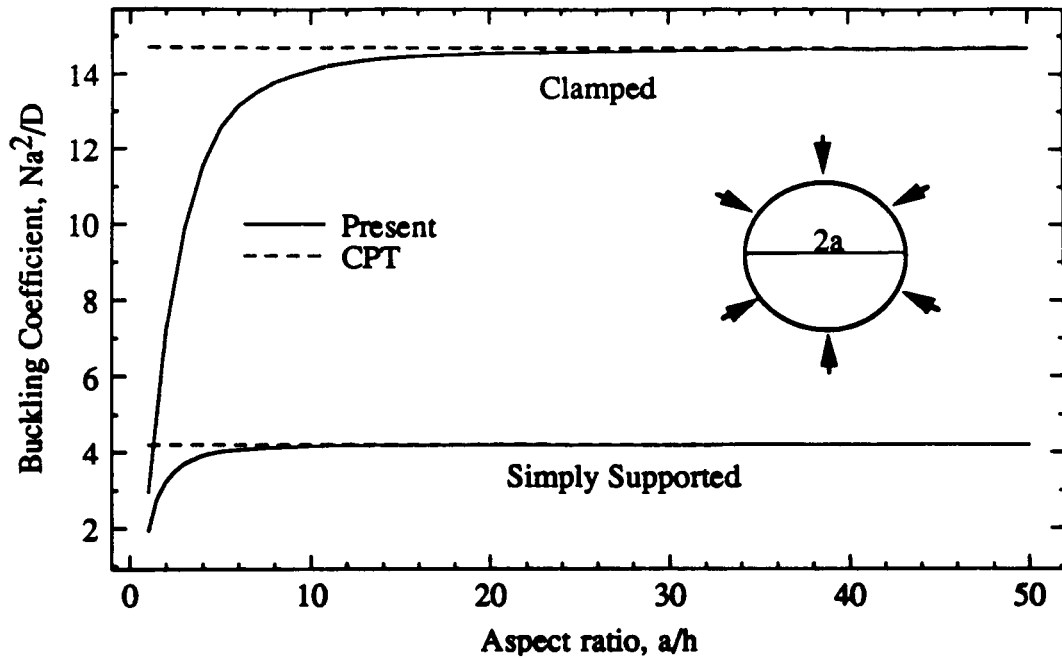


Figure 5-1 Buckling coefficients of clamped and simply supported circular aluminum plates subjected to uniform edge compression ($a = 1.0$ in.).

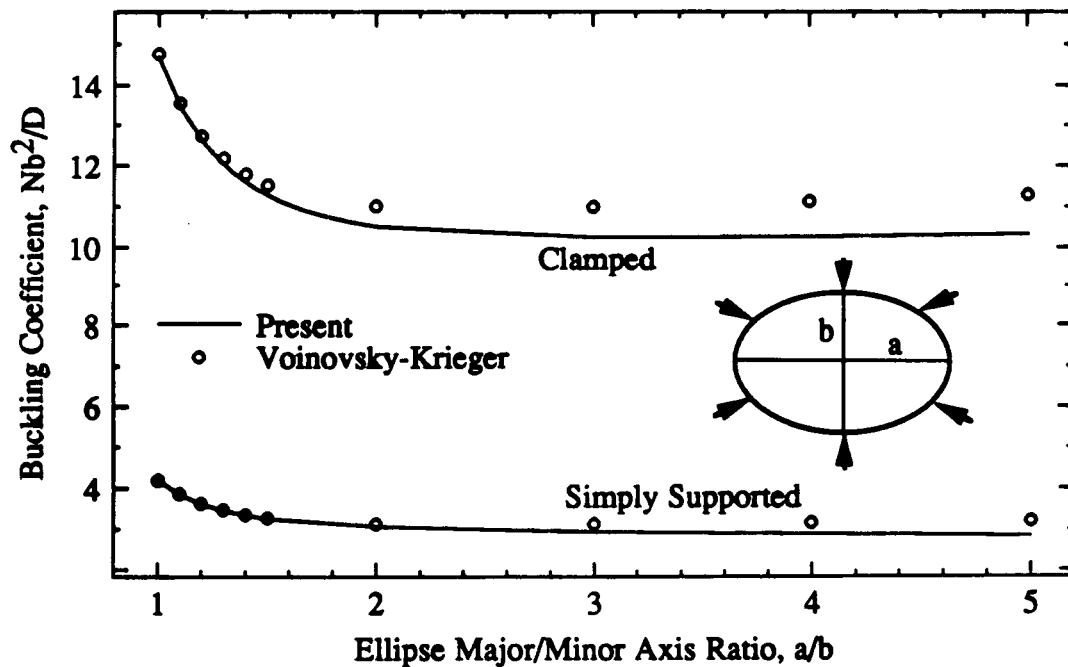


Figure 5-2 Buckling coefficients of clamped and simply supported elliptical aluminum plates subjected to uniform edge compression ($a = 1.0$ in., $h = 0.01$ in.).

include shear deformation effects, a large thickness ratio ($\frac{a}{h} = 100$) was chosen for the present calculation to minimize the effects of shear deformation. At the lower ellipticities the results are virtually identical, while at higher ellipticities the present results are slightly lower. This is to be expected since the present solution uses more terms in the approximating functions than did Voinovsky-Krieger, thereby reducing the stiffness of the approximation and lowering the buckling coefficients. The simple support prediction is included in the figure for completeness since Voinovsky-Krieger suggested that the buckling coefficients for simply supported plates could be estimated by dividing the clamped plate values by a factor of 3.5.

§5.3 Large Deflections of Circular Plates Without Delaminations

The linear theory of plate bending is usually limited to transverse deflections on the order of fractions of the plate thickness. Nonlinear theories which include moderate rotations (such as the present method) allow transverse deflections up to about two times the plate thickness.

Consider an isotropic, clamped circular plate without delaminations subjected to a uniform transverse load. The transverse deflections at the center of the plate were determined by DELAM as a function of the applied uniform load. In Figure 5-3, the present solution is compared to a perturbation method solution given by Chia [41]

$$\frac{q_o a^4}{Eh^4} = \frac{16}{3(1-\nu^2)} \frac{w_o}{h} \left[1 + \frac{1}{360} (1+\nu)(173-73\nu) \left(\frac{w_o}{h} \right)^2 \right] \quad (5.3)$$

where q_o is the transverse uniform pressure and w_o the transverse deflection at the center of a thin plate. The present solution and Chia's solution agree very well out to transverse deflections of at least twice the plate thickness. As expected, the linear solution (which omits the higher order terms in the bracket) agrees with the

nonlinear solutions to transverse deflections of only about four-tenths of the plate thickness.

§5.4 Change in Total Potential Energy of a Plate Without Delaminations

Consider an isotropic, clamped circular aluminum plate of radius a subjected to a transverse load as in the previous section. The change in total potential energy Π of the plate for an increment of the area ($A = \pi a^2$) is

$$G = -\frac{d\Pi}{da} \frac{1}{2\pi a} \quad (5.4)$$

where self-similar growth has been assumed. The change in total potential energy was calculated by DELAM as a function of the applied uniform load. For comparison, G was calculated using the perturbation method solution of Chia [41]. The total potential energy Π was calculated using the stresses, strains, and displacements as given by Chia (Appendix H), and differentiated with respect to the area A to give G . The present solution is compared to that of Chia as a function of the applied load in Figure 5-4. At lower loads, the solutions agree well. At higher loads, the perturbation solution for G is somewhat higher than the present solution, due to the use of more terms for the displacement functions in the present method.

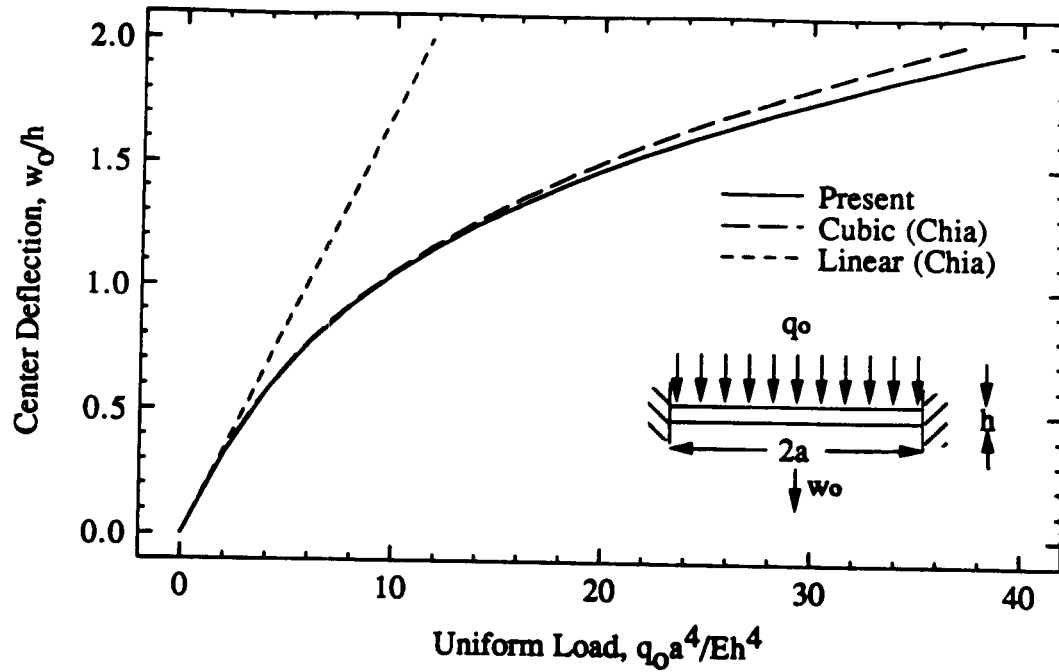


Figure 5-3 Center deflection of a circular aluminum plate subjected to a uniform applied load ($a = 1.0$ in., $h = 0.01$ in.).

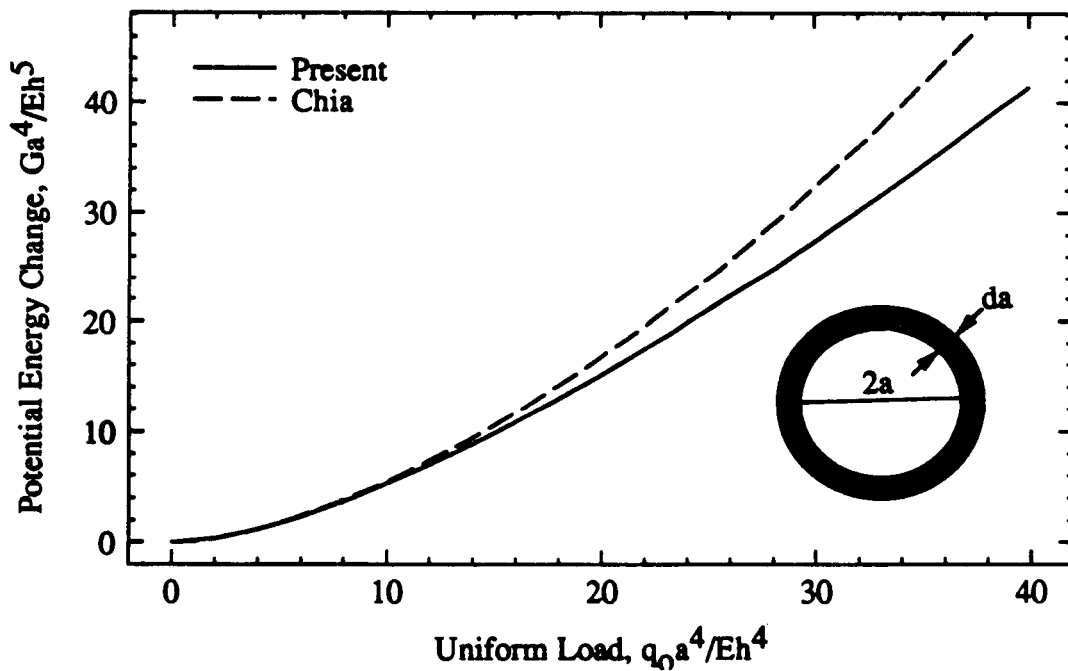


Figure 5-4 Change in total potential energy of a clamped, circular aluminum plate subjected to a uniform load ($a = 1.0$ in., $h = 0.01$ in.).

§5.5 Buckling of Elliptical Sublaminates in Plates Containing Delaminations

Several investigators have proposed approximate solutions to describe the behavior of plates containing elliptical delaminations. To compare the present sublaminate behavior model, which is quite general, to results presented in the literature, it is necessary to make several simplifications:

1. The axes of the ellipse are aligned with the load axes.
2. The sublaminate is a single layer which is either isotropic or orthotropic.
3. The base plate is isotropic, and is much thicker than the sublaminate.

The normalized critical buckling strain is defined as

$$\epsilon_n = \epsilon_{cr}(1 - \nu_{xy}\nu_{yz}) \frac{b^2}{(h_{sl})^2} \quad (5.5)$$

where ϵ_{cr} is the far field strain in the plate when the sublaminate buckles, and h is the sublaminate thickness. The normalized critical buckling strain was calculated by DELAM as a function of the plate ellipticity (a/b) for three cases: (a) an isotropic aluminum sublaminate and base plate, (b) a unidirectional sublaminate with the fibers aligned in the load direction (case A), and (c) a unidirectional sublaminate with the fibers aligned transversely to the load direction (case B). The base plate for these cases is a fictitious isotropic material. The material properties of the sublaminates and base plate are given in Table 5-1.

The DELAM predictions are compared with those of Chai and Babcock [18] and Kassapoglou [19] for the isotropic, orthotropic A, and orthotropic B sublaminates in Figures 5-5 through 5-7, respectively. For the isotropic and orthotropic A sublaminates, the present results agree well with those of Chai and Babcock and Kassapoglou. For the orthotropic B sublaminate, the present results agree with Chai and Babcock and Kassapoglou at ellipticities greater than three. At lower

ellipticities, all of the analyses show different results. The orthotropic sublaminate B is very stiff compared to the base plate in the direction transverse to the applied load. Thus, under compressive loading the transverse Poisson expansion of the base plate drives the sublaminate into tension in the fiber direction. Conversely, an applied tensile load will cause a Poisson contraction of the base plate and compression in the fiber direction of the sublaminate. Both the present solution and Chai and Babcock actually predict buckling under an applied tensile load (not shown) for case B at lower ellipticities. In any event, case B is an extreme situation for which none of the methods presently agree.

Table 5-1 Material Properties used in the Comparisons

Material	Isotropic	Orthotropic	Orthotropic	Isotropic Base Plate
Property	Aluminum	Case A	Case B	for Cases A and B
E_x	10.0	1.47	25.9	1.47
E_y	10.0	25.9	1.47	1.47
ν_{xy}	0.30	0.28	0.016	0.30
G_{xy}	3.84	1.03	1.03	0.567
G_{xz}	3.84	1.03	0.286	0.567
G_{yz}	3.84	0.286	1.03	0.567

The elastic moduli are in Msi. Poisson's ratio is dimensionless.

§5.6 Summary

The results indicate that the present analysis method can predict the buckling, postbuckling large deflection, and growth behavior of circular and elliptical plates and sublaminates subjected to various loads. Final verification of the method for the general cases of: (a) elliptical delaminations with axes arbitrarily oriented with respect to the applied in-plane loads, and (b) delaminations located between any two plies of the composite plate, will be made in Chapter 7 by comparison to experimental data.

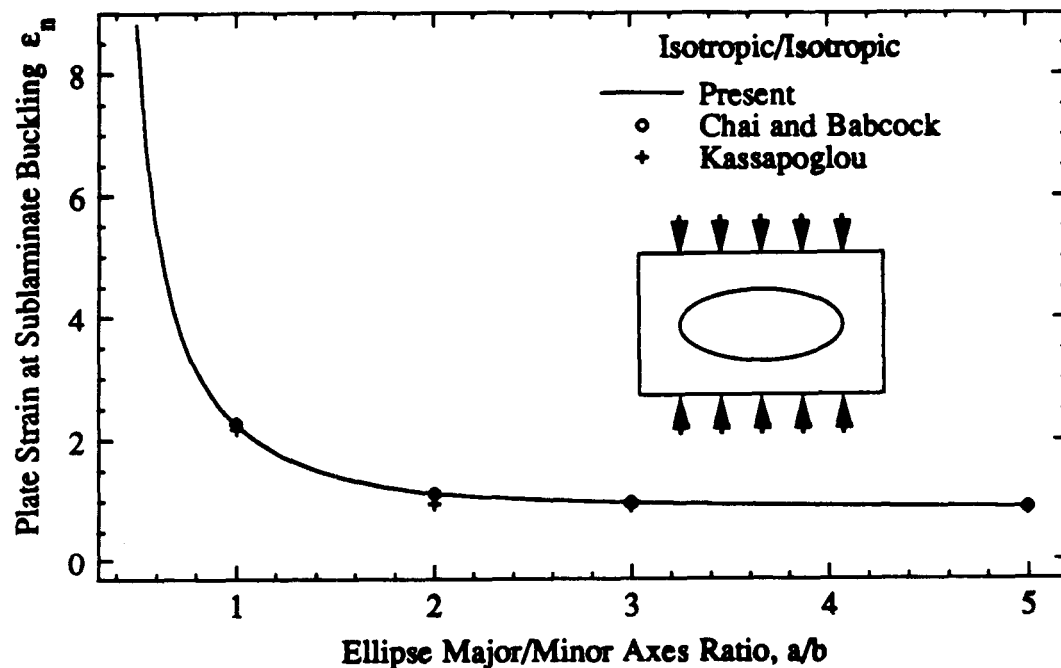


Figure 5-5 Normalized critical buckling strain. Aluminum sublaminate on an aluminum base plate (Table 5-1) ($b = 0.5$ in., $h = 0.03$ in.).

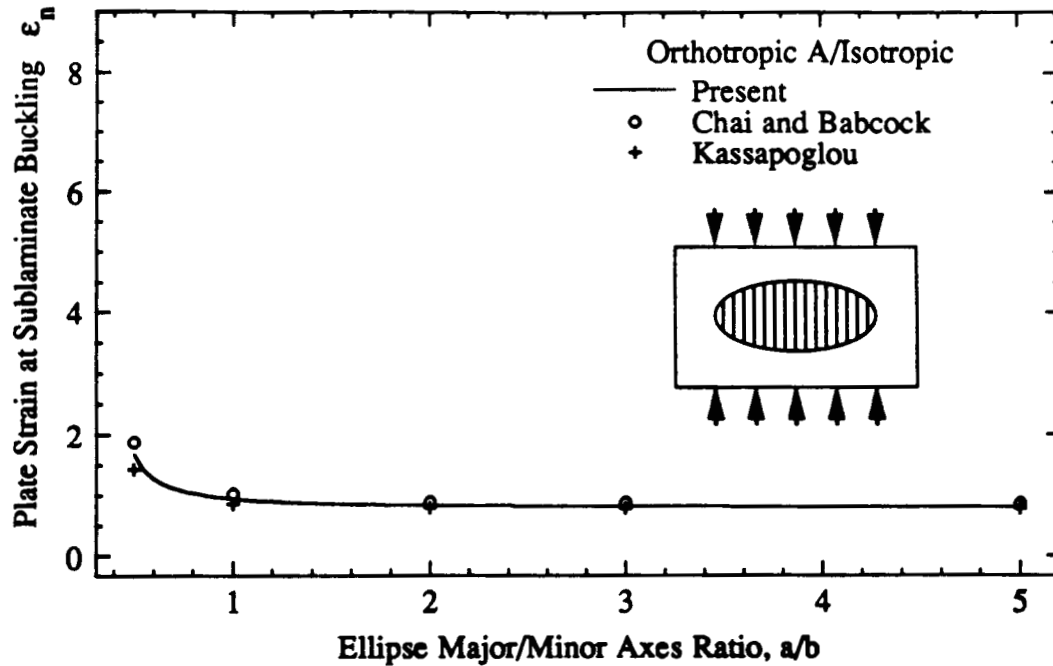


Figure 5-6 Normalized critical buckling strain. Unidirectional type A sublaminate on an isotropic base plate (Table 5-1) ($b = 0.5$ in., $h = 0.03$ in.).

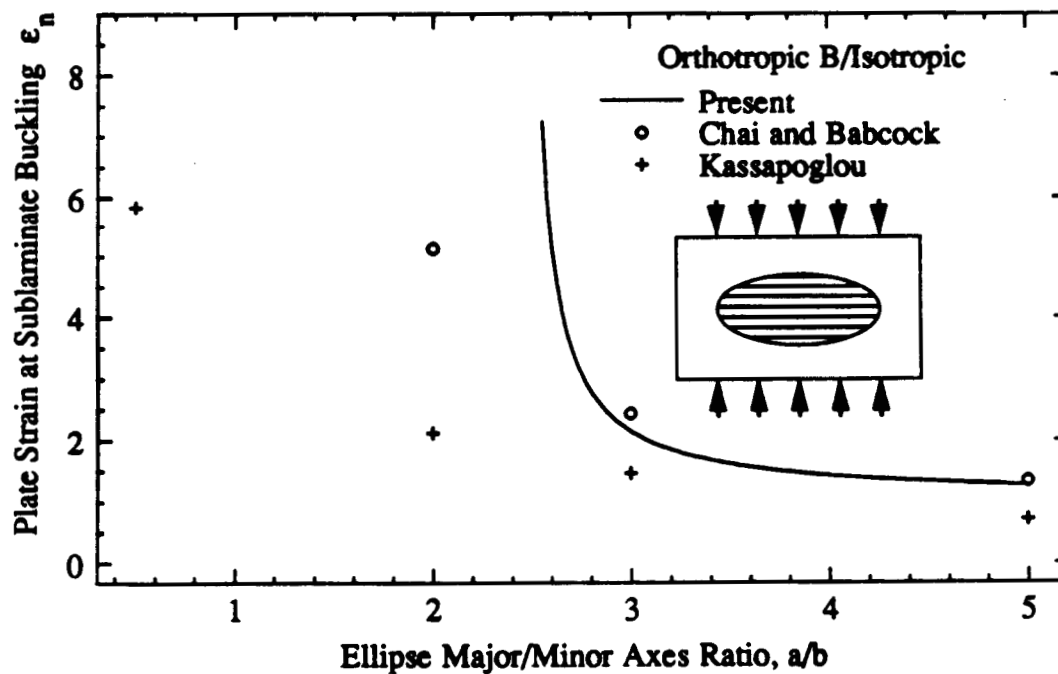


Figure 5-7 Normalized critical buckling strain. Unidirectional type B sublaminate on an isotropic base plate (Table 5-1) ($b = 0.5$ in., $h = 0.03$ in.).

Chapter 6

Experimental Procedure

§6.1 Specimen Design and Fabrication

A testing program provides experimental data against which the analytical development can easily be verified. The requirements for this experimental program were: (a) that the test specimens contain well-characterized delaminations; (b) that the specimens be exposed to uniform loads, implying a uniform far field strain; and (c) that the sublaminar deformation and growth be closely monitored.

A sandwich construction test specimen (Figure 6-1) was developed of two Fiberite T300/976 graphite/epoxy face sheets secondarily bonded to an 0.625" thick aluminum honeycomb core. The honeycomb sandwich construction provided a test specimen that could be easily loaded in compression without introducing significant bending moments. One of the face sheets contained a 0.001" thick Teflon disk between two plies simulating the presence of a delamination. The facesheets were fabricated from unidirectional T300/976 prepreg tape and cured in an autoclave at a maximum temperature of 350°F at 80 psi. The secondary bonding of the facesheet laminates to the honeycomb was accomplished using a Hysol 250°F curing film adhesive under 30 psi in the autoclave.

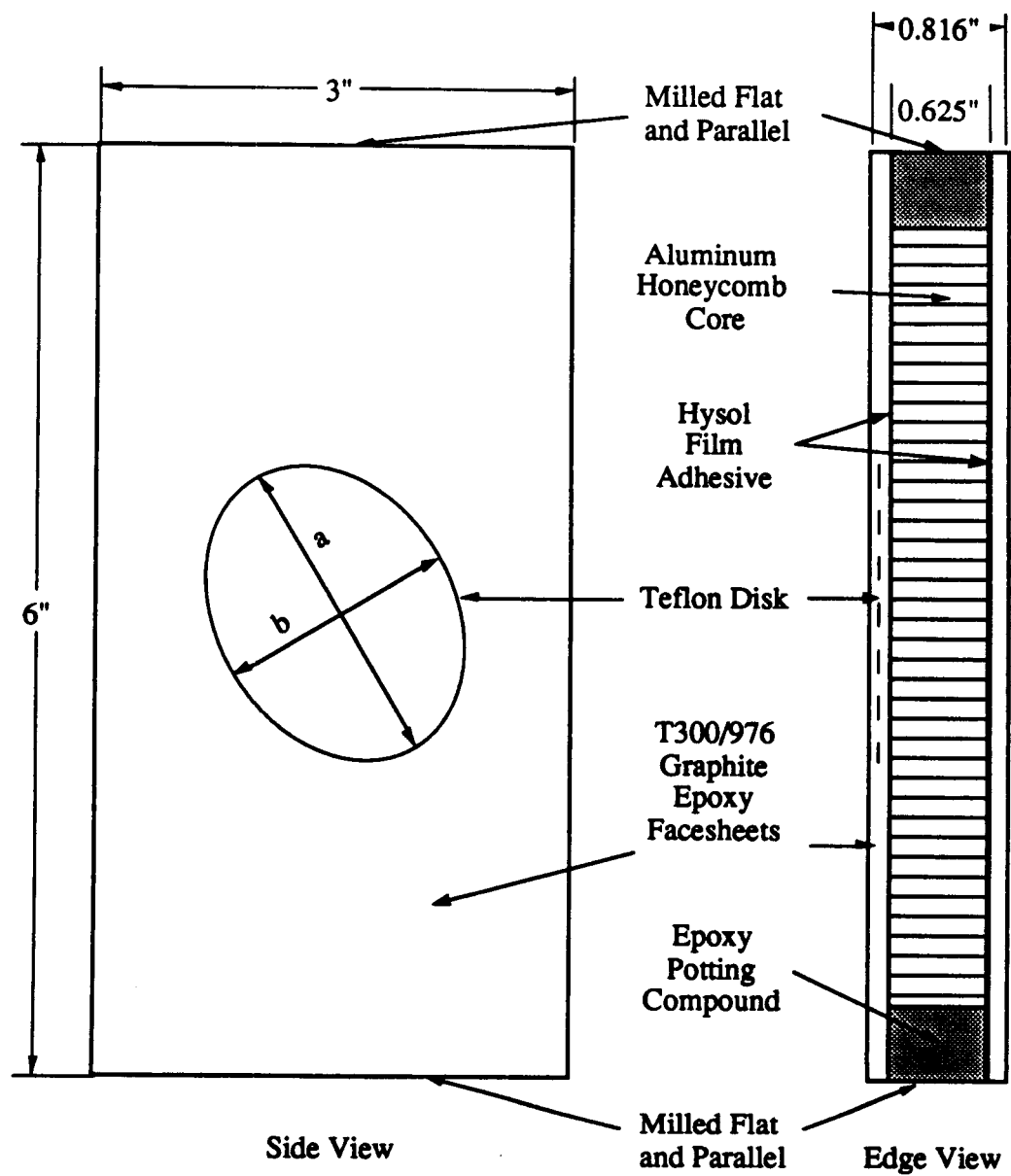


Figure 6-1 Sandwich construction test specimen containing a teflon disk in one facesheet.

The experimental parameters were delamination shape (circular or elliptical), orientation of the ellipse axes, delamination depth in the facesheet, and sublamine layup. The specimens were nominally 3" wide by 6" long, and were fabricated in six groups, designated Series 1 through 6. After trimming, the ends of the specimens were filled with epoxy potting compound and milled flat and parallel to one another in preparation for testing. Series 1 through 3 were devoted to specimen development. Series 4 through 6 comprise the test matrix, the details of which are shown in Table 6-1.

§6.2 Nondestructive Inspection

Complete characterization of the delamination required an exact determination of the Teflon insert location in the facesheet. Despite careful positioning of the inserts during fabrication of the laminates, trimming and milling operations changed the reference points. Every specimen was therefore ultrasonically C-scanned (Appendix I) and the position of the Teflon insert mapped relative to the final dimensions. The location data were essential for the later mounting of the strain gauges. The C-scan dimensions of the delaminations were often 0.1" larger than the nominal size of the Teflon inserts, probably due to two phenomena: (a) incomplete bonding of adjacent plies at the edge of the Teflon, and (b) the lateral resolution of the C-scan.

The C-scan was capable of mapping out not only the planar extent of the delamination, but also the depth of the delamination. This was useful as a check on the specimen fabrication, and particularly in the posttest inspection to determine whether delamination growth had occurred within the original ply interface or had progressed to other ply interfaces.

Table 6-1 Test Matrix

Specimen	Layup	Teflon	Orientation	Depth* (plies)
4-1	$[0_{16}H0_{16}]$	2" circle	0°	2
4-2	$[0_{16}H0_{16}]$	2" circle	0°	4
4-3	$[0_{16}H0_{16}]$	2" circle	0°	6
4-4	$[0_{16}H0_{16}]$	2" circle	0°	8
5-1	$[(0_290_20_290_2)_sH(sym)]$	2" circle	0°	3
5-2	$[(0_290_20_290_2)_sH(sym)]$	2" circle	0°	4
5-3	$[(0_290_20_290_2)_sH(sym)]$	2" circle	0°	5
5-4	$[(0_290_20_290_2)_sH(sym)]$	2" circle	0°	8
6-1	$[(0_290_20_290_2)_sH(sym)]$	2" x 1.5" ellipse	0°	4
6-2	$[(0_290_20_290_2)_sH(sym)]$	2" x 1.5" ellipse	30°	4
6-3	$[(0_290_20_290_2)_sH(sym)]$	2" x 1.5" ellipse	60°	4
6-4	$[(0_290_20_290_2)_sH(sym)]$	2" x 1.5" ellipse	90°	4

* Number of plies from the facesheet surface.

§6.3 Instrumentation

Each specimen was instrumented with nine strain gauges arranged as shown in Figure 6-2. The individual type, orientation, and purpose of each gauge are shown in Table 6-2. In general, a single gauge was located at the center of the sublaminates to record the buckling and postbuckling strains during a test. One additional gauge was mounted on the front and three on the back facesheets to measure the far field strains in the specimen. The outputs of these gauges were used to adjust the relative load distribution between the faces during setup, to determine the actual load distribution during a test, and as a check against the

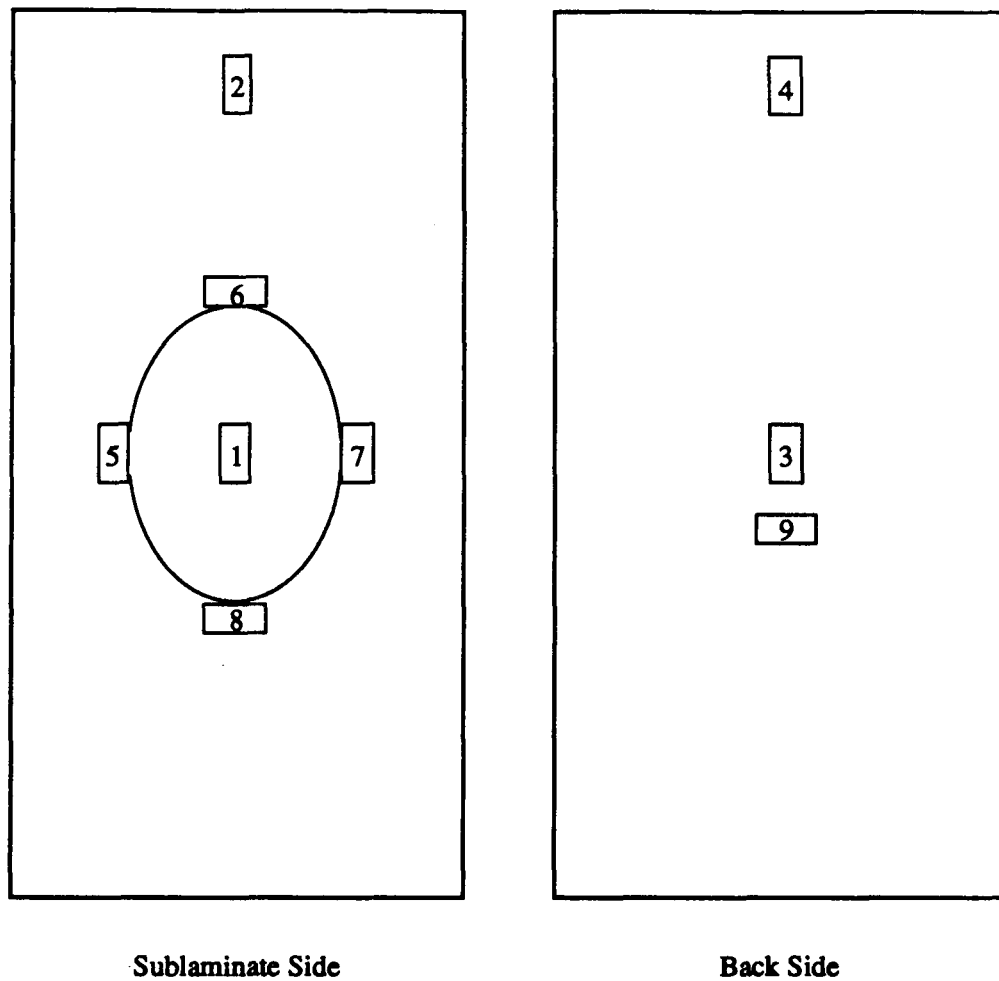


Figure 6-2 Specimen strain gauge locations and orientations.

material properties given by the prepreg manufacturers . Four gauges were mounted on the periphery of the sublamine, based on the C-scan data, to determine the onset of delamination growth. Up to the onset of growth, these gauges were also used to check the uniformity of the far field strains over the specimen.

§6.4 Testing to Failure

Each specimen was loaded in compression between platens in an MTS testing machine. One platten was a ball and socket self-aligning fixture to ensure that the loads were evenly distributed over the specimen. During each test, the plate was loaded at a constant displacement rate of .003 in/min. The outputs of all nine strain gauges (after amplification) and the MTS load cell were digitized and recorded in a spreadsheet computer file for later data reduction and plotting. Buckling of the sublamine was observed, both visually and from the output of the strain gauge located at the center of the sublamine. Growth of the delamination was detected by the four gauges surrounding the delamination. At extreme loads growth was also visually observed.

Table 6-2 Strain Gauge Locations and Purposes

Gauge Number	Gauge Type	Orientation*	Purpose
1	CEA-06-062UW-350	longitudinal	sublamine strain
2	CEA-06-125UN-350	longitudinal	far field - front
3	CEA-06-125UN-350	longitudinal	far field - back
4	CEA-06-125UN-350	longitudinal	far field - back
5	CEA-06-125UN-350	longitudinal	delamination growth
6	CEA-06-125UN-350	transverse	delamination growth
7	CEA-06-125UN-350	longitudinal	delamination growth
8	CEA-06-125UN-350	transverse	delamination growth
9	CEA-06-125UN-350	transverse	far field - back

* With respect to the load direction.

Chapter 7

Comparison of Experimental and Model Results

§7.1 Introduction

This chapter demonstrates the validity of the delamination behavior model through a comparison with experimental data. Two kinds of data are required for this validation: (a) load-strain histories of delaminated sublaminates from the onset of loading through buckling and into the postbuckling regime, and (b) the load at which growth of the sublaminate begins.

The experimental data in the literature can be divided into two types. In the first, experimental investigations have demonstrated the reduction in strength in composite plates resulting from impact damage. Data from a number of researchers have been reviewed by Baker et al. [42]. These data are important in that they were the first to show that a significant problem existed. However, the behavior of the sublaminate was not characterized in any way. In the second, researchers implanted a release agent, such as a teflon film, in the laminate during fabrication to simulate the presence of a delamination. Thus, a flaw of known shape, size, orientation, and depth in the laminate was introduced. Gillespie and Pipes [4], Wang et al. [6], Williams et al. [8], Wang and Slomiana [43], and Ramkumar [44] have simulated delaminations using through-width implants in wide columns. Whitcomb

[22], Wang and Slomiana [43], Ramkumar [44], Konishi and Johnston [45], Byers [46], Webster [47], and Geier et al. [48] have simulated delaminations using circular implants, while Jones et al. [17] and Reddy et al. [49] used rectangular implants and Kassapoglou [19] used elliptical implants. All have reported some features of the sublaminar behavior, such as buckling loads or growth loads. None, however, has reported a complete load-strain history. Therefore, an experimental investigation using implants was undertaken to generate a data base for validation of the model.

§7.2 Experimental Measurements and Material Properties

Load-strain histories during compression testing were recorded from each of the nine strain gauges mounted on each specimen. The strain data from gauge number 1, located at the center of the delamination, was used to establish the buckling and postbuckling behavior of the sublaminar. A typical response is illustrated in Figure 7-1. The onset of delamination growth and the corresponding growth load were determined from gauges 5, 6, 7, and 8, which were located on the periphery of the delamination. Typical responses are shown in Figure 7-2. As gauges 5 and 7 began to deviate significantly from a linear response, the delamination had grown to include the gauges as part of the larger sublaminar. The growth load was estimated from the first gauge to show a change in linear behavior.

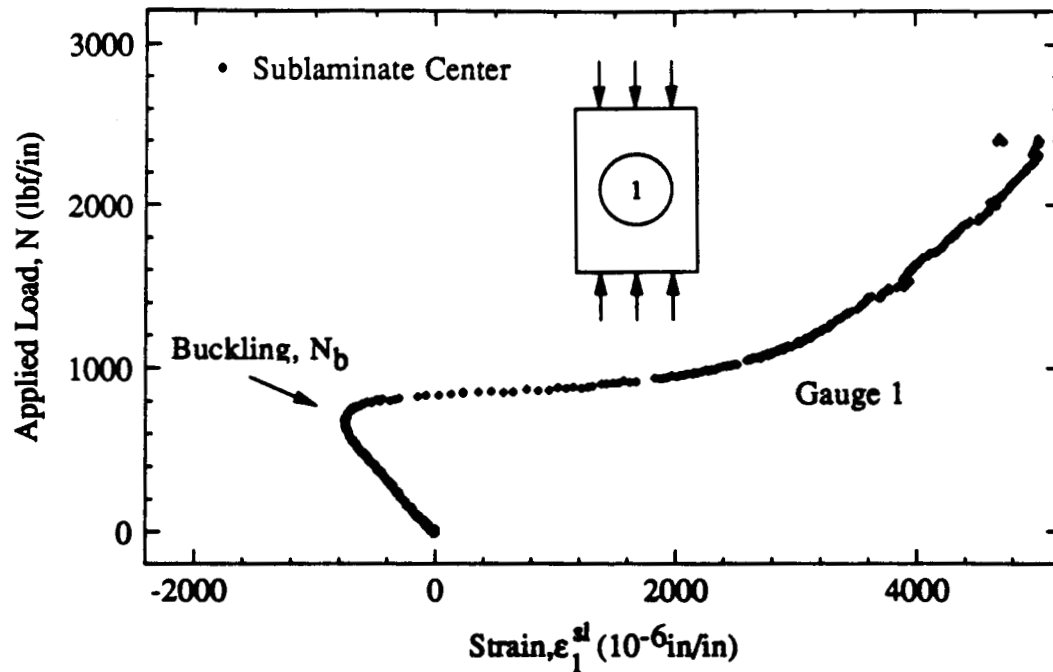


Figure 7-1 Typical sublaminate gauge 1 load-strain response.

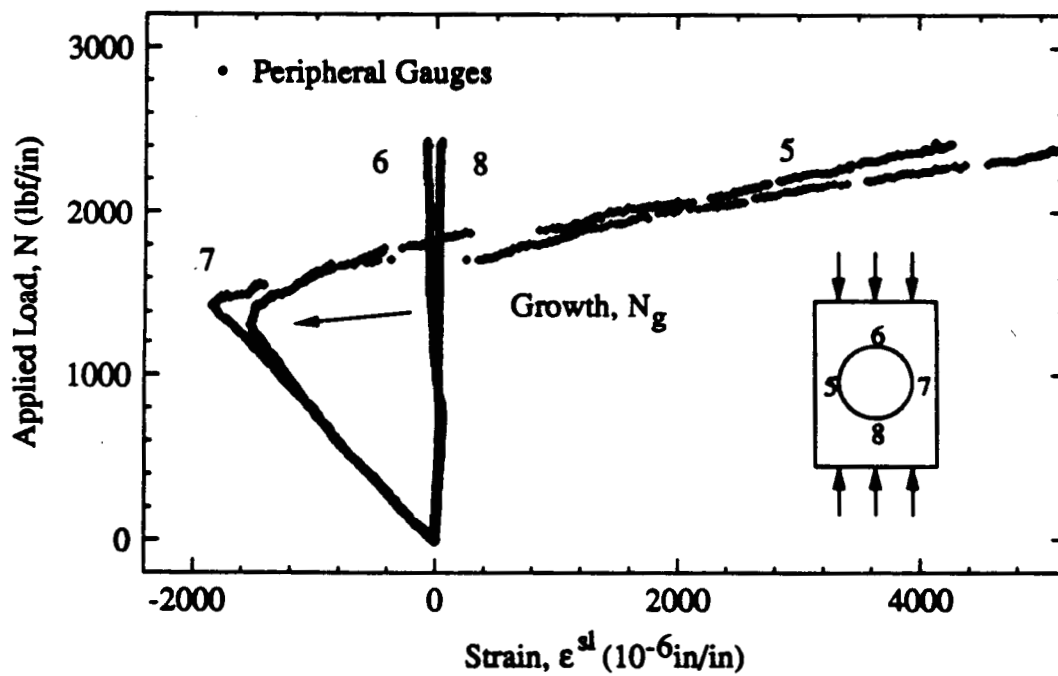


Figure 7-2 Typical sublaminate peripheral gauge 5, 6, 7, 8 load-strain responses.

The material properties of the cured laminate are shown in Table 7-1. These material properties were used in all analytical predictions. The compressive load was applied along the longitudinal x_1' axis of the specimens and the sublamine orientations were measured counterclockwise with respect to this axis. The following input data were common to all analyses (unless specified otherwise): (a) temperature difference, $\Delta T = -180^\circ F$; (b) transverse pressure difference, $\Delta P = 0$ psi; and (c) relative growth direction, $\frac{da}{db} = 0$. The strains shown in the comparisons were calculated at the outer surface of the sublamine plus 0.004 in. to allow for the strain gauge thickness ($x_1' = 0.$, $x_2' = 0.$, $x_3' = \frac{h'}{2} + 0.004$).

Table 7-1 Material Properties of Fiberite T300/976

Material Property	Value	Units
Longitudinal Young's modulus, E_x	19.5E6	psi
Transverse Young's modulus, E_y	1.32E6	psi
Poisson's ratio, ν_{xy}	0.30	-
In-plane shear modulus, G_{xy}	1.01E6	psi
Out-of-plane shear modulus, G_{xz}	1.01E6	psi
Out-of-plane shear modulus, G_{yz}	0.50E6	psi
Longitudinal thermal coeff. of expansion, α_x	0.50E-6	$\frac{\text{in}}{\text{in}-^\circ F}$
Transverse thermal coeff. of expansion, α_x	18.0E-6	$\frac{\text{in}}{\text{in}-^\circ F}$
Critical strain energy release rate, G_c [50]	0.2	$\frac{\text{in}-\text{lb}f}{\text{in}^2}$
Foundation modulus, K	1.E6	$\frac{\text{lb}f}{\text{in}^3}$

§7.3 Circular Delaminations in Unidirectional Laminated Plates

Test Series 4 investigated the effect of delamination depth on the sublamine behavior in unidirectional laminated plates containing circular delaminations. Tests 4-1 through 4-4 used delamination depths of 2, 4, 6, and 8 plies, respectively. A small hole (0.021" diameter) was drilled through the sublamine to allow air ingress to the Teflon implant to eliminate the effect of a transverse pressure differential. During the tests, specimens 4-1 through 4-3 were observed to buckle at increasing loads, while specimen 4-4 was loaded to the limit of the testing machine without buckling. Figure 7-3 shows the measured strains at the sublamine center (gauge 1) from each experiment. The predicted behavior of each experiment is shown as a solid line for comparison. The measured ply thickness ($t = 0.00556''$) was used as specific input for the analyses. Experimental and model results agree quite well. The data from the strain gauges surrounding the sublamine (gauges 5, 6, 7, 8), indicating the onset of sublamine growth, are shown in Figure 7-4. Only specimen 4-2 showed an onset of sublamine growth, which occurred at the end of the test.

§7.4 Circular Delaminations in Cross Ply Laminated Plates

Test Series 5 investigated the effect of delamination depth on sublamine behavior in cross ply ($[(0_2/90_2/0_2/90_2)_s H(sym)]$) laminated plates containing circular delaminations. Tests 5-1 through 5-4 used delamination depths of 3, 4, 5, and 8 plies, respectively. Specimens 5-1 ($[0_2/90]$ sublamine) and 5-3 ($[0_2/90_2/0]$ sublamine) were specifically intended to investigate the residual thermal strain effect, since the sublamine layups were significantly different from the facesheet layup. A small hole (0.021" diameter) was again drilled through the sublamine to allow air ingress to the Teflon implant. During the test, specimens 5-1 through 5-3 were observed to buckle at increasingly higher loads, while specimen 5-4 was loaded to

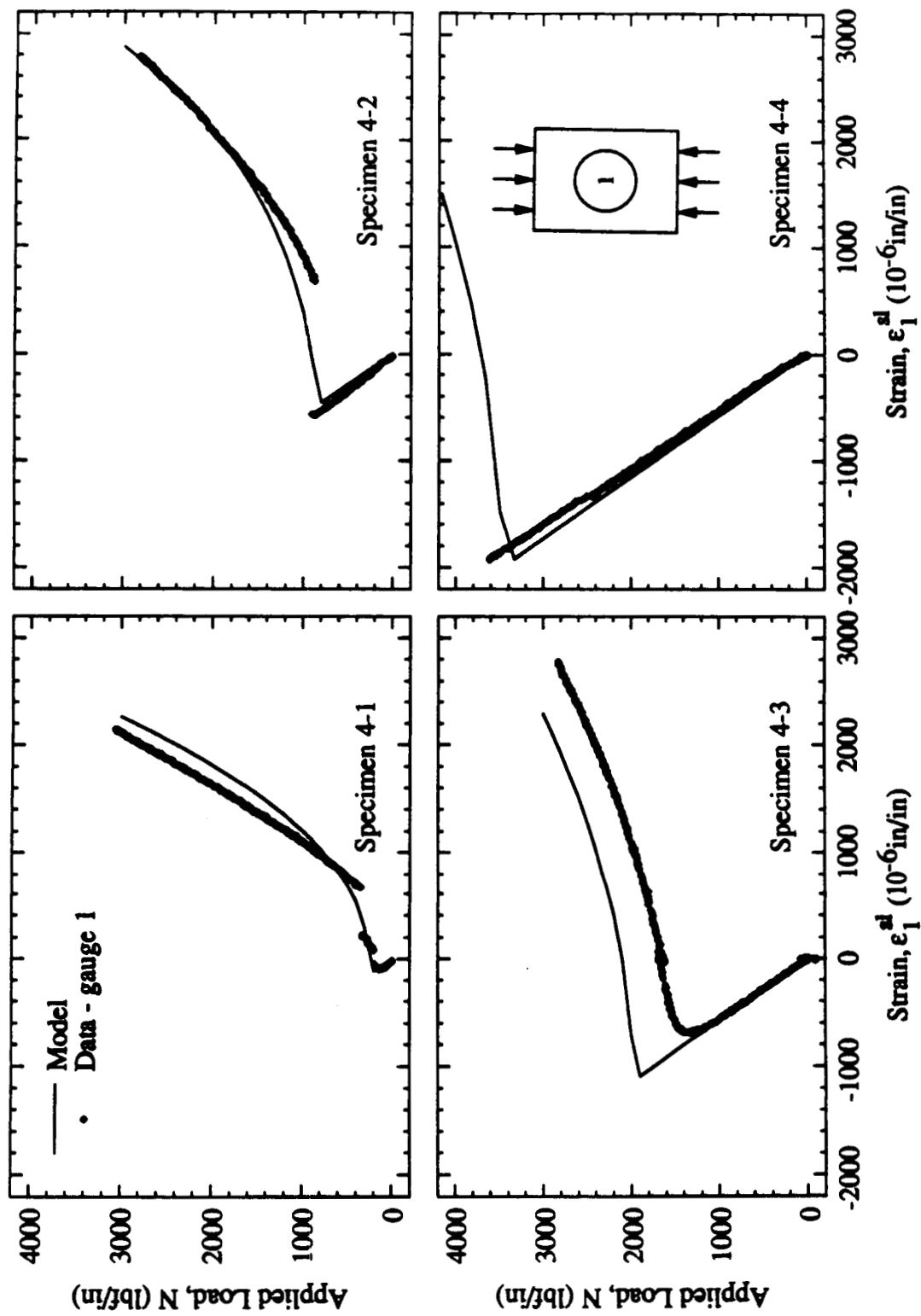


Figure 7-3 Load versus strain for a $[0_{16}H0_{16}]$ T300/976 laminate under uniaxial compression. Circular delaminations implanted at 2 (Specimen 4-1), 4 (Specimen 4-2), 6 (Specimen 4-3), and 8 (Specimen 4-4) plies from the outer surface. Strain gauge 1 was located on the surface at the center of the sublaminate (see also Tables 6-1 and 6-2 and Figures 6-1 and 6-2).

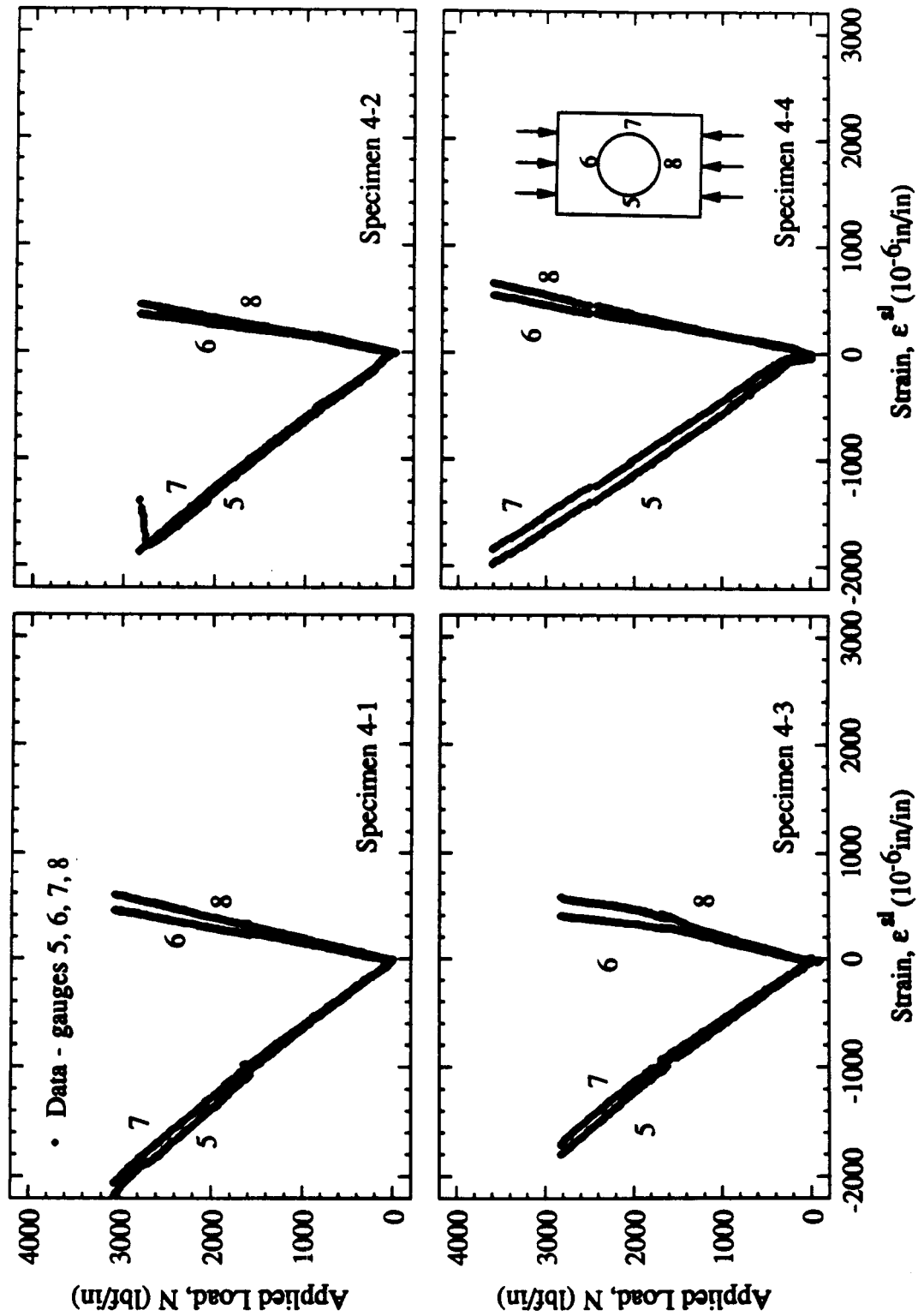


Figure 7-4 Load versus strain for a $[0_{16}H0_{16}]$ T300/976 laminate under uniaxial compression. Circular delaminations implanted at 2 (Specimen 4-1), 4 (Specimen 4-2), 6 (Specimen 4-3), and 8 (Specimen 4-4) plies from the outer surface. Strain gauges 5, 6, 7, and 8 were located around the periphery of the sublaminate (see also Tables 6-1 and 6-2 and Figures 6-1 and 6-2).

the limit of the testing machine without buckling. Figure 7-5 shows the measured strains at the sublamine center (gauge 1) from each experiment. The predicted behavior of each experiment is shown as a solid line for comparison. The laminate cured ply thickness ($t = 0.00609''$) was measured and used as specific input for the analyses. The buckled region of each specimen in this series appeared not to extend over the full Teflon implant area but rather to have a shorter buckling dimension in the loading direction. The analyses confirmed that these specimens would preferentially buckle in multiple half waves in the loading direction and a single half wave in the transverse direction. The analyses of specimens 5-1 and 5-3 also indicated a small but noticable effect of the thermally induced load, in this case reducing the buckling load. The data from the strain gauges surrounding the sublamine (gauges 5, 6, 7, 8), indicating the onset of sublamine growth, are shown in Figure 7-6. Specimens 5-1 through 5-3 experienced sublamine growth transverse to the applied load as indicated by peripheral gauges 5 and 7.

§7.5 Elliptical Delaminations in Cross Ply Laminated Plates

Test Series 6 investigated the effect of delamination orientation on sublamine behavior for cross ply ($[(0_2/90_2/0_2/90_2)_s H(sym)]$) laminated plates containing elliptical delaminations. Tests 6-1 through 6-4 used 2.0" by 1.5" elliptical Teflon implants oriented at 0° , 30° , 60° , and 90° to the applied load, respectively. Each implant was 4 plies deep in the facesheet. No hole was drilled through the sublamine so that any effect of transverse pressure might be observed. Buckling was observed in each specimen, followed by sublamine growth. As in Series 5, the buckled region of each specimen appeared not to extend over the full Teflon implant area but rather to have a shorter buckling dimension in the loading direction, which was confirmed by analysis. Figure 7-7 shows the measured strains at

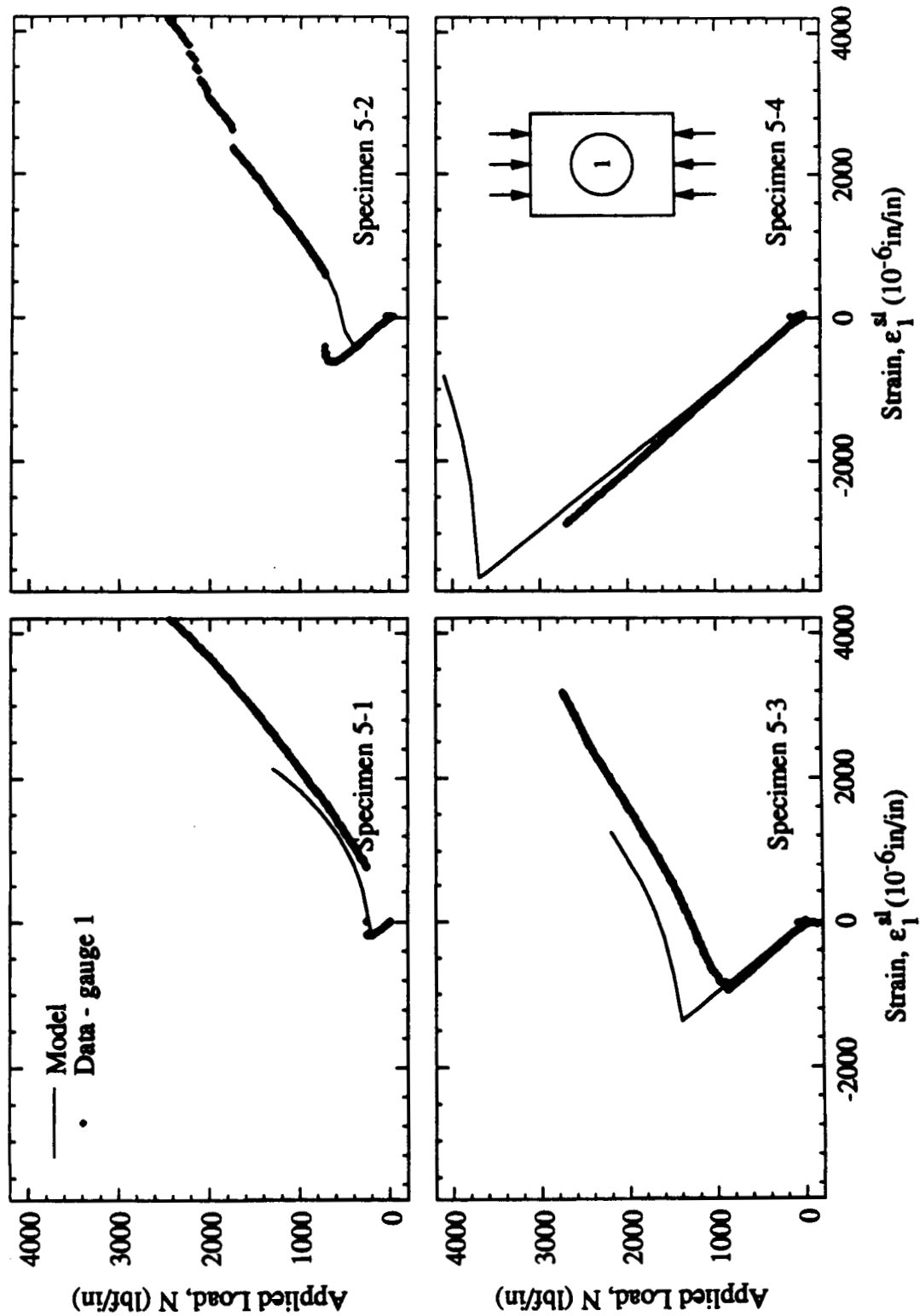


Figure 7-5 Load versus strain for a $[(0_2/90_2/0_2/90_2)_s H(0_2/90_2/0_2/90_2)]$ T300/976 laminate under uniaxial compression. Circular delaminations implanted at 3 (Specimen 5-1), 4 (Specimen 5-2), 5 (Specimen 5-3), and 8 (Specimen 5-4) plies from the outer surface. Strain gauge 1 was located on the surface at the center of the sublaminate (see also Tables 6-1 and 6-2 and Figures 6-1 and 6-2).

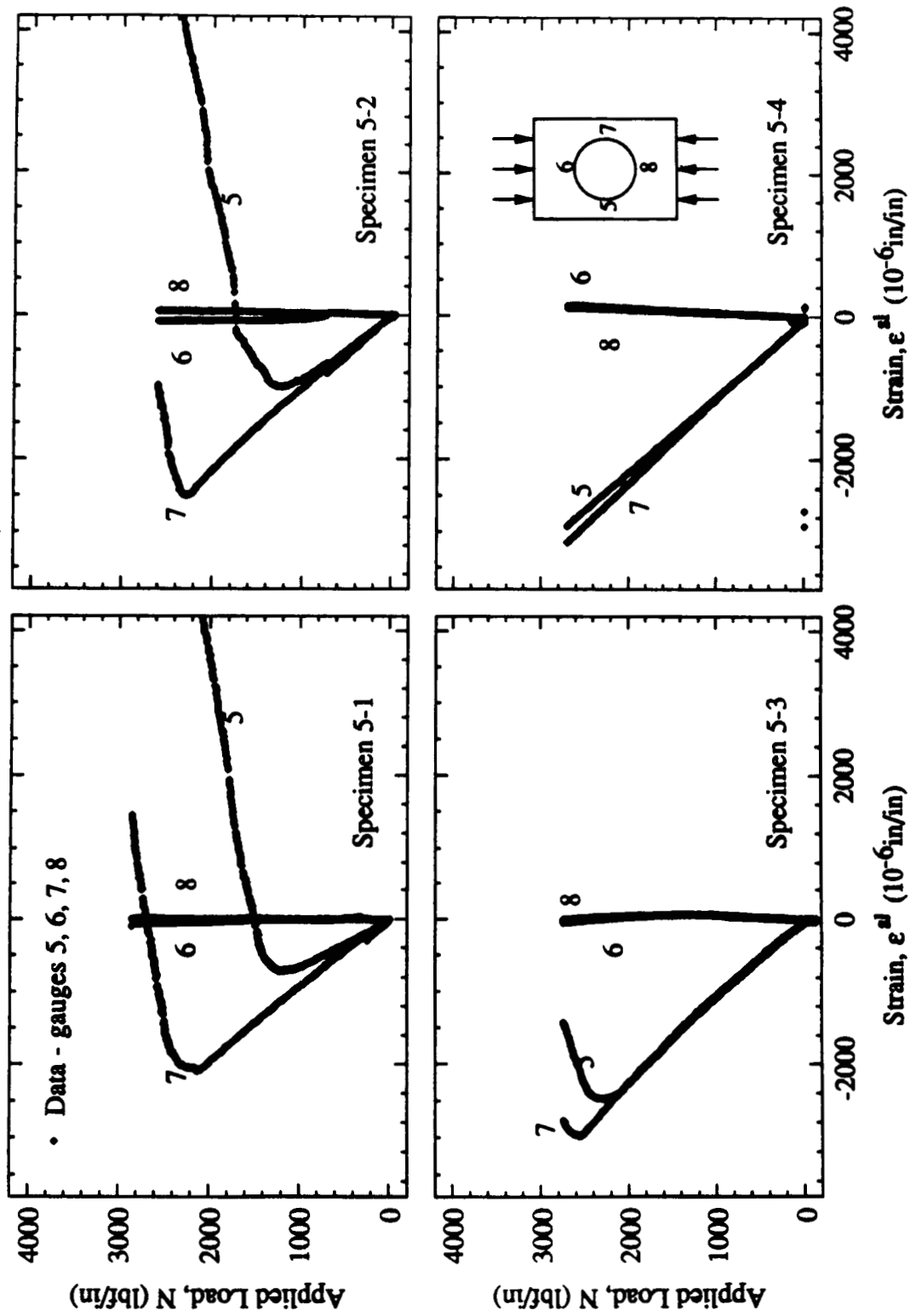


Figure 7-6 Load versus strain for a $[(0_2/90_2/0_2/90_2)_s H(0_2/90_2/0_2/90_2)]$ T300/976 laminate under uniaxial compression. Circular delaminations implanted at 3 (Specimen 5-1), 4 (Specimen 5-2), 5 (Specimen 5-3), and 8 (Specimen 5-4) plies from the outer surface. Strain gauges 5, 6, 7, and 8 were located around the periphery of the sublaminates (see also Tables 6-1 and 6-2 and Figures 6-1 and 6-2).

the sublamine center (gauge 1) from each experiment. The predicted behavior of each experiment is shown as a solid line for comparison. The laminate cured ply thickness ($t = 0.00609''$) was measured and used as specific input for the analyses. Experiment and model results generally agree quite well. The data from the strain gauges surrounding the sublamine (gauges 5, 6, 7, 8), indicating the onset of sublamine growth, are shown in Figure 7-8. The observed growth direction was transverse to the applied load as indicated by peripheral gauges 5 and 7. The predicted growth load for specimens 6-1 and 6-2 was based on a relative growth parameter of $\frac{da}{db} = 0$, while for specimens 6-3 and 6-4, it was based on $\frac{da}{db} = 100$.

§7.6 Buckling and Growth Loads

The measured buckling loads are compared to the buckling loads predicted by the nonlinear equilibrium method in Figure 7-9. The measured and predicted growth loads are shown in Figure 7-10. The figures include the experimental and prediction uncertainties (Appendix J). The error bars shown are plus and minus three standard deviations. The dashed line in each figure represents perfect agreement between experiment and calculation.

The buckling results show generally good agreement between prediction and experiment. The growth results show reasonable agreement. The prediction errors for the growth results are large due to large uncertainty in the critical strain energy release rate. Considering the uncertainties in the experimental data and the uncertainties in the analyses, it would appear that the analysis method describes with reasonable accuracy the experimental data.

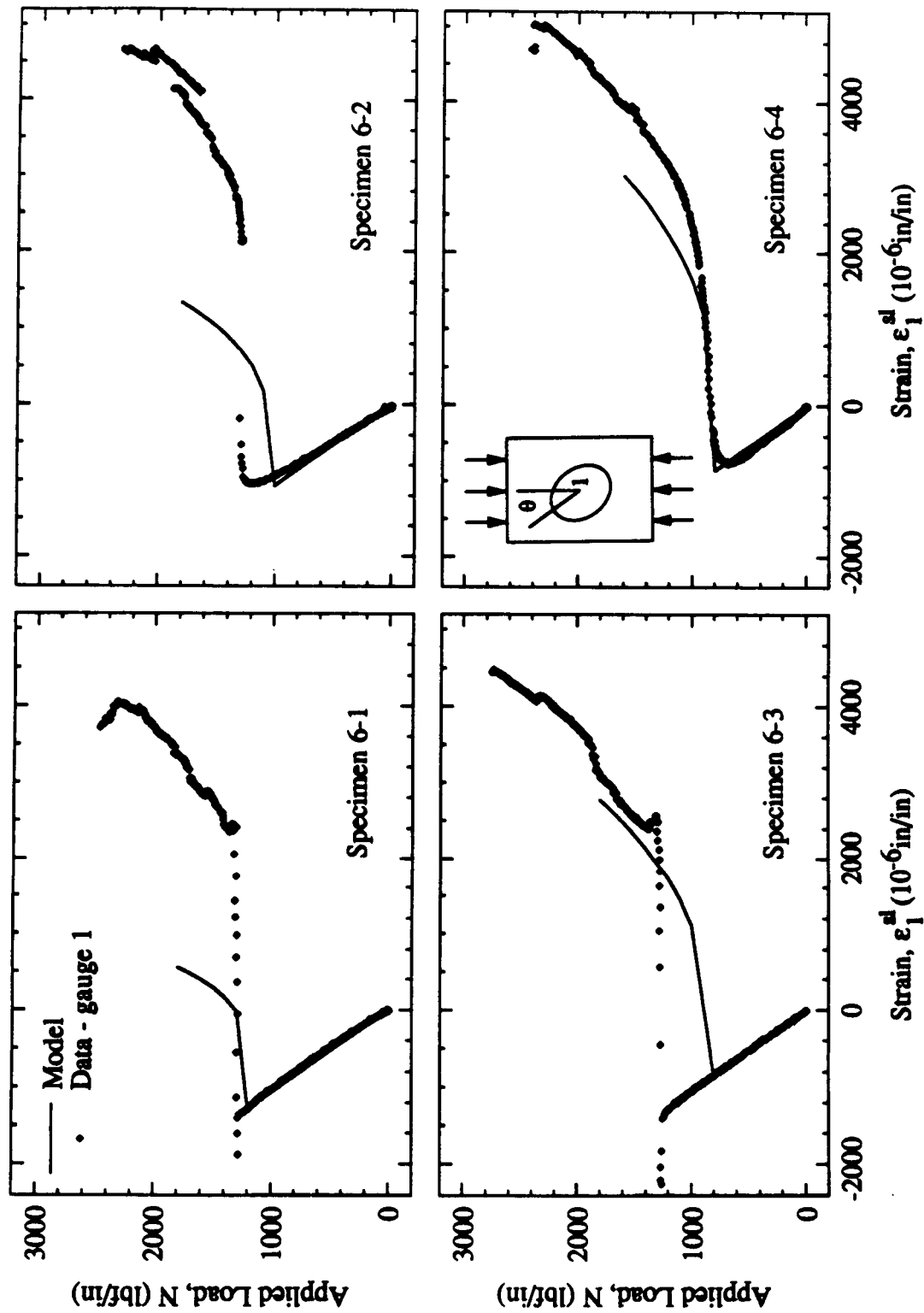


Figure 7-7 Load versus strain for a $[(0_2/90_2/0_2/90_2)_s H(0_2/90_2/0_2/90_2)_s]$ T300/976 laminate under uniaxial compression. 2.0 in. by 1.5 in. elliptical delaminations implanted 4 plies from the outer surface (all specimens). 0° (Specimen 6-1), 30° (Specimen 6-2), 60° (Specimen 6-3), and 90° (Specimen 6-4) orientations of the ellipses with respect to the load. Strain gauge 1 was located on the surface at the center of the sublaminate (see also Tables 6-1 and 6-2 and Figures 6-1 and 6-2).

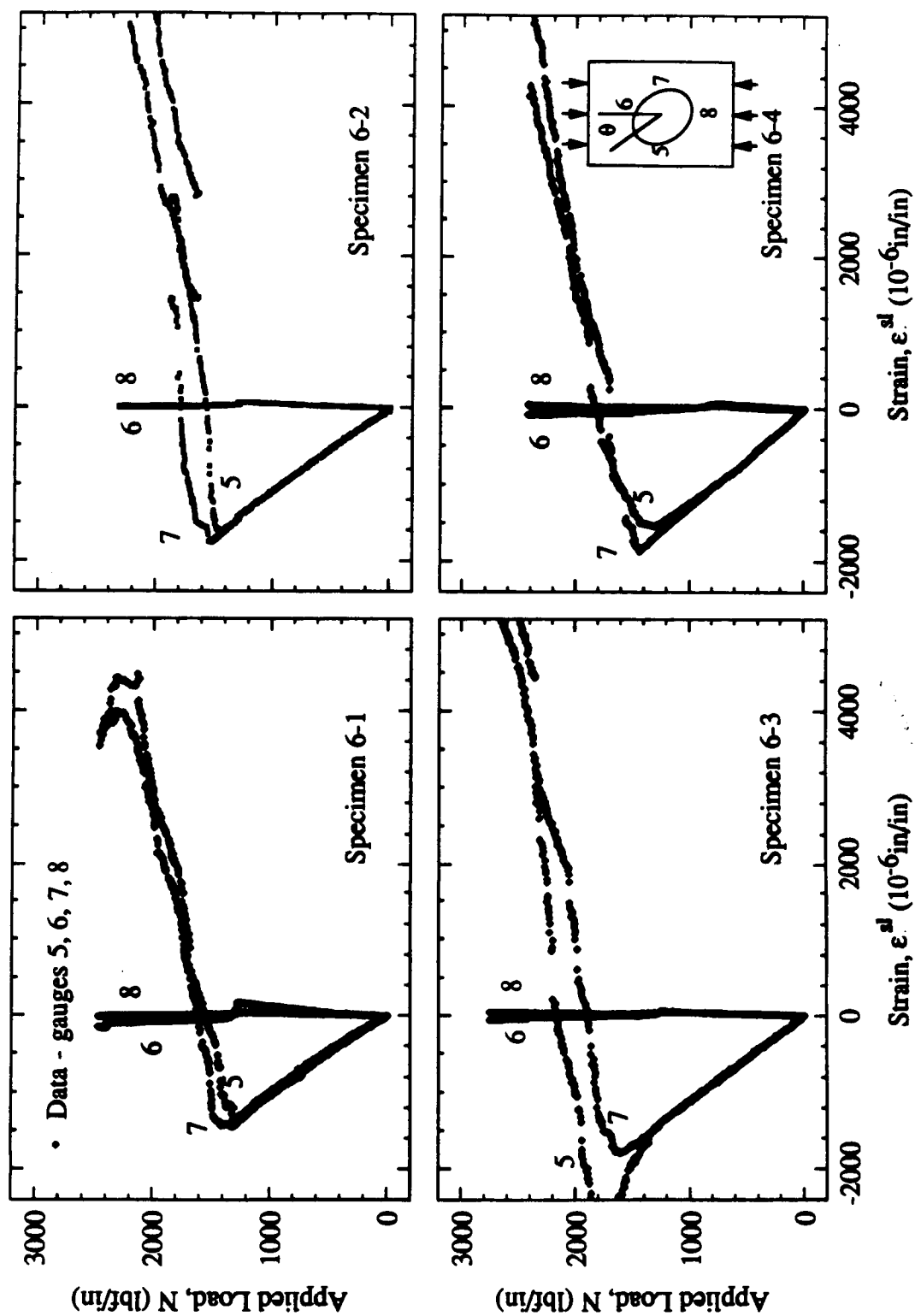


Figure 7-8 Load versus strain for a $[(0_2/90_2/0_2/90_2)_s H(0_2/90_2/0_2/90_2)_s]$ T300/976 laminate under uniaxial compression. 2.0 in. by 1.5 in. elliptical delaminations implanted 4 plies from the outer surface (all specimens). 0° (Specimen 6-1), 30° (Specimen 6-2), 60° (Specimen 6-3), and 90° (Specimen 6-4) orientations of the ellipses with respect to the load. Strain gauges 5, 6, 7, and 8 were located around the periphery of the sublaminates (see also Tables 6-1 and 6-2 and Figures 6-1 and 6-2).

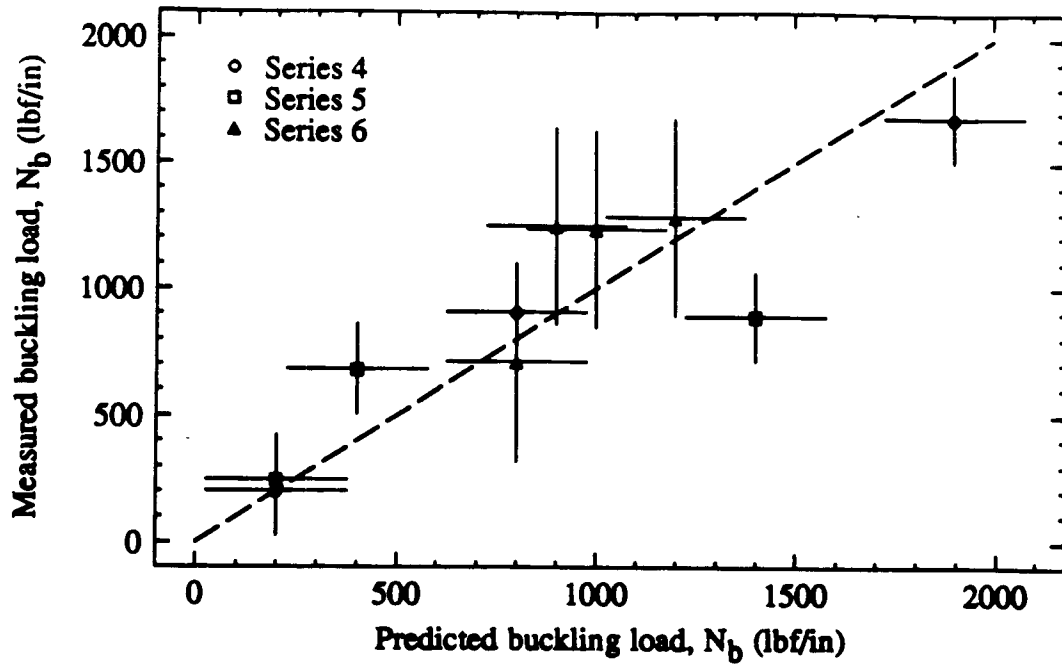


Figure 7-9 Measured versus predicted buckling loads. Error bars are plus and minus three standard deviations (see Tables J-1 and J-3).

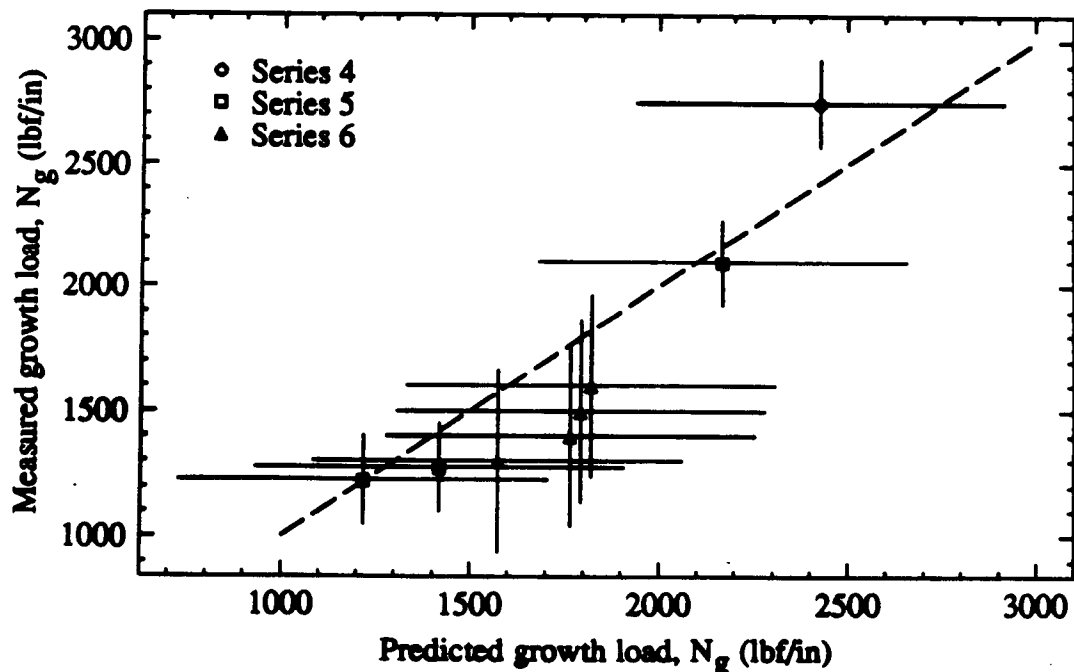


Figure 7-10 Measured versus predicted growth loads. Error bars are plus and minus three standard deviations (see Tables J-1 and J-3).

Chapter 8

Sample Problem and Discussion

§8.1 Introduction

The analytical and experimental verifications performed in Chapters 5 through 7 demonstrated the model performance over a range of input variables and loading conditions. The uncertainty analysis (Appendix J) determined not only the overall uncertainty in the experimental data and code predictions, but the relative sensitivity of the model to specific input variables. In general, the input variables can be grouped into three types in terms of their influence on the buckling load, postbuckling strain, and growth load (Table 8-1): (a) variables which are physically well-characterized and for which the results are highly sensitive, (b) variables which are physically well-characterized but for which the results show little sensitivity, and (c) variables which, for a variety of reasons, are poorly characterized and thus may exert a large influence on the results. This chapter discusses the effects of this last group of variables in the context of a sample problem.

§8.2 Sample Problem Description

The sample problem chosen corresponds to Experiment 6-1. The plate is a

16 ply symmetric cross ply laminate $([0_2/90_2/0_2/90_2]_s)$ fabricated from Fiberite T300/976 graphite/epoxy (see Table 7-1 for material properties). A 2.0 in. by 1.5 in. elliptical delamination lies 4 plies deep in the plate. The ellipse major axis is aligned with the load axis. The plate is subjected to uniform compression along the major axis of the ellipse as shown in Figure 8-1. A complete list of the nominal input variables is shown in Table 8-2. Note that x_1 , x_2 , and x_3 are the coordinates in the sublaminates, and in this instance are coincident with the x_1' , x_2' , x_3' coordinate system of the plate (see Figure 3-1). The strains shown in the examples were calculated at the outer surface of the sublaminates plus 0.004 in. to allow for the strain gauge thickness ($x_1 = 0.$, $x_2 = 0.$, $x_3 = \frac{h'}{2} + 0.004$).

Table 8-1 Code Input Variable Sensitivities

	Sensitive	Insensitive
Well-	Ellipse major semi-axis, a	Long. Young's modulus, E_x
Characterized	Ellipse minor semi-axis, b	Tran. Young's modulus, E_y
	Ellipse orientation, θ	Shear modulus, G_{xy}
	Ply thickness, t_i	Long. thermal expansion, α_x
		Tran. thermal expansion, α_y
		Temperature change, ΔT
Poorly	Critical strain energy release, G_c	
Characterized	Growth direction parameter, $\frac{da}{db}$	
	Foundation modulus, K	
	Transverse pressure load, ΔP	

In each example that follows, one variable has been allowed to change over a realistic range of possible values to illustrate the effect of that variable while holding all other input variables constant. The effects of each variable on the calculated response are shown individually in the following sections. Recommendations for designers are summarized in the last section.

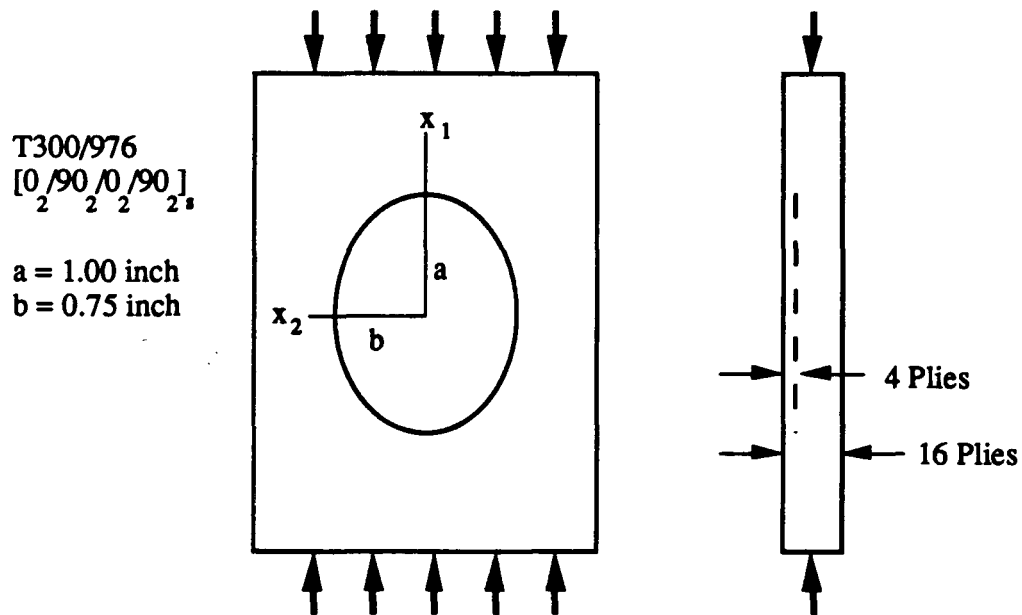


Figure 8-1 Sample problem description. Input variables are given in Table 8-2. Material properties are given in Table 7-1.

§8.3 Geometry Effects

It is well known from classical buckling theory that the buckling load of the sublaminate varies in proportion to the cube of the thickness and inversely with the square of the lateral dimensions of the sublaminate. For a designer studying the effects of manufacturing-induced disbonds or impact-caused delaminations, the thickness and shape of the sublaminate may be the source of major uncertainty.

The effect of changing the nominal ply thickness in the sample problem on the calculated load-strain history of the sublaminates is illustrated in Figure 8-2. The three cases represent successive changes of 0.0002 inch to the ply thickness. The buckling and growth loads are shown versus the ply thickness in Figure 8-3. The buckling load and growth load increase by roughly 100 lbf/in with the total 0.0005 in. thickness variation.

Table 8-2 Sample Problem Input Variables

Variable	Value	Units
Material	T300/976	
Layup	$(0_2 90_2 0_2 90_2)_s H(sym)$	
Delamination depth	4	plies
Ellipse major semi-axis, a	1.00	in
Ellipse minor semi-axis, b	0.75	in
Ellipse orientation, θ	0.	degrees
Ply thickness, t_i	0.00556	in
Critical strain energy release rate, G_c	0.20	$\frac{\text{in-lbf}}{\text{in}^2}$
Relative growth direction parameter, $\frac{da}{db}$	0	
Contact law foundation modulus, K	1.E6	$\frac{\text{lbf}}{\text{in}^3}$
Normal load in the 1 direction, γ_1	1.	
Normal load in the 2 direction, γ_2	0.	
Shear load in the 1-2 plane, γ_6	0.	
Change from reference temperature state, ΔT	-180.	$^{\circ}F$
Transverse pressure load, ΔP	3.	psi

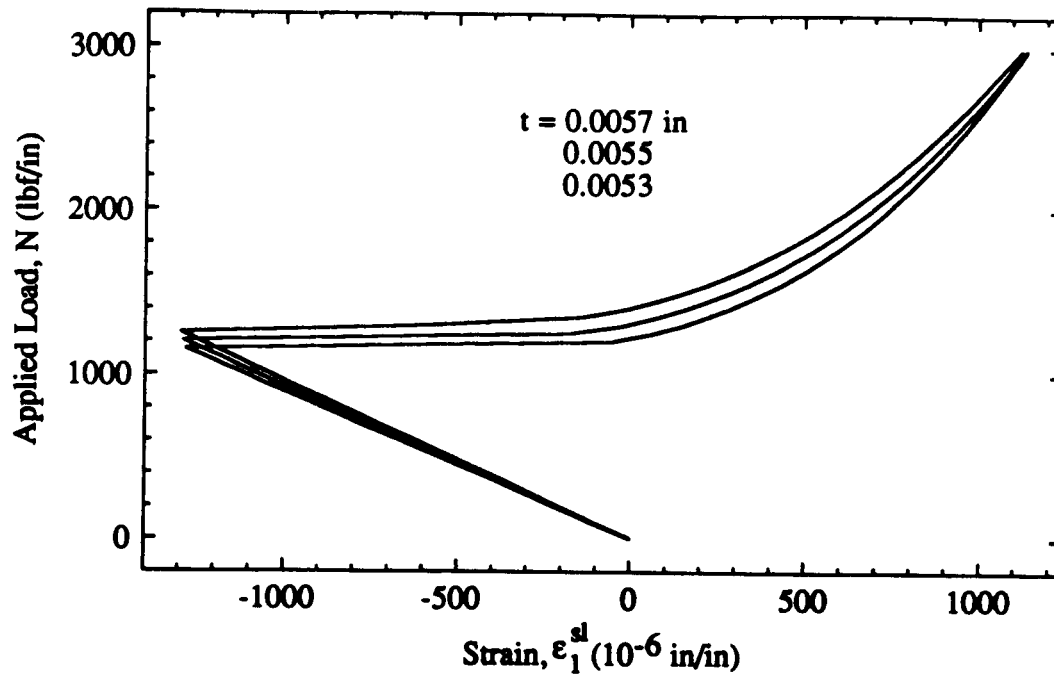


Figure 8-2 Effect of changing ply thickness on the compressive load-strain response of the sample problem described in Figure 8-1. Results calculated by the DELAM code.

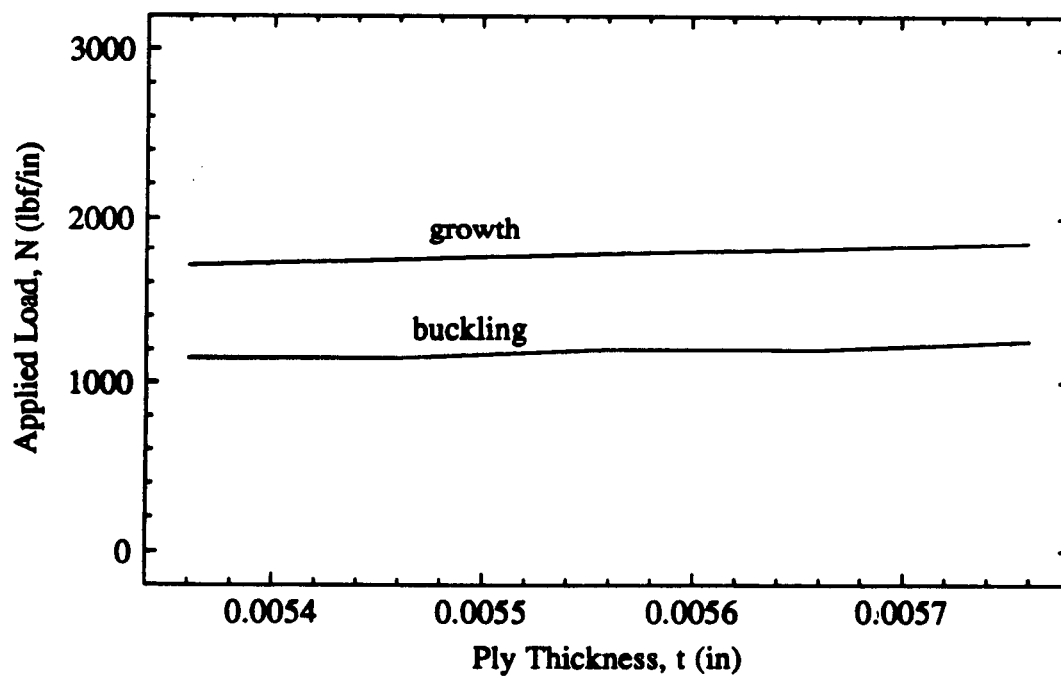


Figure 8-3 Effect of changing ply thickness on the buckling and growth loads of the sample problem described in Figure 8-1. Results calculated by the DELAM code.

The effect of a change in the lateral dimension of the sublamine on the load-strain behavior is more dramatic than the effect of a thickness change. The effect of 0.05 inch successive changes in the transverse "b" dimension of the delamination ellipse on the load-strain behavior of the sample problem sublamine is shown in Figure 8-4. The larger diameter sublaminates are much more compliant than the smaller sublaminates. The trends of the buckling and growth loads versus the ellipse semi-axis dimension are shown in Figure 8-5. As expected, the loads decrease with an increase in the semi-axis. These effects are particularly important because in practice, the lateral dimensions of a delamination may only be known to about the accuracy shown in this figure.

§8.4 Contact Model Effects

The contact model represents the physical restraint to deflection of the sublamine posed by the plate containing the delamination. The key to the model is the value of the foundation modulus K (Equation 3.31). No value for K has been measured for graphite/epoxy. A rationale for estimating K from the transverse elastic modulus of the foundation E_f and a characteristic length l_f is discussed in Appendix D. For the materials used here, $E_f \approx 1.0$ Msi and $l_f \approx 1.0$ inch yielding a foundation modulus $K \approx 1 \times 10^{-6} \frac{\text{lb}}{\text{in}^2}$ (see Equation 3.32). Figure 8-6 illustrates the effect on the load strain history of the sublamine of successive changes in the foundation modulus K . The value of $K = 0$ indicates that the contact model was not used. An increase in the foundation modulus corresponds to an increase in the stiffness of the response. Varying the value of the foundation modulus has almost no effect on the buckling and growth loads of the sublamine, as shown in Figure 8-7.

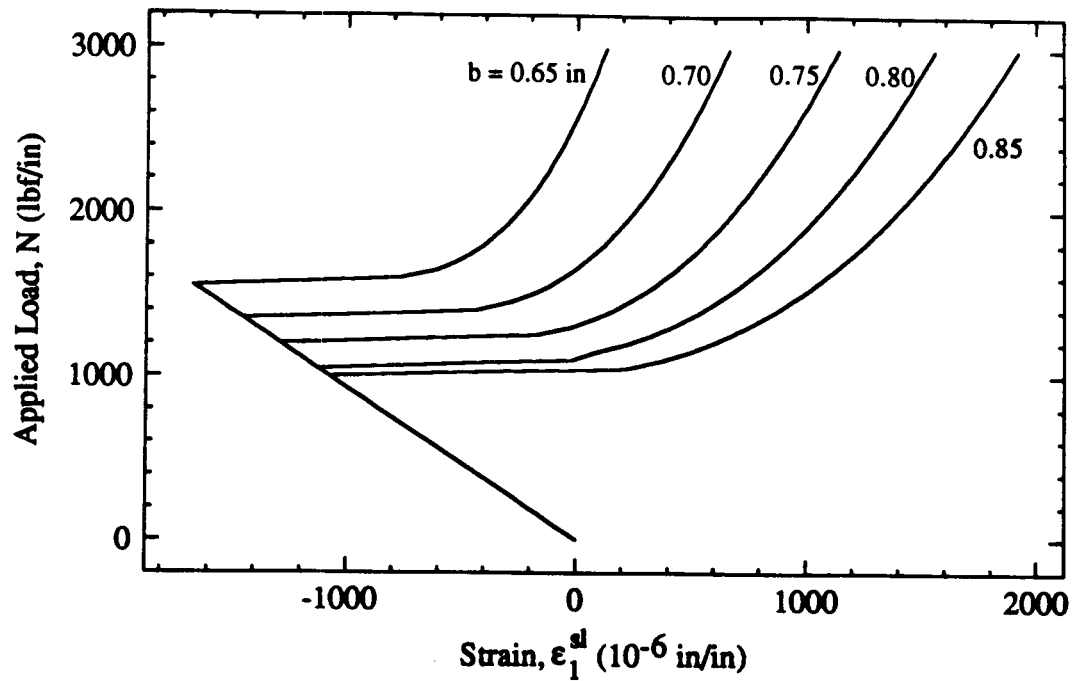


Figure 8-4 Effect of changing the semi-minor axis "b" of the ellipse on the compressive load-strain response of the sample problem described in Figure 8-1. Results calculated by the DELAM code.

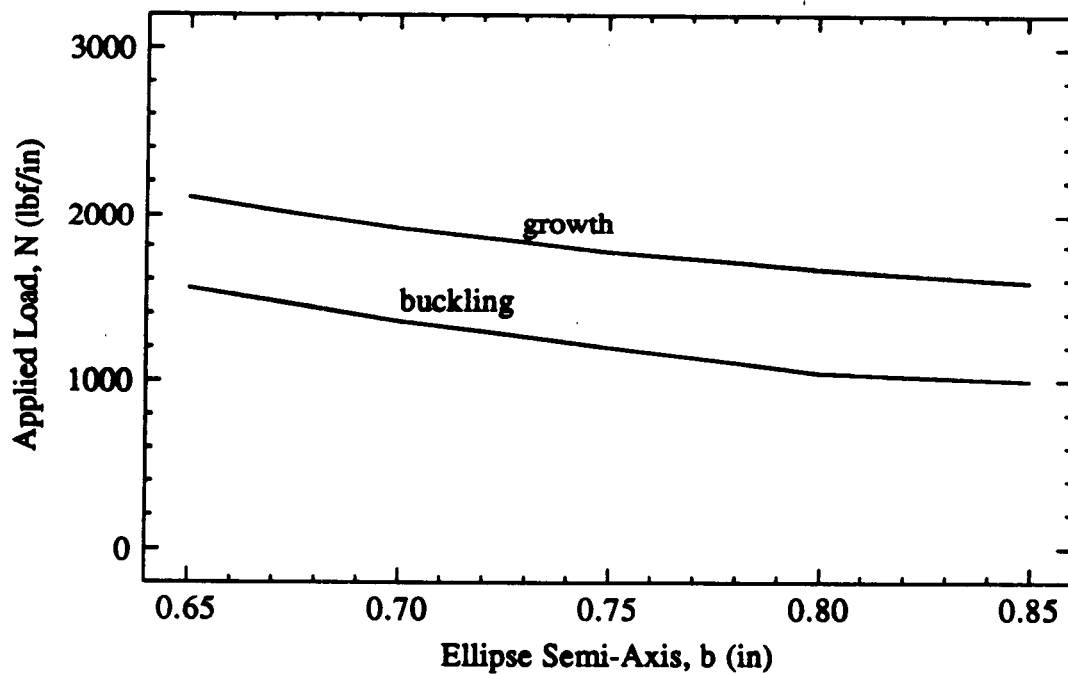


Figure 8-5 Effect of changing the semi-minor axis "b" of the ellipse on the buckling and growth loads of the sample problem described in Figure 8-1. Results calculated by the DELAM code.

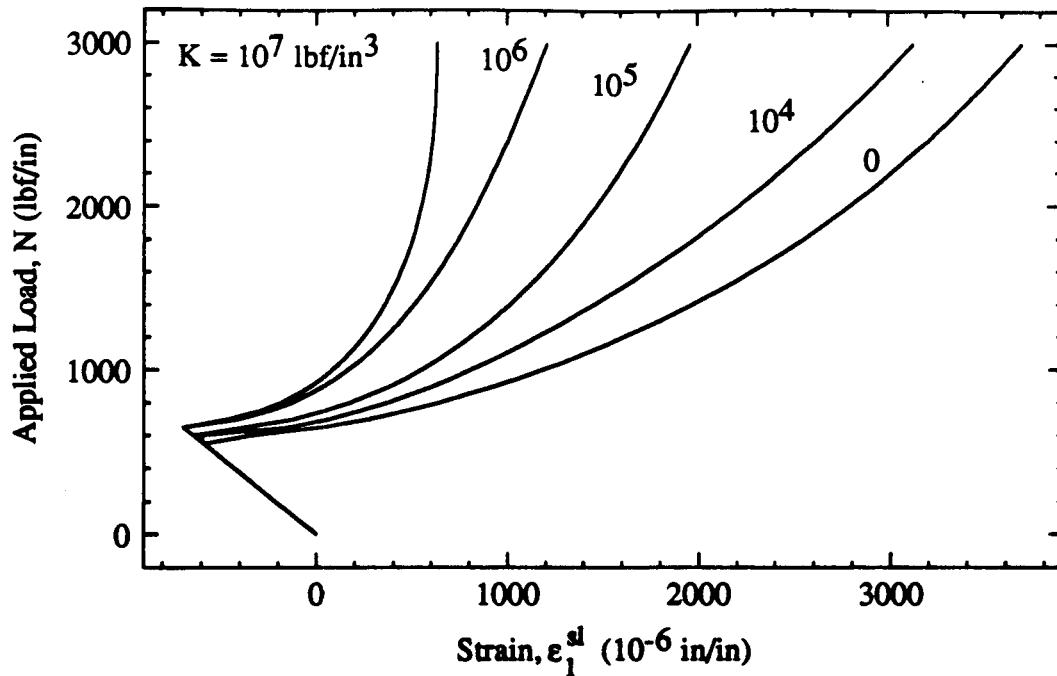


Figure 8-6 Effect of changing the contact law foundation modulus K on the compressive load-strain response of the sample problem described in Figure 8-1. Results calculated by the DELAM code.

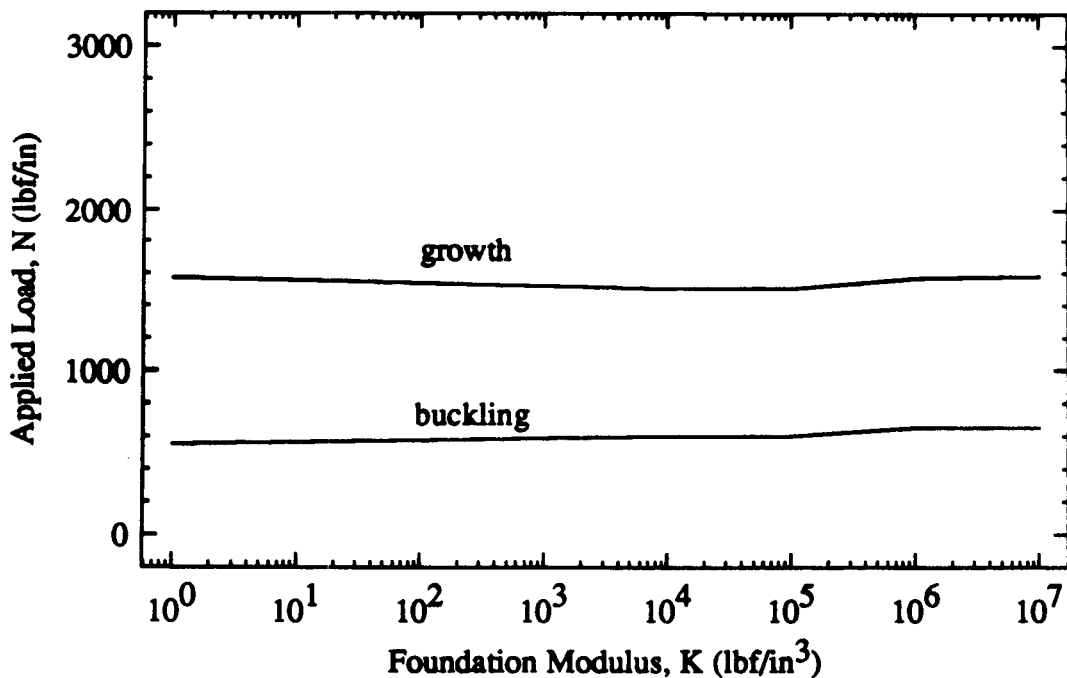


Figure 8-7 Effect of changing the contact law foundation modulus K on the buckling and growth loads of the sample problem described in Figure 8-1. Results calculated by the DELAM code.

§8.5 Transverse Pressure Effects

The transverse pressure model describes the effects of subatmospheric pressure in the cavity formed by the sublamine as it buckles away from the plate. Since there is no method to measure the actual ΔP across the sublamine, the uncertainty associated with ΔP may be large. Figure 8-8 illustrates the effect of the pressure differential on the load-strain response of the sublamine. Figure 8-9 shows the increasing buckling and growth loads with increasing pressure differential.

§8.6 Growth Model Effects

The growth model requires a parameter, $\frac{da}{db}$, describing the shape of sublamine growth, and a material property, G_c , which is the critical strain energy release rate of the material. Neither is well-characterized [50]. The effect of changing values of $\frac{da}{db}$ on the calculated growth load of the sample problem is illustrated in Figure 8-10. The lowest value is clearly $\frac{da}{db} = 0$, and the growth load increases sharply with increasing values of $\frac{da}{db}$. Figure 8-11 depicts the dependence of the growth load on the critical strain energy release rate. As shown, the growth load increases strongly with increasing G_c .

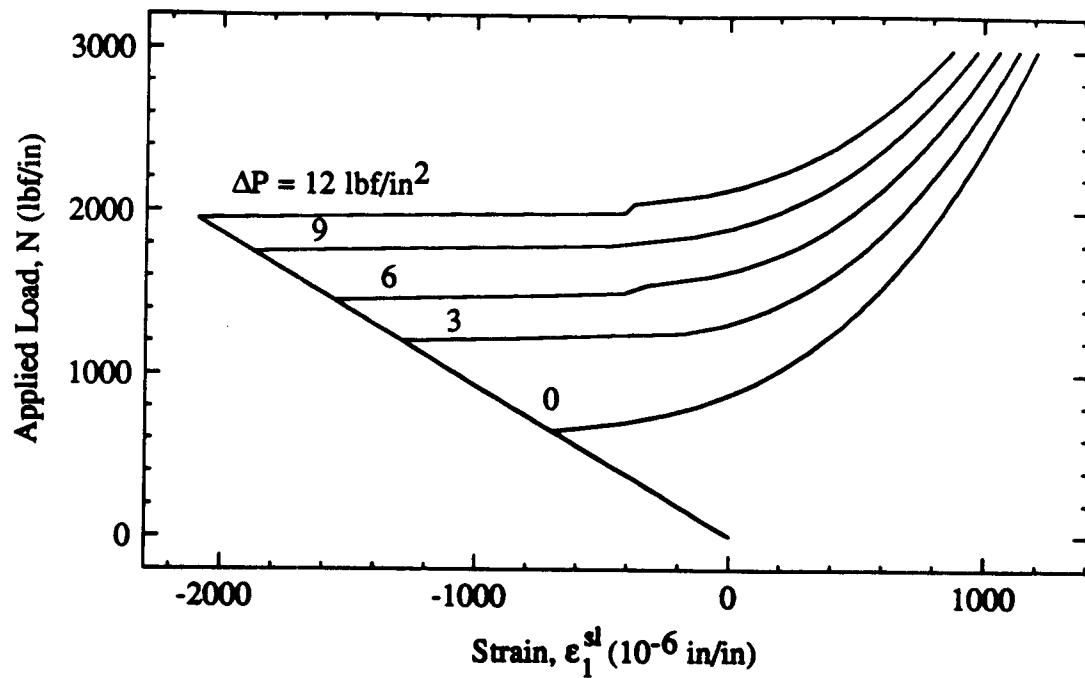


Figure 8-8 Effect of changing the transverse pressure ΔP on the compressive load-strain response of the sample problem described in Figure 8-1. Results calculated by the DELAM code.

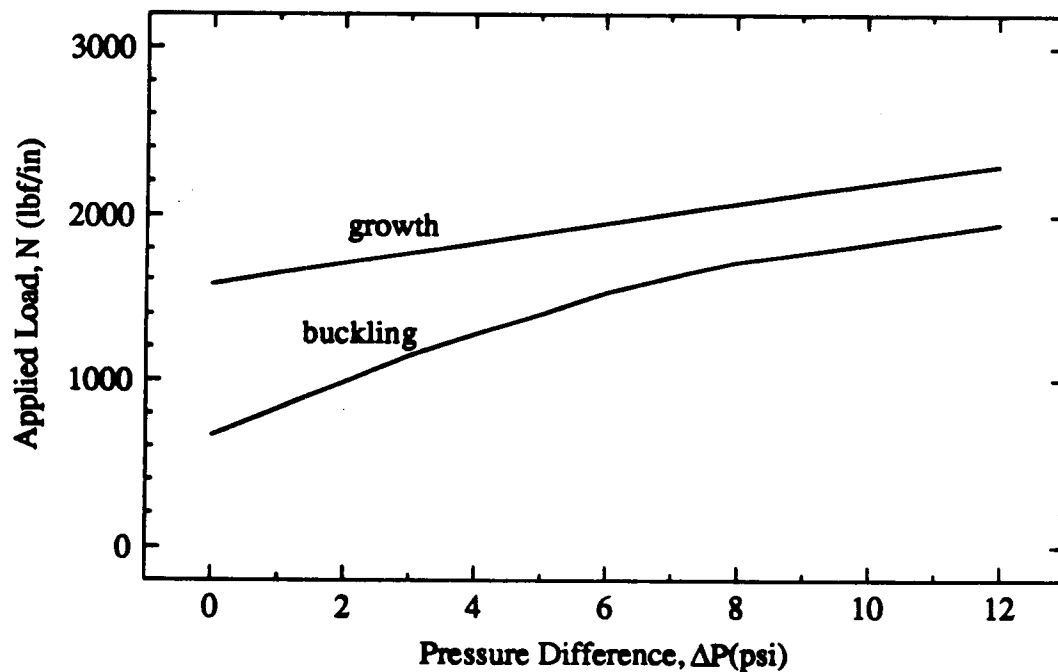


Figure 8-9 Effect of changing the transverse pressure ΔP on the buckling and growth loads of the sample problem described in Figure 8-1. Results calculated by the DELAM code.

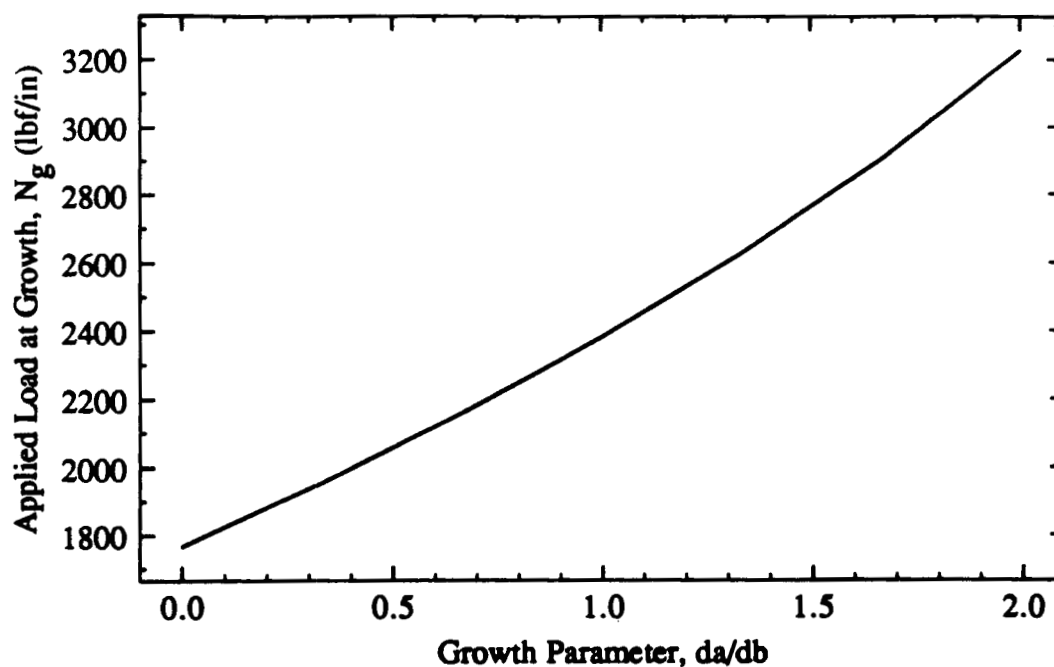


Figure 8-10 Effect of changing the growth model parameter $\frac{da}{db}$ on the compressive load-strain response of the sample problem described in Figure 8-1. Results calculated by the DELAM code.

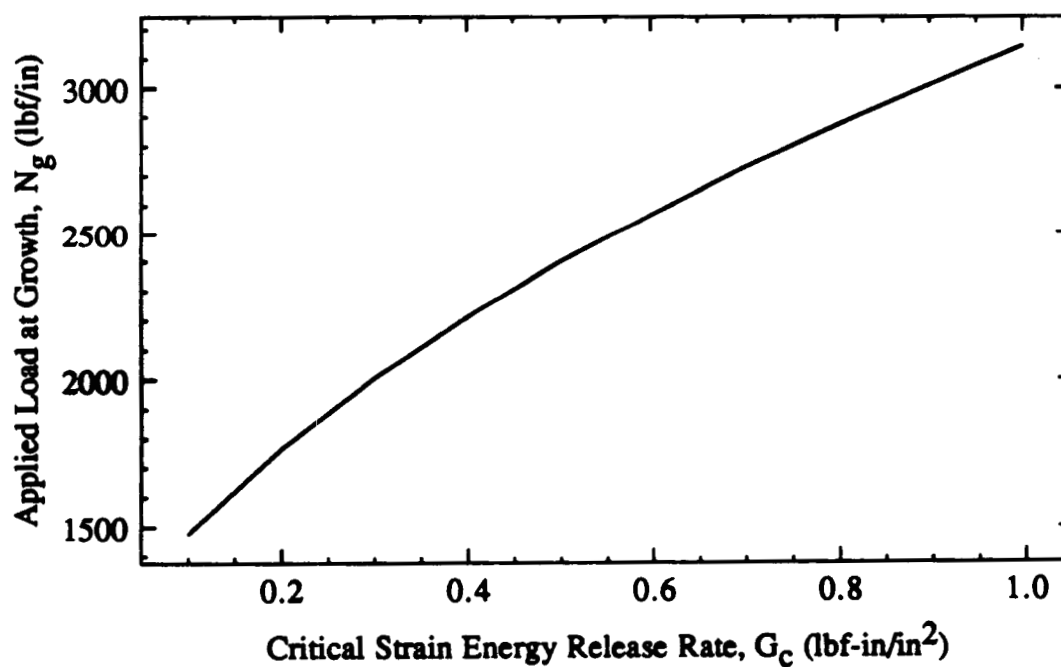


Figure 8-11 Effect of changing the critical strain energy release rate G_c on the growth loads of the sample problem described in Figure 8-1. Results calculated by the DELAM code.

§8.7 Summary and Recommendations

The sample problem shown has demonstrated the sensitivity of the model to certain input variables, in particular the sublaminate geometry, the foundation modulus, the transverse pressure differential, and the growth parameter and critical strain energy release rate. In summary, none of the variables affect the prebuckling behavior of the sublaminate whereas all of them affect the postbuckling load-strain behavior. Of the variables affecting the buckling load and growth load, the sublaminate thickness t and the foundation modulus K were shown to have a minor effect. In contrast, the sublaminate lateral dimension "b," the pressure difference ΔP , and the growth parameter $\frac{da}{db}$ and the critical strain energy release rate G_c were all shown to significantly affect the buckling and growth loads. Therefore, the following choices are recommended to designers for conservative analysis: (a) the lateral dimensions should be chosen large, (b) the pressure difference should be zero (which is likely since the pressure can equalize through cracks), (c) the growth parameter $\frac{da}{db}$ should be systematically evaluated to find the lowest growth load, and (d) the critical strain energy release rate should be as low as practical.

Chapter 9

Concluding Remarks

A model was developed to describe the behavior of delaminated composite plates subjected to compressive in-plane loads. The delaminated region is assumed to be elliptical, and may be located between any two plies of the laminate. The axes of the ellipse may be arbitrarily oriented with respect to the applied loads. The model calculates the displacements, strains, and stresses in the plate containing the delamination, and in the sublaminates created by the delamination. The model solves the nonlinear equilibrium equations describing the sublaminates up through large postbuckling deflections of the sublaminates. In particular, the model predicts the loads applied to the plate at which first buckling and then growth of the sublaminates will occur.

A computationally efficient computer implementation of the model was developed. The code has a user friendly interface, and is intended to be used for design calculations.

A new set of experimental data on the behavior of Fiberite T300/976 graphite/epoxy laminated plates containing simulated delaminations and loaded in compression was used to validate the model performance. The sublaminates load-strain histories were described at a level of detail not previously available in the literature, and will prove useful in future delamination studies.

The model currently describes a single delamination, and the behavior of the sublaminates is assumed not to affect the behavior of the plate in which it is contained. The effects of multiple delaminations, and the interaction of the sublaminates and plate, are suitable topics for future investigations.

References

- [1] Chai, H., C. D. Babcock, and W. B. Knauss, "One-Dimensional Modeling of Failure in Laminated Plates by Delamination Buckling," *Int. J. of Solids and Structures*, Vol. 17 (1981), pp. 1069-1083.
- [2] Yin, W. L., S. Sallam, and G. J. Simitses, "Ultimate Axial Load Capacity of a Delaminated Plate," AIAA/ASME/ASCE/AHS 25th Structures, Structural Dynamics and Materials Conference, Palm Springs, California, May 1984, pp. 159-165.
- [3] Simitses, G.J., S. Sallam, and W. L. Yin, "Effect of Delamination on Axially-Loaded Laminated Plates," AIAA/ASME/ASCE/AHS 25th Structures, Structural Dynamics and Materials Conference, Palm Springs, California, May 1984, pp. 351-359.
- [4] Gillespie, J. W., Jr. and R. B. Pipes, "Compressive Strength of Composite Laminates with Interlaminar Defects," *Composite Structures*, Vol. 2 (1984), pp. 49-69.
- [5] Wang, S.S., N. M. Zahlau, and H. Suemasu, "Compressive Stability of Delaminated Random Short-Fiber Composites, Part I—Modeling and Methods of Analysis," *J. of Composite Materials*, Vol. 19 (1985), pp. 296-316.
- [6] Wang, S.S., N. M. Zahlau, and H. Suemasu, "Compressive Stability of Delaminated Random Short-Fiber Composites, Part II—Experimental and Analytical Results," *J. of Composite Materials*, Vol. 19 (1985), pp. 317-333.
- [7] Sallam, A. and G. J. Simitses, "Delamination Buckling and Growth of Flat, Cross-Ply Laminates," *Composite Structures*, Vol. 4 (1985), pp. 361-381.

- [8] Williams, J. F., D. C. Stouffer, S. Ilic, and R. Jones, "An Analysis of Delamination Behavior," *Composite Structures*, Vol. 5 (1986), pp. 203-216.
- [9] El-Senussi, A. K. and J. P. H. Webber, "Blister Delamination Analysis in Fibre Reinforced Plastics Using Beam-Column Theory with an Energy Release Rate Criterion," *Composite Structures*, Vol. 6 (1986), pp. 125-141.
- [10] Vizzini, A. J. and P. A. Lagace, "The Buckling of a Delaminated Sublaminates on an Elastic Foundation," *J. of Composite Materials*, Vol. 21 (1987), pp. 1106-1117.
- [11] Yin, W.-L., "The Effects of Laminated Structure on Delamination Buckling and Growth," *J. of Composite Materials*, Vol. 22 (1988), pp. 502-517.
- [12] Kardomateas, G. A. and D. W. Schmueser, "Buckling and Postbuckling of Delaminated Composites Under Compressive Loads Including Transverse Shear Effects," *AIAA Journal*, Vol. 26 (1988), pp. 337-343.
- [13] Bottega, W. J. and A. Maewal, "Delamination Buckling and Growth in Laminates," *J. of Applied Mechanics*, Vol. 50 (1983), pp. 184-189.
- [14] Yin, W. L. and Z. Fei, "Delamination Buckling and Growth in a Clamped Circular Plate," *AIAA/ASME/ASCE/AHS 26th Structures, Structural Dynamics and Materials Conference*, Orlando, Florida, April 1985, pp. 274-282.
- [15] Bruno, D., "Delamination Buckling in Composite Laminates with Interlaminar Defects," *Theoretical and Applied Fracture Mechanics*, Vol. 9 (1988), pp. 145-159.
- [16] Konishi, D. Y., "A Rational Approach to the Analysis of Delaminated Composite Panels," *Composite Structures*, Vol. 3 (1985), pp. 383-401.
- [17] Jones, R., W. Broughton, R. F. Mousley, and R. T. Potter, "Compression Failures of Damaged Epoxy Laminates," *Composite Structures*, Vol. 3 (1985), pp. 167-186.

- [18] Chai, H. and C.D. Babcock, "Two-Dimensional Modeling of Compressive Failure in Delaminated Composites," *J. of Composite Materials*, Vol. 19 (1985), pp. 67-98.
- [19] Kassapoglou, C. "Buckling, Post-Buckling and Failure of Elliptical Delaminations in Laminates Under Compression," *Composite Structures*, Vol. 9, (1988), pp. 139-159.
- [20] Shivakumar, K. N. and J. D. Whitcomb, "Buckling of a Sublaminates in a Quasi-Isotropic Composite Laminate," *J. of Composite Materials*, Vol. 19 (1985), pp. 2-18.
- [21] Whitcomb, J. D., "Three-Dimensional Analysis of a Postbuckled Embedded Delamination," NASA Technical Paper 2823, July 1988.
- [22] Whitcomb, J. D., "Instability-Related Delamination Growth of Embedded and Edge Delaminations," NASA Technical Memorandum 100655, August 1988.
- [23] Tsai, S. W. and H. T. Hahn, *Introduction to Composite Materials*, Technomic Publishing, 1980.
- [24] Tsai, S. W., *Composites Design*, Think Composites, 1987.
- [25] von Karman, T., "Festigkeitsprobleme in Maschinenbau," *Encycl. Math. Wiss.*, Vol. 4 (1910), pp. 348-351.
- [26] Reddy, J. N., "A Refined Nonlinear Theory of Plates with Transverse Shear Deformation," *Int. J. Solids and Structures*, Vol. 20 (1984), pp. 881-896.
- [27] Reddy, J. N., "A Simple Higher-Order Theory for Laminated Composite Plates," *J. of Applied Mechanics*, Vol. 51 (1984), pp. 745-752.
- [28] Phan, N. D. and J. N. Reddy, "Analysis of Laminated Composite Plates Using a Higher-Order Shear Deformation Theory," *Int. J. for Numerical Methods in Engineering*, Vol. 21 (1985), pp. 2201-2219.
- [29] Reddy, J. N. and N. D. Phan, "Dynamic Analysis of Laminated Plates Using a

- Higher Order Theory," AIAA/ASME/ASCE /AHS 25th Structures, Structural Dynamics and Materials Conference, Palm Springs, California, May 1984 pp. 201-205.
- [30] Reddy, J. N., *Energy and Variational Methods in Applied Mechanics*, John Wiley and Sons, Inc., 1984.
- [31] Shames, I. H. and C. L. Dym, *Energy and Finite Element Methods in Structural Mechanics*, Hemisphere Publishing, 1985.
- [32] Kardomateas, G. A., "Effect of an Elastic Foundation on the Buckling and Postbuckling of Delaminated Composites under Compressive Loads," *J. of Applied Mechanics*, Vol 55, (1988), pp.238-241.
- [33] Timoshenko, S. P. and J. M. Gere, *Theory of Elastic Stability*, McGraw-Hill, 1963.
- [34] Timoshenko, S. P. and S. Woinowsky-Krieger, *Theory of Plates and Shells*, McGraw-Hill, 1959.
- [35] Brush, D. O. and B. O. Almroth, *Buckling of Bars, Plates and Shells*, McGraw-Hill, 1975.
- [36] Trefftz, E., "Zür Theorie der Stabilität des Elastischen Gleichgewichts," *Z. Angew. Math. Mech*, Vol. 13 (1933), pp. 160-165.
- [37] Broek, D., *Elementary Engineering Fracture Mechanics*, Martinus Nijhoff, 1986.
- [38] MACSYMA, Symbolics, Inc., 1988.
- [39] Press, W. H., B. P. Flannery, S. A. Teukolsky, W. T. Vetterling, *Numerical Recipes, The Art of Scientific Computing*, Cambridge University Press, 1986.
- [40] Voinovsky-Krieger, S. "The Stability of a Clamped Elliptic Plate Under Uniform Compression," *J. of Applied Mechanics*, Vol. 4 (1937), pp. A177-A178.
- [41] Chia, C.-Y., *Nonlinear Analysis of Plates*, McGraw-Hill, 1980.

- [42] Baker, A. A., R. Jones, and R. J. Callinan, "Damage Tolerance of Graphite/Epoxy Composites," *Composite Structures*, Vol. 4 (1985), pp. 15-44.
- [43] Wang, A. S. D. and M. Slomiana, *Fracture Mechancis of Delamination, Initiation and Growth*, NADC-79056-60, (1982).
- [44] Ramkumar, A. L., "Compression Fatigue Behavior of Composites in the Presence of Delaminations," *Damage in Composite Materials*, ASTM STP 775, (1982), pp. 184-210.
- [45] Konishi, D. Y. and W. R. Johnston, "Fatigue Effects on Delamination and Strength Degradation in Graphite/Epoxy Laminates," *Composite Materials: Testing and Design*, ASTM STP 674, (1979), pp. 597-619.
- [46] Byers, B. A., *Behavior of Damaged Graphite/Epoxy Laminates under Compression*, NASA-CR-159293, (1980).
- [47] Webster, J. D., *Flaw Criticality of Circular Disbond Defects in Composite Laminates*, NASA-CR-164830, (1981).
- [48] Geier, W., J. Vilismeier, and D. Weiserber, "Experimental Investigation of Delaminations in Carbon," *AGARD Conference on Characterization, Analysis and Significance of Defects in Composite Materials*, AGARD-CP-355, (1983).
- [49] Reddy, A. D., L. W. Rehfield, R. S. Haag, "Influence of Prescribed Delaminations of Stiffness-Controlled Behavior of Composite Laminates," *Effects of Defects in Composite Materials*, ASTM STP 836, (1984), pp. 71-83.
- [50] Ishai, O., A. Rotem, J. Lifshitz, *Damage Tolerance Evaluation of Structural Composite Materials*, Technion Research and Development Foundation Ltd, (1988).
- [51] Librescu, L., and R. Schmidt, "Higher Order Moderate Rotation Theories for Elastic Anisotropic Plates," *Finite Rotations in Structural Mechanics*, Springer-Verlag, (1986), pp. 158-174.

- [52] Fung, Y. C., *Foundations of Solid Mechanics*, Prentice-Hall, Inc., 1969.
- [53] Bathe, K.-J., *Finite Element Procedures in Engineering Analysis*, Prentice-Hall, Inc., 1982.
- [54] Timoshenko, S. P. and J. N. Goodier, *Theory of Elasticity*, McGraw-Hill, 1934.
- [55] Box, G. E. P., W. G. Hunter, and J. S. Hunter, *Statistics for Experimenters*, John Wiley and Sons, Inc., 1978.
- [56] Mosteller, F. and J. W. Tukey, *Data Analysis and Regression*, Addison-Wesley, 1977.
- [57] Peck, S. O., *FRAP Uncertainty Analysis Option*, EG&G Idaho, Inc., Idaho Falls, Idaho, CDAP-TR-78-024, (1978).
- [58] Peck, S. O. and C. L. Atwood, *Developmental Verification of the FRAP Uncertainty Analysis Option*, EG&G Idaho, Inc., Idaho Falls, Idaho, CDAP-TR-79-050, (1979).
- [59] Peck, S. O., *Optimization of FRAP Uncertainty Analysis Option*, EG&G Idaho, Inc., Idaho Falls, Idaho, EG&G-CDAP-5031, (1979).

Appendix A

Engineering Constants for Isotropic and Orthotropic Materials

This appendix identifies the ply plane stress reduced stiffnesses Q_{ij} used in Chapter 3 in terms of ordinary engineering elastic constants for isotropic and orthotropic materials. In addition, the transformation matrix relating on-axis and off-axis stiffnesses is given.

§A.1 Engineering Constants

The on-axis lamina constitutive relations for an orthotropic material in plane stress are

$$\begin{pmatrix} \sigma_x \\ \sigma_y \\ \sigma_p \\ \sigma_r \\ \sigma_s \end{pmatrix} = \begin{pmatrix} Q_{xx} & Q_{xy} & 0 & 0 & 0 \\ Q_{xy} & Q_{yy} & 0 & 0 & 0 \\ 0 & 0 & Q_{pp} & 0 & 0 \\ 0 & 0 & 0 & Q_{rr} & 0 \\ 0 & 0 & 0 & 0 & Q_{ss} \end{pmatrix} \begin{pmatrix} \epsilon_x \\ \epsilon_y \\ \epsilon_p \\ \epsilon_r \\ \epsilon_s \end{pmatrix} \quad (A.1)$$

where x and y are the in-plane principal material axes of the lamina, p refers to the transverse y - z plane, r to the transverse x - z plane, and s to the in-plane x - y plane.

In terms of engineering constants, the stiffnesses for an orthotropic material are

$$\begin{aligned} Q_{xx} &= \frac{E_x}{1 - \nu_{xy}\nu_{yx}} & Q_{yy} &= \frac{E_y}{1 - \nu_{xy}\nu_{yx}} & Q_{xy} &= \frac{\nu_{xy}E_y}{1 - \nu_{xy}\nu_{yx}} \\ Q_{pp} &= G_p & Q_{rr} &= G_r & Q_{ss} &= G_s \end{aligned} \quad (A.2)$$

where

E_x = Longitudinal Young's modulus

E_y = Transverse Young's modulus

ν_{xy} = Major Poisson's ratio

ν_{yx} = Minor Poisson's ratio

G_p = Transverse shear modulus in the y-z plane

G_r = Transverse shear modulus in the x-z plane

G_s = Transverse shear modulus in the x-y plane

For an isotropic material the relationships are simpler. In terms of engineering constants the stiffnesses for an isotropic material are

$$\begin{aligned} Q_{xx} &= \frac{E}{1-\nu^2} & Q_{yy} &= \frac{E}{1-\nu^2} & Q_{xy} &= \frac{\nu E}{1-\nu^2} \\ Q_{pp} &= G & Q_{rr} &= G & Q_{ss} &= G \end{aligned} \quad (A.3)$$

where

E = Young's modulus

ν = Poisson's ratio

G = Shear modulus = $\frac{E}{2(1+\nu)}$

§A.2 Transformation Matrix

The off-axis lamina constitutive relations for an orthotropic material in plane stress are

$$\begin{pmatrix} \sigma_1 \\ \sigma_2 \\ \sigma_4 \\ \sigma_5 \\ \sigma_6 \end{pmatrix} = \begin{pmatrix} Q_{11} & Q_{12} & 0 & 0 & Q_{16} \\ Q_{12} & Q_{22} & 0 & 0 & Q_{26} \\ 0 & 0 & Q_{44} & Q_{45} & 0 \\ 0 & 0 & Q_{45} & Q_{55} & 0 \\ Q_{16} & Q_{26} & 0 & 0 & Q_{66} \end{pmatrix} \begin{pmatrix} \epsilon_1 \\ \epsilon_2 \\ \epsilon_4 \\ \epsilon_5 \\ \epsilon_6 \end{pmatrix} \quad (A.4)$$

where 1 and 2 are the in-plane body axes of the lamina, 4 refers to the transverse 2-3 plane, 5 to the transverse 1-3 plane, and 6 to the in-plane 1-2 plane. The transformation matrix relating the off-axis stiffnesses to the on-axis stiffnesses is

$$\begin{pmatrix} Q_{11} \\ Q_{22} \\ Q_{12} \\ Q_{66} \\ Q_{16} \\ Q_{26} \\ Q_{44} \\ Q_{45} \\ Q_{55} \end{pmatrix} = \begin{pmatrix} m^4 & n^4 & 2m^2n^2 & 0 & 0 & 4m^2n^2 \\ n^4 & m^4 & 2m^2n^2 & 0 & 0 & 4m^2n^2 \\ m^2n^2 & m^2n^2 & m^4 + n^4 & 0 & 0 & -4m^2n^2 \\ m^2n^2 & m^2n^2 & -2m^2n^2 & 0 & 0 & (m^2 - n^2)^2 \\ m^3n & -mn^3 & mn^3 - m^3n & 0 & 0 & 2(mn^3 - m^3n) \\ mn^3 & -m^3n & m^3n - mn^3 & 0 & 0 & 2(m^3n - mn^3) \\ 0 & 0 & 0 & m^2 & n & 0 \\ 0 & 0 & 0 & -mn & mn & 0 \\ 0 & 0 & 0 & n^2 & m & 0 \end{pmatrix} \begin{pmatrix} Q_{xx} \\ Q_{yy} \\ Q_{xy} \\ Q_{pp} \\ Q_{rr} \\ Q_{ss} \end{pmatrix} \quad (A.5)$$

where $m = \cos\theta$, $n = \sin\theta$, and θ is the angle between the on-axis and off-axis coordinate systems, defined as positive in the counter-clockwise direction. Equation A.5 is given for the negative transformation, meaning that the ply on-axis stiffnesses are rotated to the body off-axis coordinates.

Appendix B

Integration of the Plate Strain Expressions

This appendix details the integration of the plate strain expressions (Equation 3.12) given in Chapter 3. The strain field in the plate is constant and uniform over the plate. The strains were derived in terms of constants c_i describing the plate (Equation 3.13), the load N , and the residual thermal strains ${}^{\circ}\epsilon_i^{pIT}$ (Equation 3.14):

$$\begin{pmatrix} {}^{\circ}\epsilon_1^{pl} \\ {}^{\circ}\epsilon_2^{pl} \\ {}^{\circ}\epsilon_6^{pl} \end{pmatrix} = \begin{pmatrix} c_1 \\ c_2 \\ c_6 \end{pmatrix} N + \begin{pmatrix} {}^{\circ}\epsilon_1^{pIT} \\ {}^{\circ}\epsilon_2^{pIT} \\ {}^{\circ}\epsilon_6^{pIT} \end{pmatrix} \quad (B.1)$$

In terms of the displacements u_i the strains are

$$\begin{pmatrix} {}^{\circ}\epsilon_1^{pl} \\ {}^{\circ}\epsilon_2^{pl} \\ {}^{\circ}\epsilon_6^{pl} \end{pmatrix} = \begin{pmatrix} \frac{\partial u_1^{pl}}{\partial x_1} \\ \frac{\partial u_2^{pl}}{\partial x_2} \\ \frac{\partial u_1^{pl}}{\partial x_2} + \frac{\partial u_2^{pl}}{\partial x_1} \end{pmatrix} \quad (B.2)$$

Combining Equations B.1 and B.2 and integrating the first two expressions yields

$$\begin{aligned} u_1^{pl} &= (c_1 N + {}^{\circ}\epsilon_1^{pIT})x_1 + f(x_2) \\ u_2^{pl} &= (c_2 N + {}^{\circ}\epsilon_2^{pIT})x_2 + g(x_1) \end{aligned} \quad (B.3)$$

where f and g are arbitrary functions of x_2 and x_1 , respectively. The in-plane shear strain ${}^{\circ}\epsilon_6^{pl}$ can then be expressed as

$${}^{\circ}\epsilon_6^{pl} = \frac{\partial {}^{\circ}u_1^{pl}}{\partial x_2} + \frac{\partial {}^{\circ}u_2^{pl}}{\partial x_1} = \frac{df(x_2)}{dx_2} + \frac{dg(x_1)}{dx_1} = c_6 N + {}^{\circ}\epsilon_6^{plT} \quad (B.4)$$

Since the strains in Equation B.1 are constant, $f(x_2)$ and $g(x_1)$ can be at most linear functions of x_2 and x_1 , respectively. Assuming that no rigid body rotation of the plate occurs, then [54]

$$\frac{\partial {}^{\circ}u_1^{pl}}{\partial x_2} - \frac{\partial {}^{\circ}u_2^{pl}}{\partial x_1} = 0 \quad (B.5)$$

or, combining Equations B.4 and B.5

$$\frac{\partial {}^{\circ}u_1^{pl}}{\partial x_2} = \frac{\partial {}^{\circ}u_2^{pl}}{\partial x_1} = \frac{1}{2}(c_6 N + {}^{\circ}\epsilon_6^{plT}) \quad (B.6)$$

Finally, $\frac{df(x_2)}{dx_2}$ and $\frac{dg(x_1)}{dx_1}$ are easily integrated and substituted into Equation B.3 to yield the in-plane displacements in the plate

$$\begin{aligned} {}^{\circ}u_1^{pl} &= (c_1 N + {}^{\circ}\epsilon_1^{plT})x_1 + \frac{1}{2}(c_6 N + {}^{\circ}\epsilon_6^{plT})x_2 \\ {}^{\circ}u_2^{pl} &= \frac{1}{2}(c_6 N + {}^{\circ}\epsilon_6^{plT})x_1 + (c_2 N + {}^{\circ}\epsilon_2^{plT})x_2 \end{aligned} \quad (B.7)$$

Appendix C

Basic Assumptions of Nonlinear Plate Theory

This appendix states the basic assumptions of the nonlinear plate theory used in the main text. In particular, the plausibility of some of the assumptions is demonstrated via an order of magnitude calculation. The motivation for this chapter was derived from the realization that the Kirchhoff-Love assumption (that normals to the midsurface remain normal) was an integral assumption in von Karman's nonlinear large deflection plate theory. The appropriate and consistent nonlinear strain measures for the shear deformable plate theory are developed subsequently [41, 51].

§C.1 Basic Assumptions

Given: A plate geometry. A body B is defined by two parallel surfaces and an edge surface joining them such that characteristic in-plane (x_1 and x_2 coordinates) lengths (L) are much greater than the through-the-thickness (x_3) length (h).

$$h \ll L \tag{C.1}$$

Assumption 1: Tangential displacements u_1 and u_2 are infinitesimal but the trans-

verse displacement u_3 is on the order of the plate thickness.

$$\begin{aligned} u_1, u_2 &\sim \text{small} \\ u_3 &\sim O(h) \end{aligned} \quad (C.2)$$

Assumption 2: Derivatives of displacements are moderate to small.

$$\frac{\partial u_i}{\partial x_j} \sim O\left(\frac{h}{L}\right) \text{ or } O\left(\frac{h}{L}\right)^2 \quad i, j = 1, 2, 3 \quad (C.3)$$

Assumption 3: Linear strain parameters e_{ij} are small, and linear rotation parameters ω_{ij} are moderate.

$$e_{ij} = \frac{1}{2} \left(\frac{\partial u_i}{\partial x_j} + \frac{\partial u_j}{\partial x_i} \right) \sim O\left(\frac{h}{L}\right)^2 \quad i, j = 1, 2, 3 \quad (C.4.a)$$

$$\omega_{ij} = \frac{1}{2} \left(\frac{\partial u_i}{\partial x_j} - \frac{\partial u_j}{\partial x_i} \right) \sim O\left(\frac{h}{L}\right) \quad i, j = 1, 2, 3 \quad (C.5.b)$$

Assumption 4: In-plane rotations are small.

$$\omega_{12} \sim O\left(\frac{h}{L}\right)^2 \quad (C.6)$$

§C.2 Order of Magnitude Estimates

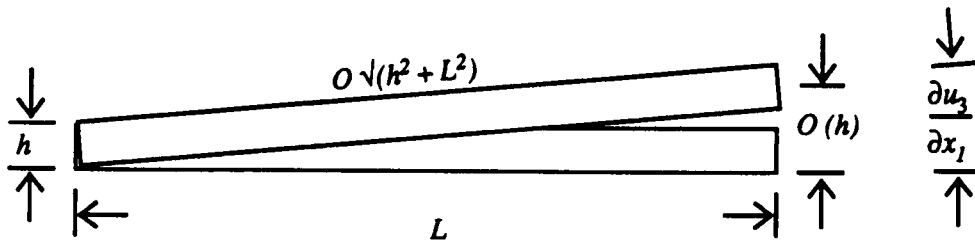


Figure C-1 Order of Magnitude Estimates for Displacements and Derivatives

To see why the above assumptions are reasonable, consider a plate with length dimensions of L and thickness h , with a transverse displacement on the order of h at one end (Figure C-1). In the deformed configuration the plate will have been stretched, rotated, and thinned by this displacement with respect to the original configuration. With respect to a Cartesian coordinate system fixed in the original reference configuration (Lagrangian description), the change in tangential in-plane displacement with respect to the in-plane coordinate is of the order

$$\begin{aligned}
 \frac{\partial u_1}{\partial x_1} &\sim O\left(\frac{\sqrt{L^2 + h^2} - L}{L}\right) \\
 &\sim O\left(\frac{L\sqrt{1 + (\frac{h}{L})^2} - L}{L}\right) \\
 &\sim O\left(1 + \frac{1}{2}\left(\frac{h}{L}\right)^2 + \dots - 1\right) \\
 &\sim O\left(\frac{h}{L}\right)^2
 \end{aligned} \tag{C.7}$$

Similarly, the change in transverse displacement with respect to the in-plane coordinate is of the order

$$\frac{\partial u_3}{\partial x_1} \sim O\left(\frac{h}{L}\right) \tag{C.8}$$

The change in the transverse displacement with respect to the transverse coordinate due to rotation (the shear effect is smaller) is of the order

$$\begin{aligned}
 \frac{\partial u_3}{\partial x_3} &\sim O\left(\frac{h(\cos \frac{\partial u_1}{\partial x_1} - 1)}{h}\right) \\
 &\sim O\left(1 - \frac{1}{2}\left(\frac{\partial u_1}{\partial x_1}\right)^2 + \dots - 1\right) \\
 &\sim O\left(\frac{h}{L}\right)^2
 \end{aligned} \tag{C.9}$$

Similar estimates for the remaining derivatives can be made so that, in summary,

the derivative order of magnitudes are

$$\begin{aligned}
 \frac{\partial u_1}{\partial x_1} &\sim O\left(\frac{h}{L}\right)^2 & \frac{\partial u_2}{\partial x_1} &\sim O\left(\frac{h}{L}\right)^2 & \frac{\partial u_3}{\partial x_1} &\sim O\left(\frac{h}{L}\right) \\
 \frac{\partial u_1}{\partial x_2} &\sim O\left(\frac{h}{L}\right)^2 & \frac{\partial u_2}{\partial x_2} &\sim O\left(\frac{h}{L}\right)^2 & \frac{\partial u_3}{\partial x_2} &\sim O\left(\frac{h}{L}\right) \\
 \frac{\partial u_1}{\partial x_3} &\sim O\left(\frac{h}{L}\right) & \frac{\partial u_2}{\partial x_3} &\sim O\left(\frac{h}{L}\right) & \frac{\partial u_3}{\partial x_3} &\sim O\left(\frac{h}{L}\right)^2
 \end{aligned} \tag{C.10}$$

as stated in (C.3).

Using the estimates for the magnitudes of derivatives (C.10), the plausibility of Assumption 3 for linear strain and and rotation parameters can be checked. For example,

$$e_{11} = \frac{\partial u_1}{\partial x_1} \sim O\left(\frac{h}{L}\right)^2 \quad e_{22} = \frac{\partial u_2}{\partial x_2} \sim O\left(\frac{h}{L}\right)^2 \quad e_{33} = \frac{\partial u_3}{\partial x_3} \sim O\left(\frac{h}{L}\right)^2 \tag{C.11}$$

The linear shear strain parameters and the rotation parameters must be examined carefully. In particular, the algebraic values of the derivatives $\frac{\partial u_i}{\partial x_j}$ are opposite in sign to the algebraic values of $\frac{\partial u_i}{\partial x_i}$ for a rigid body rotation. Thus, the linear shear strain parameters are really difference equations and the rotations simply additive. Therefore, Assumption 3 actually states that the difference in derivatives is small. That is,

$$\begin{aligned}
 e_{12} &= \frac{1}{2} \left(\frac{\partial u_1}{\partial x_2} + \frac{\partial u_2}{\partial x_1} \right) \sim O\left(\frac{h}{L}\right)^2 - O\left(\frac{h}{L}\right)^2 \sim O\left(\frac{h}{L}\right)^3 \\
 e_{13} &= \frac{1}{2} \left(\frac{\partial u_1}{\partial x_3} + \frac{\partial u_3}{\partial x_1} \right) \sim O\left(\frac{h}{L}\right) - O\left(\frac{h}{L}\right) \sim O\left(\frac{h}{L}\right)^2 \\
 e_{23} &= \frac{1}{2} \left(\frac{\partial u_2}{\partial x_3} + \frac{\partial u_3}{\partial x_2} \right) \sim O\left(\frac{h}{L}\right) - O\left(\frac{h}{L}\right) \sim O\left(\frac{h}{L}\right)^2 \\
 \omega_{12} &= \frac{1}{2} \left(\frac{\partial u_1}{\partial x_2} - \frac{\partial u_2}{\partial x_1} \right) \sim O\left(\frac{h}{L}\right)^2 + O\left(\frac{h}{L}\right)^2 \sim O\left(\frac{h}{L}\right)^2 \\
 \omega_{13} &= \frac{1}{2} \left(\frac{\partial u_1}{\partial x_3} - \frac{\partial u_3}{\partial x_1} \right) \sim O\left(\frac{h}{L}\right) + O\left(\frac{h}{L}\right) \sim O\left(\frac{h}{L}\right) \\
 \omega_{23} &= \frac{1}{2} \left(\frac{\partial u_2}{\partial x_3} - \frac{\partial u_3}{\partial x_2} \right) \sim O\left(\frac{h}{L}\right) + O\left(\frac{h}{L}\right) \sim O\left(\frac{h}{L}\right)
 \end{aligned} \tag{C.12}$$

§C.3 Rationale and Consequences

In the above, we implicitly used a Lagrangian description of the system. That is, within a fixed Cartesian coordinated system, the deformation of the plate was described in terms of the reference undeformed configuration of the plate. The appropriate stress measure in the Lagrangian description [52] is the 2nd Piola-Kirchhoff stress tensor σ_{ij}^{P-K} which, in terms of the Cauchy stresses σ_{ij}^C , is

$$\sigma_{ij}^{P-K} = \frac{\rho_o}{\rho_c} \frac{\partial x_i^o}{\partial x_\alpha^c} \frac{\partial x_j^o}{\partial x_\beta^c} \sigma_{\alpha\beta}^C \quad (C.13)$$

where ρ_o and ρ_c are the mass densities in the reference and current configurations, respectively, and x_i^o and x_α^c particle locations in the reference and current configurations. The appropriate strain measure [52] for the Lagrangian description is the Green-Lagrange strain tensor

$$\epsilon_{ij} = \frac{1}{2} \left(\frac{\partial u_i}{\partial x_j} + \frac{\partial u_j}{\partial x_i} + \frac{\partial u_k}{\partial x_i} \frac{\partial u_k}{\partial x_j} \right) \quad (C.14)$$

The 2nd Piola-Kirchhoff stress tensor and the Green-Lagrange strain tensor are energy conjugate to one another [53]. That is, the strain energy of the system calculated by these two measures in the reference coordinates is equal to the strain energy calculated in the current coordinates using Cauchy stresses and infinitesimal strains. Thus, we have defined a plate theory involving large transverse deflections, moderate rotations, and small strains. For nonlinear analysis, the following observations can be made.

C.3.1 Stresses

The Cauchy stresses, expressed in terms of the 2nd Piola-Kirchhoff stresses and the derivatives of displacement already discussed, are

$$\sigma_{ij}^C = \frac{\rho_c}{\rho_o} \left\{ \sigma_{ij}^{P-K} + (\delta_{j\beta} \frac{\partial u_i}{\partial x_\alpha} + \delta_{i\alpha} \frac{\partial u_j}{\partial x_\beta} + \frac{\partial u_i}{\partial x_\alpha} \frac{\partial u_j}{\partial x_\beta}) \sigma_{\beta\alpha}^{P-K} \right\} \quad (C.15)$$

where δ_{ij} is the Kronecker delta and u_i and x_i are with respect to the reference configuration. Given the magnitudes of the displacement derivatives (C.10), the consequence of these assumptions is that, to first order, the Cauchy stresses and 2nd Piola-Kirchhoff stresses are equal. Therefore, the stress and moment resultants defined elsewhere in this thesis will also be approximately equal. There is no further need to distinguish reference and current configurations when discussing stress.

C.3.2 Strains

The components of the Green-Lagrange strain tensor (C.14) and the order of magnitude of the various displacement derivatives are:

$$\begin{aligned}\epsilon_{11} &= \frac{\partial u_1}{\partial x_1} + \frac{1}{2} \left(\left(\frac{\partial u_1}{\partial x_1} \right)^2 + \left(\frac{\partial u_2}{\partial x_1} \right)^2 + \left(\frac{\partial u_3}{\partial x_1} \right)^2 \right) \\ \epsilon_{11} &\sim O\left\{ \left(\frac{h}{L} \right)^2, \quad \left(\frac{h}{L} \right)^4, \quad \left(\frac{h}{L} \right)^4, \quad \left(\frac{h}{L} \right)^2 \right\}\end{aligned}\tag{C.16}$$

$$\begin{aligned}\epsilon_{22} &= \frac{\partial u_2}{\partial x_2} + \frac{1}{2} \left(\left(\frac{\partial u_1}{\partial x_2} \right)^2 + \left(\frac{\partial u_2}{\partial x_2} \right)^2 + \left(\frac{\partial u_3}{\partial x_2} \right)^2 \right) \\ \epsilon_{22} &\sim O\left\{ \left(\frac{h}{L} \right)^2, \quad \left(\frac{h}{L} \right)^4, \quad \left(\frac{h}{L} \right)^4, \quad \left(\frac{h}{L} \right)^2 \right\}\end{aligned}\tag{C.17}$$

$$\begin{aligned}\epsilon_{33} &= \frac{\partial u_3}{\partial x_3} + \frac{1}{2} \left(\left(\frac{\partial u_1}{\partial x_3} \right)^2 + \left(\frac{\partial u_2}{\partial x_3} \right)^2 + \left(\frac{\partial u_3}{\partial x_3} \right)^2 \right) \\ \epsilon_{33} &\sim O\left\{ \left(\frac{h}{L} \right)^2, \quad \left(\frac{h}{L} \right)^2, \quad \left(\frac{h}{L} \right)^2, \quad \left(\frac{h}{L} \right)^4 \right\}\end{aligned}\tag{C.18}$$

$$\begin{aligned}\epsilon_{12} &= \frac{1}{2} \left(\frac{\partial u_1}{\partial x_2} + \frac{\partial u_2}{\partial x_1} + \frac{\partial u_1}{\partial x_1} \frac{\partial u_1}{\partial x_2} + \frac{\partial u_2}{\partial x_1} \frac{\partial u_2}{\partial x_2} + \frac{\partial u_3}{\partial x_1} \frac{\partial u_3}{\partial x_2} \right) \\ \epsilon_{12} &\sim O\left\{ \left(\frac{h}{L} \right)^2, \quad \left(\frac{h}{L} \right)^2, \quad \left(\frac{h}{L} \right)^4, \quad \left(\frac{h}{L} \right)^4, \quad \left(\frac{h}{L} \right)^2 \right\}\end{aligned}\tag{C.19}$$

$$\begin{aligned}\epsilon_{13} &= \frac{1}{2} \left(\frac{\partial u_1}{\partial x_3} + \frac{\partial u_3}{\partial x_1} + \frac{\partial u_1}{\partial x_1} \frac{\partial u_1}{\partial x_3} + \frac{\partial u_2}{\partial x_1} \frac{\partial u_2}{\partial x_3} + \frac{\partial u_3}{\partial x_1} \frac{\partial u_3}{\partial x_3} \right) \\ \epsilon_{13} &\sim O\left\{ \left(\frac{h}{L} \right), \quad \left(\frac{h}{L} \right), \quad \left(\frac{h}{L} \right)^3, \quad \left(\frac{h}{L} \right)^3, \quad \left(\frac{h}{L} \right)^3 \right\}\end{aligned}\tag{C.20}$$

$$\begin{aligned}\epsilon_{23} &= \frac{1}{2} \left(\frac{\partial u_2}{\partial x_3} + \frac{\partial u_3}{\partial x_2} + \frac{\partial u_1}{\partial x_2} \frac{\partial u_1}{\partial x_3} + \frac{\partial u_2}{\partial x_2} \frac{\partial u_2}{\partial x_3} + \frac{\partial u_3}{\partial x_2} \frac{\partial u_3}{\partial x_3} \right) \\ \epsilon_{23} &\sim O\left\{\left(\frac{h}{L}\right), \quad \left(\frac{h}{L}\right), \quad \left(\frac{h}{L}\right)^3, \quad \left(\frac{h}{L}\right)^3, \quad \left(\frac{h}{L}\right)^3\right\}\end{aligned}\quad (C.21)$$

Neglecting terms of $(\frac{h}{L})^3$ and higher, and recalling the arguments for the magnitudes of the linear portions of the strains (C.12), it is apparent that

- 1.) Only the in-plane strains retain nonlinear terms, and
- 2.) With the exception of ϵ_{33} , these terms are derivatives of the transverse displacement u_3 .

In this regard ϵ_{33} deserves a special note. Recalling the estimate of the magnitude of $\frac{\partial u_3}{\partial x_3}$ due to rotation (C.9), it is apparent that $\frac{\partial u_3}{\partial x_3}$ and $\frac{\partial u_1}{\partial x_3}$ are algebraically opposite (similar to the linear shear strain terms). This makes sense in that a strict rigid body rotation should produce no strain. For moderate rotation deformation the rigid body portion of that motion should vanish. The difference between these terms will be due to any effect of shear on ϵ_{33} (arguably of order $(\frac{h}{L})^3$) and the term $\frac{\partial u_2}{\partial x_3}$ will be due to Poisson thinning. (These are obviously beam-like simplifications.) Thus, a reasonable summation of appropriate nonlinear strain measures for the above assumptions in a compact form is

$$\epsilon_{ij} = \frac{1}{2} \left(\frac{\partial u_i}{\partial x_j} + \frac{\partial u_j}{\partial x_i} + \frac{\partial u_3}{\partial x_i} \frac{\partial u_3}{\partial x_j} \right) \quad i, j = 1, 2, 3 \quad (C.22)$$

That is, the strain-displacement relations von Karman assumed are entirely appropriate in the context of moderate rotation, small strain shear deformation theory. For large strains, particularly large shear strains, appropriate nonlinear terms will have to include the effects of the assumed shear deformation mode in the nonlinearities.

Appendix D

Contact Model Foundation Modulus

The contact model requires the foundation modulus K of the plate as a material property input. For graphite/epoxy composite materials no measured value of K is available. The purpose of this appendix is to describe a method for estimating this property. The vertical displacement v of a semi-infinite plate subjected to a uniform pressure load q acting on a portion of the plate, as shown in Figure D-1, is [54]

$$v = -\frac{2q}{\pi E} 2a \log a \quad (D.1)$$

where the displacement is evaluated at the origin, E is Young's modulus, and $2a$ is the width over which the pressure acts. Rearranging Equation D.1 gives

$$q = -\frac{\pi E}{4a \log a} v \quad (D.2)$$

The contact model is stated as

$$f = \begin{cases} \Delta P - K u_3^{sl} & u_3^{sl} \geq 0 \\ \Delta P & u_3^{sl} < 0 \end{cases} \quad (D.3)$$

where f is the contact force per unit area and u^{sl} is the displacement of the sub-laminate. Identifying q with f and v with u^{sl} , the foundation modulus K may be

estimated from

$$K = \frac{\pi E}{4a \log a} \quad (D.4)$$

More simply, the foundation modulus is estimated by

$$K \approx \frac{E_f}{l_f} \quad (D.5)$$

where E_f is the elastic modulus of the foundation and l_f a characteristic length.

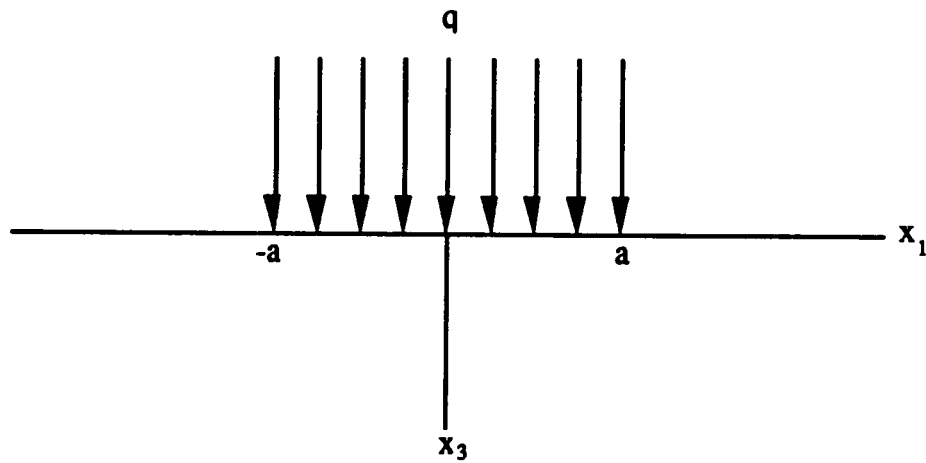


Figure D-1 Uniform pressure load acting on a semi-infinite plate.

Appendix E

Parallel Axes Theorem for Unsymmetric Laminates

This appendix describes the calculation of laminate stiffnesses for generally unsymmetric laminates. A_{ij} , B_{ij} , D_{ij} , E_{ij} , F_{ij} , H_{ij} are laminate stiffnesses defined in Equation 3.34 as

$$\begin{aligned} (A_{ij}, B_{ij}, D_{ij}, E_{ij}, F_{ij}, H_{ij}) &= \int_{-\frac{h^s}{2}}^{\frac{h^s}{2}} Q_{ij}(1, x_3, x_3^2, x_3^3, x_3^4, x_3^6) dx_3 \quad i, j = 1, 2, 6 \\ (A_{ij}, D_{ij}, F_{ij}) &= \int_{-\frac{h^s}{2}}^{\frac{h^s}{2}} Q_{ij}(1, x_3^2, x_3^4) dx_3 \quad i, j = 4, 5 \end{aligned} \quad (E.1)$$

For a laminate composed of plies of varying thicknesses or an odd number of plies the laminate midsurface may fall within a given ply. It is computationally simple to calculate the laminate stiffnesses in a coordinate system originating on the laminate outer surface, and then to use the parallel axis theorem [23] to determine the stiffnesses in a coordinate system located at the laminate midsurface.

For a primed coordinate system located a distance d from the laminate midsurface as shown in Figure E-1, the laminate stiffnesses are calculated from

$$\begin{aligned}
 (A'_{ij}, B'_{ij}, D'_{ij}, E'_{ij}, F'_{ij}, G'_{ij}, H'_{ij}) &= \int_{d-\frac{h^*l}{2}}^{d+\frac{h^*l}{2}} Q_{ij}(1, x_3, x_3^2, x_3^3, x_3^4, x_3^5, x_3^6) dx'_3 \quad i, j = 1, 2, 6 \\
 (A'_{ij}, D'_{ij}, F'_{ij}) &= \int_{d-\frac{h^*l}{2}}^{d+\frac{h^*l}{2}} Q_{ij}(1, x_3^2, x_3^4) dx'_3 \quad i, j = 4, 5
 \end{aligned}
 \tag{E.2}$$

Notice that the stiffness G'_{ij} is required. The laminate stiffnesses in the unprimed plate midsurface coordinate system are then determined using the parallel axis theorem as

$$\begin{aligned}
 A_{ij} &= A'_{ij} \\
 B_{ij} &= B'_{ij} - dA_{ij} \\
 D_{ij} &= D'_{ij} - 2dB_{ij} - d^2A_{ij} \\
 E_{ij} &= E'_{ij} - 3dD_{ij} - 3d^2B_{ij} - d^3A_{ij} \\
 F_{ij} &= F'_{ij} - 4dE_{ij} - 6d^2D_{ij} - 4d^3B_{ij} - d^4A_{ij} \\
 G_{ij} &= G'_{ij} - 5dF_{ij} - 10d^2E_{ij} - 10d^3D_{ij} - 5d^4B_{ij} - d^5A_{ij} \\
 H_{ij} &= H'_{ij} - 6dG_{ij} - 15d^2F_{ij} - 20d^3E_{ij} - 15d^4D_{ij} - 6d^5B_{ij} - d^6A_{ij}
 \end{aligned}
 \tag{E.3}$$

Each equation requires the result of the previous equation to complete the calculation. The distance d is, in general, arbitrary. However, in the particular case here, d is equal to half the sublamine thickness $\frac{h^*l}{2}$.

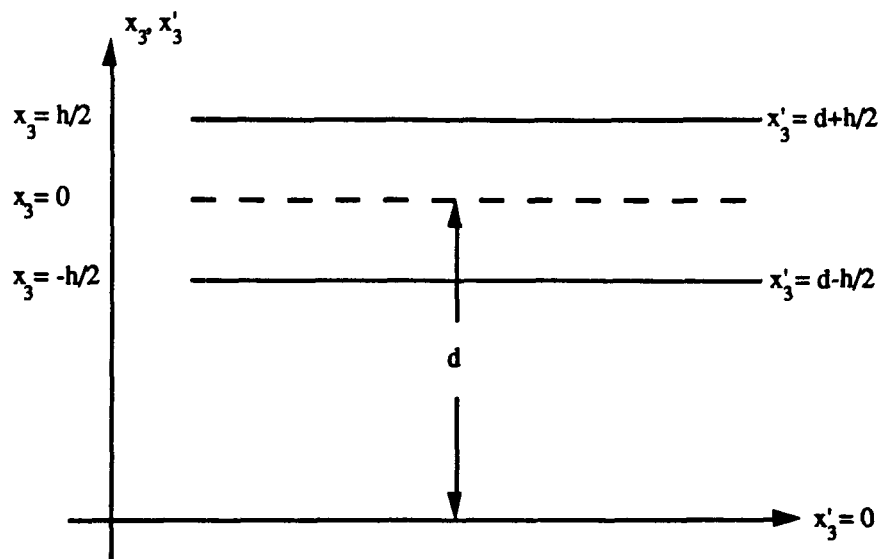


Figure E-1 Laminate thickness direction coordinate systems located at the plate midsurface (x_3) and an arbitrary distance d from the plate midsurface (x'_3).

Appendix F

Strain Energy Release of an Elliptical Sublaminates

This appendix details the derivation of the strain energy release of an elliptical sublaminates (Equations 3.41 and 3.43). The total potential energy Π and area A of an elliptical plate are functions of the semi-major and semi-minor axes a and b , respectively, of the ellipse.

$$\Pi = \Pi(a, b, \dots) \quad A = \pi ab \quad (F.1)$$

Taking differentials of both yields

$$d\Pi = \frac{\partial \Pi}{\partial a} da + \frac{\partial \Pi}{\partial b} db \quad dA = \pi(b da + a db) \quad (F.2)$$

Combining the differentials gives the strain energy release per unit area

$$\frac{d\Pi}{dA} = \frac{\frac{\partial \Pi}{\partial a} da + \frac{\partial \Pi}{\partial b} db}{\pi(b da + a db)} \quad (F.3)$$

or

$$\frac{d\Pi}{dA} = \frac{\frac{\partial \Pi}{\partial a} \frac{da}{db} + \frac{\partial \Pi}{\partial b}}{\pi(b \frac{da}{db} + a)} \quad (F.4)$$

In the particular instance of a sublaminates in a composite plate, the calculation is made for each system, Π^{pl} and Π^{sl} .

DELAM SAMPLE INPUT/OUTPUT

THIS IS PROGRAM DELAM.

COPYRIGHT 1989 BY SCOTT OWEN PECK

STRUCTURES AND COMPOSITES LABORATORY
DEPARTMENT OF AERONAUTICS AND ASTRONAUTICS
STANFORD UNIVERSITY, STANFORD, CALIFORNIA
(415) 723-4135

GIVEN A LAMINATED COMPOSITE PLATE CONTAINING AN
ELLIPTICALLY SHAPED DELAMINATION, DELAM WILL
CALCULATE THE FOLLOWING:

- (1) THE CRITICAL LOAD APPLIED TO THE PLATE NECESSARY
TO CAUSE BUCKLING OF THE SUBLAMINATE CREATED BY
THE DELAMINATION,
- (2) THE NONLINEAR LOAD-STRAIN HISTORY OF THE
SUBLAMINATE, AND
- (3) THE CRITICAL LOAD APPLIED TO THE PLATE NECESSARY
TO CAUSE THE ONSET OF DELAMINATION GROWTH.

DELAM IS BASED ON A NONLINEAR PLATE THEORY
INCLUDING THE EFFECTS OF LARGE TRANSVERSE DEFLECTIONS
OF THE SUBLAMINATE AND TRANSVERSE SHEAR DEFORMATION.
THE ASSUMPTIONS ABOUT THE PLATE AND SUBLAMINATE ARE:

- (1) THE PLATE CONTAINING THE DELAMINATION IS
SYMMETRICALLY LAMINATED.
- (2) THE DELAMINATION MAY OCCUR BETWEEN ANY TWO
PLIES, AND THEREFORE THE SUBLAMINATE MAY
BE UNSYMMETRICALLY LAMINATED.
- (3) THE ELLIPTICAL SUBLAMINATE MAY BE ARBITRARILY
ORIENTED WITH RESPECT TO THE APPLIED LOADS.
- (4) THE PLATE FORMS A DETACHED ELASTIC FOUNDATION
FOR THE SUBLAMINATE, WHICH MODELS POSSIBLE
CONTACT BETWEEN THE TWO.
- (5) A TRANSVERSE PRESSURE DIFFERENTIAL MAY ACT
ACROSS THE SUBLAMINATE THICKNESS DUE TO
SUBATMOSPHERIC PRESSURES IN THE CAVITY FORMED
BETWEEN THE SUBLAMINATE AND PLATE.
- (6) GROWTH OF THE SUBLAMINATE WILL OCCUR
WHEN THE TOTAL POTENTIAL ENERGY RELEASED BY
SUBLAMINATE - PLATE SYSTEM EXCEEDS THE
CRITICAL VALUE FOR THE PARTICULAR MATERIAL.

DELAM OPERATES IN ONE OF TWO MODES: PROMPTED
AND DATA FILE. IN THE PROMPTED MODE YOU WILL BE QUERIED
FOR EACH INPUT PARAMETER. IN THE DATA FILE MODE, THE
INPUT DATA IS ASSUMED TO BE IN A USER DATA FILE,
AND YOU WILL BE ASKED ONLY FOR THE NAME OF THE FILE.
AT THE END OF THE INPUT PROCESS IN PROMPTED MODE,
YOU WILL BE ASKED WHETHER YOU WOULD LIKE THE INPUT
TO BE SAVED IN AN INPUT FILE FOR FUTURE ANALYSES.

WOULD YOU LIKE THE NORMAL PRINTOUT (0),
MORE PRINTOUT (1), OR LOTS OF PRINTOUT (2) ?
0
WOULD YOU PREFER PROMPTED INPUT (P)
OR TO READ YOUR INPUT FROM A DATA FILE (D)?
P

THE FOLLOWING INPUT DESCRIBES THE GEOMETRY AND
MATERIALS OF THE ELLIPTICAL DELAMINATION.
THE INPUT UNITS ARE IN ANY SELF-CONSISTENT
SYSTEM THE USER DESIRES.

ELLIPSE SEMI-MAJOR AXIS?
1.0

ELLIPSE SEMI-MINOR AXIS?
0.75

ROTATION OF THE ELLIPSE W.R.T. THE PLATE?
0.

NUMBER OF PLIES IN THE WHOLE PLATE?
16

NUMBER OF PLIES IN THE SUBLAMINATE?
4

THE PLIES ARE NUMBERED FROM THE TOP SURFACE TO THE BOTTOM SURFACE.
SHOULD EACH PLY HAVE THE SAME THICKNESS? (Y/N)
Y

PLY THICKNESS -
.00556

THE ORIENTATION OF EACH PLY IS POSITIVE FROM THE PLATE COORDINATE AXIS
TO THE PLY AXIS.

PLY NUMBER 1 ORIENTATION -
0.

PLY NUMBER 2 ORIENTATION -
0.

PLY NUMBER 3 ORIENTATION -
90.

PLY NUMBER 4 ORIENTATION -
90.

PLY NUMBER 5 ORIENTATION -
0.

PLY NUMBER 6 ORIENTATION -
0.

PLY NUMBER 7 ORIENTATION -
90.

PLY NUMBER 8 ORIENTATION -
90.

PLY NUMBER 9 ORIENTATION -
90.

PLY NUMBER 10 ORIENTATION -
90.

PLY NUMBER 11 ORIENTATION -
0.

PLY NUMBER 12 ORIENTATION -
0.

PLY NUMBER 13 ORIENTATION -
90.

PLY NUMBER 14 ORIENTATION -
90.

PLY NUMBER 15 ORIENTATION -
0.

PLY NUMBER 16 ORIENTATION -
0.

SHOULD EACH PLY HAVE THE SAME SET OF ENGINEERING CONSTANTS? (Y/N)
Y

LONGITUDINAL YOUNGS MODULUS EX -
19.5E6

TRANSVERSE YOUNGS MODULUS EY -
1.32E6

LONGITUDINAL TO TRANSVERSE POISSON RATIO NUXY -
.30

SHEAR MODULUS GXY -
1.01E6

SHEAR MODULUS GXZ -
1.01E6

SHEAR MODULUS GYZ =
0.50E6

110

LONG. THERMAL (HYGRO) COEFF. OF EXP. ALPX(1) =
0.50E-6

TRAN. THERMAL (HYGRO) COEFF. OF EXP. ALPY(1) =
18.E-6

THE FOLLOWING INPUT DESCRIBES THE LOADING
CONDITIONS ON THE PLATE:

TEMPERATURE (HYGRO) DIFFERENCE FROM REF. DELTA T =
-180.

TRANSVERSE PRESSURE LOADING DELTA P =
3.

USE CONTACT LAW? (Y/N)
Y

CONTACT LAW COEFF CON1?
1.E6

CRITICAL STRAIN ENERGY RELEASE PER UNIT AREA =
0.2

RELATIVE GROWTH DIRECTION DA/DB =
0.

THE RELATIVE LOAD MAGNITUDES IN THE PLATE
COORDINATE SYSTEM (1-PRIME, 2-PRIME).
(FOR EXAMPLE, BN1 = 1, BN2 = 0, BN6 = 0
IS A SINGLE LOAD APPLIED IN THE 1-PRIME
DIRECTION.)

BN1 =
1.0

BN2 =
0.

BN6 =
0.

AT HOW MANY LOCATIONS IN THE DELAMINATION DO YOU
WISH STRESS/STRAIN CALCULATIONS?

NLIST =

1

INPUT 1 PAIRS OF COORDINATES:

LISTX(1) =

0.

LISTY(1) =

0.

WOULD YOU LIKE THE STRESSES/STRAINS TO BE CALCULATED
AT THE TOP (T), MIDDLE (M), OR BOTTOM (B) OF EACH PLY?
THE THROUGH-THICKNESS COORDINATE ORIGINATES WITH THE FIRST
PLY OF THE SUBLAMINATE AND PROCEEDS UNTIL THE LAST PLY OF THE
PLATE. THUS, THE BOTTOM OF THE FIRST PLY IS THE SUBLAMINATE
OUTER SURFACE, AND SO ON.

M

THE FOLLOWING INPUT PRESCRIBES WHICH CODE
ANALYSIS OPTIONS WILL BE RUN:

NONLINEAR LOAD-STRAIN HISTORY? (Y/N)

Y

OUTPUT STRAIN FILE NAME?
SAMPLE.STRAIN

OUTPUT STRESS FILE NAME?
SAMPLE.STRESS

MAXIMUM LOAD FOR POSTBUCKLING PLOT?
-3000.

NUMBER OF LOAD INCREMENTS FOR PLOT?
5

CALCULATE POSTBUCKLING GROWTH LOAD? (Y/N)
Y

CALCULATE LINEAR BUCKLING LOAD? (Y/N)
Y

SHOULD THE INPUT DATA BE WRITTEN TO A FILE FOR FUTURE USE? (Y/N)
Y

OUTPUT FILE NAME?
SAMPLE.INPUT

INITIAL Z COORDINATES

PLY	Z
1	0.00e+00
2	0.56e-02
3	0.11e-01
4	0.17e-01
5	0.22e-01
6	0.28e-01
7	0.33e-01
8	0.39e-01
9	0.44e-01
10	0.50e-01
11	0.56e-01
12	0.61e-01
13	0.67e-01
14	0.72e-01
15	0.78e-01
16	0.83e-01
17	0.89e-01

PLANE STRESS REDUCED STIFFNESSES FOR EACH PLY

PLY	QXX	QYY	QXY	QSS	QXZXZ	QYZYZ
1	0.20e+08	0.13e+07	0.40e+06	0.10e+07	0.10e+07	0.50e+06
2	0.20e+08	0.13e+07	0.40e+06	0.10e+07	0.10e+07	0.50e+06
3	0.20e+08	0.13e+07	0.40e+06	0.10e+07	0.10e+07	0.50e+06
4	0.20e+08	0.13e+07	0.40e+06	0.10e+07	0.10e+07	0.50e+06
5	0.20e+08	0.13e+07	0.40e+06	0.10e+07	0.10e+07	0.50e+06
6	0.20e+08	0.13e+07	0.40e+06	0.10e+07	0.10e+07	0.50e+06
7	0.20e+08	0.13e+07	0.40e+06	0.10e+07	0.10e+07	0.50e+06
8	0.20e+08	0.13e+07	0.40e+06	0.10e+07	0.10e+07	0.50e+06
9	0.20e+08	0.13e+07	0.40e+06	0.10e+07	0.10e+07	0.50e+06
10	0.20e+08	0.13e+07	0.40e+06	0.10e+07	0.10e+07	0.50e+06
11	0.20e+08	0.13e+07	0.40e+06	0.10e+07	0.10e+07	0.50e+06
12	0.20e+08	0.13e+07	0.40e+06	0.10e+07	0.10e+07	0.50e+06
13	0.20e+08	0.13e+07	0.40e+06	0.10e+07	0.10e+07	0.50e+06
14	0.20e+08	0.13e+07	0.40e+06	0.10e+07	0.10e+07	0.50e+06
15	0.20e+08	0.13e+07	0.40e+06	0.10e+07	0.10e+07	0.50e+06
16	0.20e+08	0.13e+07	0.40e+06	0.10e+07	0.10e+07	0.50e+06

OFF-AXIS REDUCED STIFFNESSES IN THE PLATE COORDINATES

113

PLY	Q11	Q22	Q12	Q66	Q16	Q26
1	0.20e+08	0.13e+07	0.40e+06	0.10e+07	0.00e+00	0.00e+00
2	0.20e+08	0.13e+07	0.40e+06	0.10e+07	0.00e+00	0.00e+00
3	0.13e+07	0.20e+08	0.40e+06	0.10e+07	0.00e+00	0.00e+00
4	0.13e+07	0.20e+08	0.40e+06	0.10e+07	0.00e+00	0.00e+00
5	0.20e+08	0.13e+07	0.40e+06	0.10e+07	0.00e+00	0.00e+00
6	0.20e+08	0.13e+07	0.40e+06	0.10e+07	0.00e+00	0.00e+00
7	0.13e+07	0.20e+08	0.40e+06	0.10e+07	0.00e+00	0.00e+00
8	0.13e+07	0.20e+08	0.40e+06	0.10e+07	0.00e+00	0.00e+00
9	0.13e+07	0.20e+08	0.40e+06	0.10e+07	0.00e+00	0.00e+00
10	0.13e+07	0.20e+08	0.40e+06	0.10e+07	0.00e+00	0.00e+00
11	0.20e+08	0.13e+07	0.40e+06	0.10e+07	0.00e+00	0.00e+00
12	0.20e+08	0.13e+07	0.40e+06	0.10e+07	0.00e+00	0.00e+00
13	0.13e+07	0.20e+08	0.40e+06	0.10e+07	0.00e+00	0.00e+00
14	0.13e+07	0.20e+08	0.40e+06	0.10e+07	0.00e+00	0.00e+00
15	0.20e+08	0.13e+07	0.40e+06	0.10e+07	0.00e+00	0.00e+00
16	0.20e+08	0.13e+07	0.40e+06	0.10e+07	0.00e+00	0.00e+00

PLY	Q44	Q45	Q55
1	0.50e+06	0.00e+00	0.10e+07
2	0.50e+06	0.00e+00	0.10e+07
3	0.10e+07	0.00e+00	0.50e+06
4	0.10e+07	0.00e+00	0.50e+06
5	0.50e+06	0.00e+00	0.10e+07
6	0.50e+06	0.00e+00	0.10e+07
7	0.10e+07	0.00e+00	0.50e+06
8	0.10e+07	0.00e+00	0.50e+06
9	0.10e+07	0.00e+00	0.50e+06
10	0.10e+07	0.00e+00	0.50e+06
11	0.50e+06	0.00e+00	0.10e+07
12	0.50e+06	0.00e+00	0.10e+07
13	0.10e+07	0.00e+00	0.50e+06
14	0.10e+07	0.00e+00	0.50e+06
15	0.50e+06	0.00e+00	0.10e+07
16	0.50e+06	0.00e+00	0.10e+07

OFF-AXIS REDUCED STIFFNESSES IN THE SUBLAMINATE COORDINATES

PLY	Q11	Q22	Q12	Q66	Q16	Q26
1	0.20e+08	0.13e+07	0.40e+06	0.10e+07	0.00e+00	0.00e+00
2	0.20e+08	0.13e+07	0.40e+06	0.10e+07	0.00e+00	0.00e+00
3	0.13e+07	0.20e+08	0.40e+06	0.10e+07	0.00e+00	0.00e+00
4	0.13e+07	0.20e+08	0.40e+06	0.10e+07	0.00e+00	0.00e+00

PLY	Q44	Q45	Q55
1	0.50e+06	0.00e+00	0.10e+07
2	0.50e+06	0.00e+00	0.10e+07
3	0.10e+07	0.00e+00	0.50e+06
4	0.10e+07	0.00e+00	0.50e+06

LAMINATE STIFFNESSES FOR THE PLATE

114

A11	A22	A12	A66	A16	A26
0.93e+06	0.93e+06	0.35e+05	0.90e+05	0.00e+00	0.00e+00

A44	A45	A55
0.67e+05	0.00e+00	0.67e+05

B11	B22	B12	B66	B16	B26
0.73e-11	0.00e+00	-.68e-12	0.45e-12	0.00e+00	0.00e+00

D44	D45	D55
0.39e+02	0.00e+00	0.50e+02

F11	F22	F12	F66	F16	F26
0.11e+01	0.36e+00	0.28e-01	0.70e-01	0.00e+00	0.00e+00

F44	F45	F55
0.42e-01	0.00e+00	0.63e-01

H11	H22	H12	H66	H16	H26
0.17e-02	0.36e-03	0.39e-04	0.99e-04	0.00e+00	0.00e+00

LAMINATE STIFFNESSES FOR THE SUBLAMINATE

A11	A22	A12	A66	A16	A26
0.23e+06	0.23e+06	0.89e+04	0.22e+05	0.00e+00	0.00e+00

A44	A45	A55
0.17e+05	0.00e+00	0.17e+05

B11	B22	B12	B66	B16	B26
-.11e+04	0.11e+04	-.11e-12	-.28e-12	0.00e+00	0.00e+00

D44	D45	D55
0.69e+00	0.00e+00	0.69e+00

F11	F22	F12	F66	F16	F26
0.71e-03	0.71e-03	0.27e-04	0.69e-04	0.00e+00	0.00e+00

115

F44	F45	F55
0.51e-04	0.00e+00	0.51e-04

H11	H22	H12	H66	H16	H26
0.63e-07	0.63e-07	0.24e-08	0.61e-08	0.00e+00	0.00e+00

LINEAR BUCKLING LOAD CALCULATION:

THE LINEAR BUCKLING LOAD IS -0.67792e+03

GROWTH LOAD CALCULATION:

WARNING: CONTACT BETWEEN SUBLAMINATE AND PLATE

WARNING: CONTACT BETWEEN SUBLAMINATE AND PLATE

WARNING: CONTACT BETWEEN SUBLAMINATE AND PLATE

WARNING: CONTACT BETWEEN SUBLAMINATE AND PLATE

WARNING: CONTACT BETWEEN SUBLAMINATE AND PLATE

WARNING: CONTACT BETWEEN SUBLAMINATE AND PLATE

WARNING: CONTACT BETWEEN SUBLAMINATE AND PLATE

THE GROWTH LOAD IS -0.17666e+04 ITER = 5

STRESSES AND STRAINS AT (X,Y) = (0.000e+00, 0.000e+00)
FOR LOAD N = -0.17666e+04

116

OFF-AXIS STRESSES IN THE SUBLAMINATE FRAME

PLY	S1	S2	S3	S4	S5	S6
1	-.17e+05	0.73e+04	0.00e+00	0.00e+00	0.00e+00	0.00e+00
2	-.38e+05	0.57e+04	0.00e+00	0.00e+00	0.00e+00	0.00e+00
3	0.46e+03	0.18e+05	0.00e+00	0.00e+00	0.00e+00	0.00e+00
4	-.13e+04	0.22e+03	0.00e+00	0.00e+00	0.00e+00	0.00e+00

OFF-AXIS STRAINS IN THE SUBLAMINATE FRAME

PLY	E1	E2	E3	E4	E5	E6
1	-.10e-02	0.58e-02	0.00e+00	0.00e+00	0.00e+00	0.00e+00
2	-.20e-02	0.49e-02	0.00e+00	0.00e+00	0.00e+00	0.00e+00
3	0.76e-04	0.90e-03	0.00e+00	0.00e+00	0.00e+00	0.00e+00
4	-.96e-03	0.31e-04	0.00e+00	0.00e+00	0.00e+00	0.00e+00

ON-AXIS STRESSES IN THE PLY FRAME

PLY	S1	S2	S3	S4	S5	S6
1	-.17e+05	0.73e+04	0.00e+00	0.00e+00	0.00e+00	0.00e+00
2	-.38e+05	0.57e+04	0.00e+00	0.00e+00	0.00e+00	0.00e+00
3	0.18e+05	0.46e+03	0.00e+00	0.00e+00	0.00e+00	0.00e+00
4	0.22e+03	-.13e+04	0.00e+00	0.00e+00	0.00e+00	0.00e+00

ON-AXIS STRAINS IN THE PLY FRAME

PLY	E1	E2	E3	E4	E5	E6
1	-.10e-02	0.58e-02	0.00e+00	0.00e+00	0.00e+00	0.00e+00
2	-.20e-02	0.49e-02	0.00e+00	0.00e+00	0.00e+00	0.00e+00
3	0.90e-03	0.76e-04	0.00e+00	0.00e+00	0.00e+00	0.00e+00
4	0.31e-04	-.96e-03	0.00e+00	0.00e+00	0.00e+00	0.00e+00

OFF-AXIS STRESSES IN THE PLATE FRAME

PLY	S1	S2	S3	S4	S5	S6
1	-.17e+05	0.73e+04	0.00e+00	0.00e+00	0.00e+00	0.00e+00
2	-.38e+05	0.57e+04	0.00e+00	0.00e+00	0.00e+00	0.00e+00
3	0.46e+03	0.18e+05	0.00e+00	0.00e+00	0.00e+00	0.00e+00
4	-.13e+04	0.22e+03	0.00e+00	0.00e+00	0.00e+00	0.00e+00

PLY	E1	E2	E3	E4	E5	E6
1	-.75e-03	0.29e-02	0.00e+00	0.00e+00	0.00e+00	0.00e+00
2	-.18e-02	0.20e-02	0.00e+00	0.00e+00	0.00e+00	0.00e+00
3	-.28e-02	0.11e-02	0.00e+00	0.00e+00	0.00e+00	0.00e+00
4	-.39e-02	0.28e-03	0.00e+00	0.00e+00	0.00e+00	0.00e+00

NONLINEAR LOAD-STRAIN HISTORY CALCULATION:

STRESSES AND STRAINS AT (X,Y) = (0.000e+00, 0.000e+00)
FOR LOAD N = 0.00000e+00

OFF-AXIS STRESSES IN THE SUBLAMINATE FRAME

PLY	S1	S2	S3	S4	S5	S6
1	-.37e+04	0.38e+04	0.00e+00	0.00e+00	0.00e+00	0.00e+00
2	-.38e+04	0.38e+04	0.00e+00	0.00e+00	0.00e+00	0.00e+00
3	0.38e+04	-.37e+04	0.00e+00	0.00e+00	0.00e+00	0.00e+00
4	0.38e+04	-.38e+04	0.00e+00	0.00e+00	0.00e+00	0.00e+00

OFF-AXIS STRAINS IN THE SUBLAMINATE FRAME

PLY	E1	E2	E3	E4	E5	E6
1	-.25e-03	0.29e-02	0.00e+00	0.00e+00	0.00e+00	0.00e+00
2	-.25e-03	0.29e-02	0.00e+00	0.00e+00	0.00e+00	0.00e+00
3	0.29e-02	-.25e-03	0.00e+00	0.00e+00	0.00e+00	0.00e+00
4	0.29e-02	-.25e-03	0.00e+00	0.00e+00	0.00e+00	0.00e+00

ON-AXIS STRESSES IN THE PLY FRAME

PLY	S1	S2	S3	S4	S5	S6
1	-.37e+04	0.38e+04	0.00e+00	0.00e+00	0.00e+00	0.00e+00
2	-.38e+04	0.38e+04	0.00e+00	0.00e+00	0.00e+00	0.00e+00
3	-.37e+04	0.38e+04	0.00e+00	0.00e+00	0.00e+00	0.00e+00
4	-.38e+04	0.38e+04	0.00e+00	0.00e+00	0.00e+00	0.00e+00

ON-AXIS STRAINS IN THE PLY FRAME

PLY	E1	E2	E3	E4	E5	E6
1	-.25e-03	0.29e-02	0.00e+00	0.00e+00	0.00e+00	0.00e+00
2	-.25e-03	0.29e-02	0.00e+00	0.00e+00	0.00e+00	0.00e+00
3	-.25e-03	0.29e-02	0.00e+00	0.00e+00	0.00e+00	0.00e+00
4	-.25e-03	0.29e-02	0.00e+00	0.00e+00	0.00e+00	0.00e+00

OFF-AXIS STRESSES IN THE PLATE FRAME

118

PLY	S1	S2	S3	S4	S5	S6
1	-.37e+04	0.38e+04	0.00e+00	0.00e+00	0.00e+00	0.00e+00
2	-.38e+04	0.38e+04	0.00e+00	0.00e+00	0.00e+00	0.00e+00
3	0.38e+04	-.37e+04	0.00e+00	0.00e+00	0.00e+00	0.00e+00
4	0.38e+04	-.38e+04	0.00e+00	0.00e+00	0.00e+00	0.00e+00

OFF-AXIS MECHANICAL STRAINS IN THE PLATE FRAME

PLY	E1	E2	E3	E4	E5	E6
1	0.11e-06	0.80e-06	0.00e+00	0.00e+00	0.00e+00	0.00e+00
2	-.80e-07	0.47e-06	0.00e+00	0.00e+00	0.00e+00	0.00e+00
3	-.27e-06	0.13e-06	0.00e+00	0.00e+00	0.00e+00	0.00e+00
4	-.47e-06	-.21e-06	0.00e+00	0.00e+00	0.00e+00	0.00e+00

STRESSES AND STRAINS AT (X,Y) = (0.000e+00, 0.000e+00)
 FOR LOAD N = -0.60000e+03

OFF-AXIS STRESSES IN THE SUBLAMINATE FRAME

PLY	S1	S2	S3	S4	S5	S6
1	-.16e+05	0.35e+04	0.00e+00	0.00e+00	0.00e+00	0.00e+00
2	-.16e+05	0.35e+04	0.00e+00	0.00e+00	0.00e+00	0.00e+00
3	0.29e+04	-.35e+04	0.00e+00	0.00e+00	0.00e+00	0.00e+00
4	0.29e+04	-.35e+04	0.00e+00	0.00e+00	0.00e+00	0.00e+00

OFF-AXIS STRAINS IN THE SUBLAMINATE FRAME

PLY	E1	E2	E3	E4	E5	E6
1	-.89e-03	0.29e-02	0.00e+00	0.00e+00	0.00e+00	0.00e+00
2	-.90e-03	0.29e-02	0.00e+00	0.00e+00	0.00e+00	0.00e+00
3	0.23e-02	-.23e-03	0.00e+00	0.00e+00	0.00e+00	0.00e+00
4	0.23e-02	-.23e-03	0.00e+00	0.00e+00	0.00e+00	0.00e+00

ON-AXIS STRESSES IN THE PLY FRAME

PLY	S1	S2	S3	S4	S5	S6
1	-.16e+05	0.35e+04	0.00e+00	0.00e+00	0.00e+00	0.00e+00
2	-.16e+05	0.35e+04	0.00e+00	0.00e+00	0.00e+00	0.00e+00
3	-.35e+04	0.29e+04	0.00e+00	0.00e+00	0.00e+00	0.00e+00
4	-.35e+04	0.29e+04	0.00e+00	0.00e+00	0.00e+00	0.00e+00

ON-AXIS STRAINS IN THE PLY FRAME

119

PLY	E1	E2	E3	E4	E5	E6
1	-.89e-03	0.29e-02	0.00e+00	0.00e+00	0.00e+00	0.00e+00
2	-.90e-03	0.29e-02	0.00e+00	0.00e+00	0.00e+00	0.00e+00
3	-.23e-03	0.23e-02	0.00e+00	0.00e+00	0.00e+00	0.00e+00
4	-.23e-03	0.23e-02	0.00e+00	0.00e+00	0.00e+00	0.00e+00

OFF-AXIS STRESSES IN THE PLATE FRAME

PLY	S1	S2	S3	S4	S5	S6
1	-.16e+05	0.35e+04	0.00e+00	0.00e+00	0.00e+00	0.00e+00
2	-.16e+05	0.35e+04	0.00e+00	0.00e+00	0.00e+00	0.00e+00
3	0.29e+04	-.35e+04	0.00e+00	0.00e+00	0.00e+00	0.00e+00
4	0.29e+04	-.35e+04	0.00e+00	0.00e+00	0.00e+00	0.00e+00

OFF-AXIS MECHANICAL STRAINS IN THE PLATE FRAME

PLY	E1	E2	E3	E4	E5	E6
1	-.64e-03	0.25e-04	0.00e+00	0.00e+00	0.00e+00	0.00e+00
2	-.64e-03	0.25e-04	0.00e+00	0.00e+00	0.00e+00	0.00e+00
3	-.65e-03	0.25e-04	0.00e+00	0.00e+00	0.00e+00	0.00e+00
4	-.65e-03	0.24e-04	0.00e+00	0.00e+00	0.00e+00	0.00e+00

STRESSES AND STRAINS AT (X,Y) = (0.000e+00, 0.000e+00)
FOR LOAD N = -0.12000e+04

OFF-AXIS STRESSES IN THE SUBLAMINATE FRAME

PLY	S1	S2	S3	S4	S5	S6
1	-.29e+05	0.33e+04	0.00e+00	0.00e+00	0.00e+00	0.00e+00
2	-.29e+05	0.33e+04	0.00e+00	0.00e+00	0.00e+00	0.00e+00
3	0.21e+04	-.33e+04	0.00e+00	0.00e+00	0.00e+00	0.00e+00
4	0.21e+04	-.33e+04	0.00e+00	0.00e+00	0.00e+00	0.00e+00

OFF-AXIS STRAINS IN THE SUBLAMINATE FRAME

PLY	E1	E2	E3	E4	E5	E6
1	-.15e-02	0.29e-02	0.00e+00	0.00e+00	0.00e+00	0.00e+00
2	-.15e-02	0.29e-02	0.00e+00	0.00e+00	0.00e+00	0.00e+00
3	0.16e-02	-.20e-03	0.00e+00	0.00e+00	0.00e+00	0.00e+00
4	0.16e-02	-.20e-03	0.00e+00	0.00e+00	0.00e+00	0.00e+00

ON-AXIS STRESSES IN THE PLY FRAME

120

PLY	S1	S2	S3	S4	S5	S6
1	-.29e+05	0.33e+04	0.00e+00	0.00e+00	0.00e+00	0.00e+00
2	-.29e+05	0.33e+04	0.00e+00	0.00e+00	0.00e+00	0.00e+00
3	-.33e+04	0.21e+04	0.00e+00	0.00e+00	0.00e+00	0.00e+00
4	-.33e+04	0.21e+04	0.00e+00	0.00e+00	0.00e+00	0.00e+00

ON-AXIS STRAINS IN THE PLY FRAME

PLY	E1	E2	E3	E4	E5	E6
1	-.15e-02	0.29e-02	0.00e+00	0.00e+00	0.00e+00	0.00e+00
2	-.15e-02	0.29e-02	0.00e+00	0.00e+00	0.00e+00	0.00e+00
3	-.20e-03	0.16e-02	0.00e+00	0.00e+00	0.00e+00	0.00e+00
4	-.20e-03	0.16e-02	0.00e+00	0.00e+00	0.00e+00	0.00e+00

OFF-AXIS STRESSES IN THE PLATE FRAME

PLY	S1	S2	S3	S4	S5	S6
1	-.29e+05	0.33e+04	0.00e+00	0.00e+00	0.00e+00	0.00e+00
2	-.29e+05	0.33e+04	0.00e+00	0.00e+00	0.00e+00	0.00e+00
3	0.21e+04	-.33e+04	0.00e+00	0.00e+00	0.00e+00	0.00e+00
4	0.21e+04	-.33e+04	0.00e+00	0.00e+00	0.00e+00	0.00e+00

OFF-AXIS MECHANICAL STRAINS IN THE PLATE FRAME

PLY	E1	E2	E3	E4	E5	E6
1	-.13e-02	0.50e-04	0.00e+00	0.00e+00	0.00e+00	0.00e+00
2	-.13e-02	0.50e-04	0.00e+00	0.00e+00	0.00e+00	0.00e+00
3	-.13e-02	0.49e-04	0.00e+00	0.00e+00	0.00e+00	0.00e+00
4	-.13e-02	0.49e-04	0.00e+00	0.00e+00	0.00e+00	0.00e+00

WARNING: CONTACT BETWEEN SUBLAMINATE AND PLATE

STRESSES AND STRAINS AT (X,Y) = (0.000e+00, 0.000e+00)
 FOR LOAD N = -0.18000e+04

OFF-AXIS STRESSES IN THE SUBLAMINATE FRAME

PLY	S1	S2	S3	S4	S5	S6
1	-.17e+05	0.74e+04	0.00e+00	0.00e+00	0.00e+00	0.00e+00
2	-.38e+05	0.58e+04	0.00e+00	0.00e+00	0.00e+00	0.00e+00
3	0.41e+03	0.18e+05	0.00e+00	0.00e+00	0.00e+00	0.00e+00
4	-.13e+04	0.67e+03	0.00e+00	0.00e+00	0.00e+00	0.00e+00

OFF-AXIS STRAINS IN THE SUBLAMINATE FRAME

121

PLY	E1	E2	E3	E4	E5	E6
1	-.10e-02	0.58e-02	0.00e+00	0.00e+00	0.00e+00	0.00e+00
2	-.21e-02	0.50e-02	0.00e+00	0.00e+00	0.00e+00	0.00e+00
3	0.30e-04	0.93e-03	0.00e+00	0.00e+00	0.00e+00	0.00e+00
4	-.10e-02	0.55e-04	0.00e+00	0.00e+00	0.00e+00	0.00e+00

ON-AXIS STRESSES IN THE PLY FRAME

PLY	S1	S2	S3	S4	S5	S6
1	-.17e+05	0.74e+04	0.00e+00	0.00e+00	0.00e+00	0.00e+00
2	-.38e+05	0.58e+04	0.00e+00	0.00e+00	0.00e+00	0.00e+00
3	0.18e+05	0.41e+03	0.00e+00	0.00e+00	0.00e+00	0.00e+00
4	0.67e+03	-.13e+04	0.00e+00	0.00e+00	0.00e+00	0.00e+00

ON-AXIS STRAINS IN THE PLY FRAME

PLY	E1	E2	E3	E4	E5	E6
1	-.10e-02	0.58e-02	0.00e+00	0.00e+00	0.00e+00	0.00e+00
2	-.21e-02	0.50e-02	0.00e+00	0.00e+00	0.00e+00	0.00e+00
3	0.93e-03	0.30e-04	0.00e+00	0.00e+00	0.00e+00	0.00e+00
4	0.55e-04	-.10e-02	0.00e+00	0.00e+00	0.00e+00	0.00e+00

OFF-AXIS STRESSES IN THE PLATE FRAME

PLY	S1	S2	S3	S4	S5	S6
1	-.17e+05	0.74e+04	0.00e+00	0.00e+00	0.00e+00	0.00e+00
2	-.38e+05	0.58e+04	0.00e+00	0.00e+00	0.00e+00	0.00e+00
3	0.41e+03	0.18e+05	0.00e+00	0.00e+00	0.00e+00	0.00e+00
4	-.13e+04	0.67e+03	0.00e+00	0.00e+00	0.00e+00	0.00e+00

OFF-AXIS MECHANICAL STRAINS IN THE PLATE FRAME

PLY	E1	E2	E3	E4	E5	E6
1	-.75e-03	0.29e-02	0.00e+00	0.00e+00	0.00e+00	0.00e+00
2	-.18e-02	0.21e-02	0.00e+00	0.00e+00	0.00e+00	0.00e+00
3	-.29e-02	0.12e-02	0.00e+00	0.00e+00	0.00e+00	0.00e+00
4	-.39e-02	0.31e-03	0.00e+00	0.00e+00	0.00e+00	0.00e+00

WARNING: CONTACT BETWEEN SUBLAMINATE AND PLATE

STRESSES AND STRAINS AT (X,Y) = (0.000e+00, 0.000e+00)
FOR LOAD N = -0.24000e+04

122

OFF-AXIS STRESSES IN THE SUBLAMINATE FRAME

PLY	S1	S2	S3	S4	S5	S6
1	-.19e+05	0.85e+04	0.00e+00	0.00e+00	0.00e+00	0.00e+00
2	-.47e+05	0.66e+04	0.00e+00	0.00e+00	0.00e+00	0.00e+00
3	-.38e+03	0.30e+05	0.00e+00	0.00e+00	0.00e+00	0.00e+00
4	-.27e+04	0.92e+04	0.00e+00	0.00e+00	0.00e+00	0.00e+00

OFF-AXIS STRAINS IN THE SUBLAMINATE FRAME

PLY	E1	E2	E3	E4	E5	E6
1	-.11e-02	0.67e-02	0.00e+00	0.00e+00	0.00e+00	0.00e+00
2	-.25e-02	0.57e-02	0.00e+00	0.00e+00	0.00e+00	0.00e+00
3	-.74e-03	0.15e-02	0.00e+00	0.00e+00	0.00e+00	0.00e+00
4	-.22e-02	0.51e-03	0.00e+00	0.00e+00	0.00e+00	0.00e+00

ON-AXIS STRESSES IN THE PLY FRAME

PLY	S1	S2	S3	S4	S5	S6
1	-.19e+05	0.85e+04	0.00e+00	0.00e+00	0.00e+00	0.00e+00
2	-.47e+05	0.66e+04	0.00e+00	0.00e+00	0.00e+00	0.00e+00
3	0.30e+05	-.38e+03	0.00e+00	0.00e+00	0.00e+00	0.00e+00
4	0.92e+04	-.27e+04	0.00e+00	0.00e+00	0.00e+00	0.00e+00

ON-AXIS STRAINS IN THE PLY FRAME

PLY	E1	E2	E3	E4	E5	E6
1	-.11e-02	0.67e-02	0.00e+00	0.00e+00	0.00e+00	0.00e+00
2	-.25e-02	0.57e-02	0.00e+00	0.00e+00	0.00e+00	0.00e+00
3	0.15e-02	-.74e-03	0.00e+00	0.00e+00	0.00e+00	0.00e+00
4	0.51e-03	-.22e-02	0.00e+00	0.00e+00	0.00e+00	0.00e+00

OFF-AXIS STRESSES IN THE PLATE FRAME

PLY	S1	S2	S3	S4	S5	S6
1	-.19e+05	0.85e+04	0.00e+00	0.00e+00	0.00e+00	0.00e+00
2	-.47e+05	0.66e+04	0.00e+00	0.00e+00	0.00e+00	0.00e+00
3	-.38e+03	0.30e+05	0.00e+00	0.00e+00	0.00e+00	0.00e+00
4	-.27e+04	0.92e+04	0.00e+00	0.00e+00	0.00e+00	0.00e+00

OFF-AXIS MECHANICAL STRAINS IN THE PLATE FRAME

123

PLY	E1	E2	E3	E4	E5	E6
1	-.84e-03	0.38e-02	0.00e+00	0.00e+00	0.00e+00	0.00e+00
2	-.22e-02	0.28e-02	0.00e+00	0.00e+00	0.00e+00	0.00e+00
3	-.36e-02	0.18e-02	0.00e+00	0.00e+00	0.00e+00	0.00e+00
4	-.51e-02	0.76e-03	0.00e+00	0.00e+00	0.00e+00	0.00e+00

WARNING: CONTACT BETWEEN SUBLAMINATE AND PLATE

STRESSES AND STRAINS AT (X,Y) = (0.000e+00, 0.000e+00)
 FOR LOAD N = -0.30000e+04

OFF-AXIS STRESSES IN THE SUBLAMINATE FRAME

PLY	S1	S2	S3	S4	S5	S6
1	-.21e+05	0.93e+04	0.00e+00	0.00e+00	0.00e+00	0.00e+00
2	-.55e+05	0.72e+04	0.00e+00	0.00e+00	0.00e+00	0.00e+00
3	-.11e+04	0.40e+05	0.00e+00	0.00e+00	0.00e+00	0.00e+00
4	-.38e+04	0.18e+05	0.00e+00	0.00e+00	0.00e+00	0.00e+00

OFF-AXIS STRAINS IN THE SUBLAMINATE FRAME

PLY	E1	E2	E3	E4	E5	E6
1	-.12e-02	0.74e-02	0.00e+00	0.00e+00	0.00e+00	0.00e+00
2	-.29e-02	0.63e-02	0.00e+00	0.00e+00	0.00e+00	0.00e+00
3	-.15e-02	0.21e-02	0.00e+00	0.00e+00	0.00e+00	0.00e+00
4	-.32e-02	0.99e-03	0.00e+00	0.00e+00	0.00e+00	0.00e+00

ON-AXIS STRESSES IN THE PLY FRAME

PLY	S1	S2	S3	S4	S5	S6
1	-.21e+05	0.93e+04	0.00e+00	0.00e+00	0.00e+00	0.00e+00
2	-.55e+05	0.72e+04	0.00e+00	0.00e+00	0.00e+00	0.00e+00
3	0.40e+05	-.11e+04	0.00e+00	0.00e+00	0.00e+00	0.00e+00
4	0.18e+05	-.38e+04	0.00e+00	0.00e+00	0.00e+00	0.00e+00

ON-AXIS STRAINS IN THE PLY FRAME

PLY	E1	E2	E3	E4	E5	E6
1	-.12e-02	0.74e-02	0.00e+00	0.00e+00	0.00e+00	0.00e+00
2	-.29e-02	0.63e-02	0.00e+00	0.00e+00	0.00e+00	0.00e+00
3	0.21e-02	-.15e-02	0.00e+00	0.00e+00	0.00e+00	0.00e+00
4	0.99e-03	-.32e-02	0.00e+00	0.00e+00	0.00e+00	0.00e+00

OFF-AXIS STRESSES IN THE PLATE FRAME

124

PLY	S1	S2	S3	S4	S5	S6
1	-.21e+05	0.93e+04	0.00e+00	0.00e+00	0.00e+00	0.00e+00
2	-.55e+05	0.72e+04	0.00e+00	0.00e+00	0.00e+00	0.00e+00
3	-.11e+04	0.40e+05	0.00e+00	0.00e+00	0.00e+00	0.00e+00
4	-.38e+04	0.18e+05	0.00e+00	0.00e+00	0.00e+00	0.00e+00

OFF-AXIS MECHANICAL STRAINS IN THE PLATE FRAME

PLY	E1	E2	E3	E4	E5	E6
1	-.96e-03	0.45e-02	0.00e+00	0.00e+00	0.00e+00	0.00e+00
2	-.27e-02	0.34e-02	0.00e+00	0.00e+00	0.00e+00	0.00e+00
3	-.44e-02	0.23e-02	0.00e+00	0.00e+00	0.00e+00	0.00e+00
4	-.61e-02	0.12e-02	0.00e+00	0.00e+00	0.00e+00	0.00e+00

THE LINEAR BUCKLING LOAD OF THE DELAMINATION IS -0.67792e+03

THE GROWTH LOAD OF THE DELAMINATION IS -0.17666e+04

Appendix H

Total Potential Energy Change of an Isotropic Plate

The change in the total potential energy G of an isotropic, circular plate subjected to a transverse pressure q_0 with respect to a change in the area $A = \pi a^2$ of the plate is

$$G = -\frac{d\Pi}{da} \frac{1}{2\pi a} \quad (H.1)$$

where the total potential energy Π is calculated from

$$\Pi = \frac{1}{2} \int_0^{2\pi} \int_{-\frac{h}{2}}^{\frac{h}{2}} \int_0^a (\sigma_r \epsilon_r + \sigma_t \epsilon_t) r dr dz d\theta - \int_0^{2\pi} \int_0^a q_0 w r dr d\theta \quad (H.2)$$

The plate thickness is h , the radius a , and (r, θ, z) are cylindrical coordinates. The transverse displacement of the plate is w . The radial and circumferential stresses, respectively, are calculated as

$$\sigma_r = \frac{N_r}{h} - 12D \frac{z}{h^3} \left(\frac{d^2 w}{dr^2} + \nu \frac{1}{r} \frac{dw}{dr} \right) \quad (H.3)$$

$$\sigma_t = \frac{N_t}{h} - 12D \frac{z}{h^3} \left(\nu \frac{d^2 w}{dr^2} + \frac{1}{r} \frac{dw}{dr} \right) \quad (H.4)$$

where N_r and N_t are the radial and circumferential stress resultants and the bending stiffness D of the plate is

$$D = \frac{Eh^3}{12(1 - \nu^2)} \quad (H.5)$$

E is Young's modulus, and ν is Poisson's ratio. The radial and circumferential strains, respectively, are

$$\epsilon_r = \frac{du_r}{dr} + 0.5\left(\frac{dw}{dr}\right)^2 - z\frac{d^2w}{dr^2} \quad (H.6)$$

$$\epsilon_t = \frac{u_r}{r} - \frac{z}{r}\frac{dw}{dr} \quad (H.7)$$

where u_r is the radial displacement of the plate. The circumferential stress resultant N_t is related to the radial stress resultant by

$$N_t = \frac{d}{dr}(rN_r) \quad (H.8)$$

and the radial displacement u_r is related to the radial stress resultant by

$$u_r = \frac{r}{Eh}\left(r\frac{dN_r}{dr} + (1 - \nu)N_r\right) \quad (H.9)$$

A perturbation solution is developed by Chia [41] by expanding the transverse displacement w , the pressure q_o , and the radial stress resultant N_r in terms of the displacement at the center of the plate w_o . The transverse displacement is expanded as

$$w = h\left(w_1\frac{w_o}{h} + w_3\left(\frac{w_o}{h}\right)^3\right) \quad (H.10)$$

where

$$w_1 = \xi^2 \quad (H.11)$$

$$w_3 = \frac{1}{360}(1 - \nu^2)\xi^2(1 - \xi)\left(\frac{83 - 43\nu}{1 - \nu} + 23\xi + 8\xi^2 + 2\xi^3\right) \quad (H.12)$$

and

$$\xi = 1 - \frac{r^2}{a^2} \quad (H.13)$$

The radial stress resultant is expanded in terms of the center displacement as

$$N_r = \frac{Eh^3}{a^2}\left(s_2\left(\frac{w_o}{h}\right)^2 + s_4\left(\frac{w_o}{h}\right)^4\right) \quad (H.14)$$

where

$$s_2 = \frac{1}{6}\left(\frac{2}{1 - \nu} + \xi + \xi^2 + \xi^3\right) \quad (H.15)$$

and

$$s_4 = \frac{(1 - \nu^2)}{7560}\left(\frac{160 - 104\nu}{1 - \nu^2} + \frac{80 - 52\nu}{1 - \nu}(\xi + \xi^2 + \xi^3) - \frac{501 - 249\nu}{1 - \nu}\xi^4 - 123\xi^5 - 39\xi^6 - 9\xi^7\right) \quad (H.16)$$

The transverse pressure load is expanded in terms of the center displacement as

$$q_o = \frac{16Eh^4}{3(1 - \nu^2)a^4}\left(\frac{w_o}{h} + \frac{1}{360}(1 + \nu)(173 - 73\nu)\left(\frac{w_o}{h}\right)^3\right) \quad (H.17)$$

For a Poisson's ratio $\nu = 0.3$, the change in the total potential energy (Eq. H.1) was evaluated as a function of the normalized center displacement as

$$\frac{Ga^4}{Eh^5} = 2.930\left(\frac{w_o}{h}\right)^2 + 1.586\left(\frac{w_o}{h}\right)^4 + 0.1279\left(\frac{w_o}{h}\right)^6 + 0.003048\left(\frac{w_o}{h}\right)^8 + 8.0064E-5\left(\frac{w_o}{h}\right)^{10} \quad (H.18)$$

Similarly, the transverse pressure (Eq. H.17) was evaluated as

$$\frac{q_o a^4}{E h^4} = 5.860 \left(\frac{w_o}{h} \right) + 3.657 \left(\frac{w_o}{h} \right)^3 \quad (H.19)$$

These equations were then parametrically evaluated to determine the relationship between the applied transverse pressure and the change in total potential energy.

Appendix I

Ultrasonic Nondestructive Examination

Every specimen in the experimental portion of this dissertation was ultrasonically examined before and after compression testing. The ultrasonic scanning, commonly known as C-scanning, was performed in the Structures and Composites Laboratory on equipment built and programmed by the author. The C-scans provided a planar map of each specimen showing the lateral extent of delamination and, in particular, the depth in number of plies of the delamination at every point. The data were used before testing to precisely locate the teflon implants to apply strain gauges to the specimen surface, and to map the extent of delamination growth after testing.

The C-scan equipment consists of: (a) an ultrasonic flaw detector (Krautkramer Branson USL 48), (b) an immersion tank and specimen positioning fixtures, (c) a bridge with stepper motors to drive the ultrasonic transducers back and forth over the specimen (Trienco Model 705), and (d) a computer to perform data acquisition and control functions as well as to display the color output (IBM PC/AT with IBM data acquisition card). The C-scan was operated by a FORTRAN computer program that controlled the movement of the transducer bridge, collected the data, and converted the data into a graphical display.

The C-scan operation is based on generating a pulse of ultrasonic sound by a

transducer. The pulse travels through a coupling medium (water) to the specimen. At every interface between two dissimilar media, part of the signal will be reflected and part transmitted. Thus, there will be reflected signals from the top and bottom surfaces of the specimen as well as from any delaminated surfaces in between. In the pulse/echo method, the first signal returning from the top surface is used as a trigger and the time for subsequent signals to arrive is measured. Knowing the speed of sound in the material, the time of flight measurements are converted to thicknesses. The thicknesses are finally displayed as depths to the delamination at that point or, if there is no delamination, as the overall thickness of the specimen.

Appendix J

Uncertainty Analysis

§J.1 Experimental Uncertainty

Uncertainty in the experimental data occurs due to variations in specimen fabrication, preparation, strain gauging, testing, data acquisition, and data reduction. The purpose of this analysis is to estimate the uncertainty in a measured load associated with a given value of strain. Each experiment had four strain gauges mounted away from the delamination whose purpose was to measure the far field strain (gauges 2, 3, 4, and 9, Figure 6-2, Chapter 6). The response of these gauges should nominally be the same for a given experiment series, and thus may serve as replicate strain readings. For example, Figure J-1 shows the measured load versus strain from gauge 3 for each of the four experiments in Series 5.

The method used to calculate the experimental uncertainty is to first fit a linear least squares regression line to the data, and then to estimate the experimental uncertainty from the differences, or residuals, between the regression line and each data point [55, 56]. The estimate of the data experimental uncertainty, σ_d , is calculated from

$$\sigma_d^2 = \frac{N_i N_i - \frac{(N_i \epsilon_i)^2}{\epsilon_i \epsilon_i}}{n - 1} \quad (J.1)$$

where σ_ϵ is one standard deviation, N_i is the applied load per unit specimen width corresponding to a single data point, ϵ_i the associated strain, and n the number of data points (repeated subscripts imply summation). The estimated experimental uncertainties for gauges 2, 3, and 4 from each test series are summarized in Table J-1. Gauge 9 was not included because it was transversely oriented, and therefore substantively different from gauge 1, the gauge of primary interest in the delamination studies. The estimated uncertainty for Test Series 4 gauge 3 is very large. One gauge from this series was clearly different from the others, indicating a systematic and not random variation.

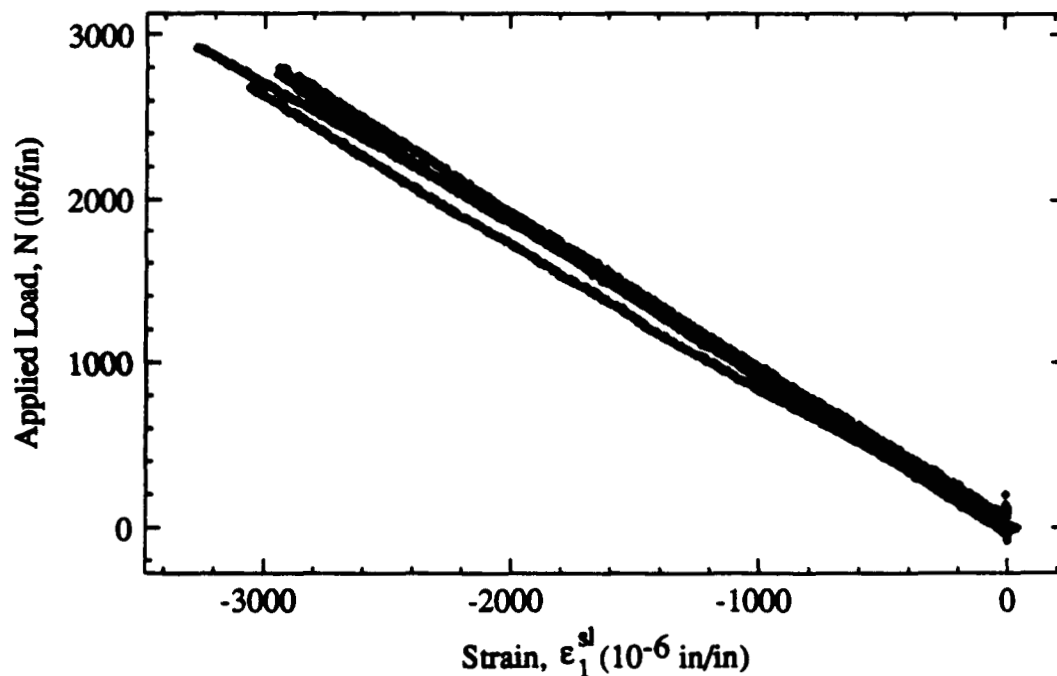


Figure J-1 Load versus strain from each gauge 3 of Experiment Series 5.

Table J-1 Estimated Standard Deviation σ_d in the Data

	Gauge 2	Gauge 3	Gauge 4
Test Series 4	43.7	604.	52.5
Test Series 5	57.6	63.8	68.5
Test Series 6	150.	126.	142.

§J.2 Prediction Uncertainty

Random uncertainty in the model predictions is due to errors in the input data propagating through the code. The response surface method may be used to estimate this uncertainty [57, 58, 59]. The model predictions N are evaluated for different combinations of perturbations to the input data x_i , termed the experimental design, where the perturbations are plus or minus one standard deviation σ_i of the input variable about its nominal mean value μ_i . The model responses so generated are used to fit a truncated Taylor's series expansion in the input variables, which is then used to estimate the prediction uncertainty. The Taylor's series expansion of the model is

$$N(x_i) = N(\mu_i) + \frac{\partial N}{\partial x_i}(x_i - \mu_i) + \dots \quad (J.2)$$

The model prediction uncertainty σ_N for a calculated load N is estimated to first order from

$$\sigma_N^2 = \left(\frac{\partial N}{\partial x_i} \sigma_i \right)^2 \quad (J.3)$$

where the σ_i are one standard deviations of the input variables.

The uncertainty in the model prediction was estimated for the particular case of Experiment 6-2. Table J-2 lists the means and standard deviations for fourteen

input variables considered in the analysis. The experimental design was a 2^{14-10} fractional factorial design, meaning that 2^{14} cases would have to be run to include every possible combination of plus and minus factors, but that only a 2^{10} fraction of the full design was run (16 cases). In this case only the linear terms of the Taylor's series expansion could be estimated.

The model prediction uncertainties were estimated for four different loads: (a) the linear buckling load, (b) the nonlinear buckling load, (c) the growth load, and (d) the load at 1000 microstrain (postbuckling regime). The mean values of the model predictions and the associated one standard deviations are listed in Table J-3. The transverse pressure was specifically not included in the uncertainty analysis even though the model is known to be sensitive to it since there was no way of estimating the uncertainty in it. For a graphical sense of the model prediction uncertainty, Figure J-2 shows the load versus strain responses corresponding to the sixteen different cases run in the uncertainty analysis.

The uncertainty in the growth load is dominated by the uncertainty in the critical strain energy release rate which, as discussed in Chapter 7, is not well characterized for the material used in these experiments. By contrast, the estimated prediction uncertainty in the growth load without a contribution from the critical strain energy release rate is 54.9 lbf/in. Similarly, the uncertainty in the postbuckling load is dominated by the strain gauge thickness uncertainty. Without this contribution the uncertainty in the load at 1000 microstrain is 177. lbf/in.

Table J-2 Input Variable Uncertainties in Experiment 6-2

	Variable	μ	σ	Units
1	Contact law, K	1.E6	0.5E6	$\frac{lbf}{in^3}$
2	Sublamine major semi-axis, a	1.000	0.033	in
3	Sublamine minor semi-axis, b	0.750	0.033	in
4	Sublamine angle with respect to loads, θ	30	2	degrees
5	Ply thickness, t	5.56E-3	0.093E-3	in
6	Longitudinal Young's modulus, E_x	19.5E6	0.65E6	psi
7	Transverse Young's modulus, E_y	1.32E6	0.04E6	psi
8	Poisson's ratio, ν_{xy}	0.30	0.01	-
9	In-plane shear modulus, G_{xy}	1.01E6	0.03E6	psi
10	Longitudinal thermal coeff. of expansion, α_x	0.50E-6	0.017E-6	$\frac{in}{in-^{\circ}F}$
11	Transverse thermal coeff. of expansion, α_y	18.0E-6	0.6E-6	$\frac{in}{in-^{\circ}F}$
12	Temperature change, ΔT	-180	20	$^{\circ}F$
13	Critical strain energy release rate, G_c	0.3	0.05	$\frac{in-lbf}{in^2}$
14	Gauge thickness, t_g	0.003	0.001	in

Table J-3 Prediction Uncertainty Analysis

	μ_N	σ_N	Units
Linear buckling load, N_b^l	619.	58.1	lbf/in
Nonlinear buckling load, N_b	1012.	58.6	lbf/in
Growth Load, N_g	1763.	162.	lbf/in
Load at 1000 microstrain, N_{1000}	1541.	245.	lbf/in

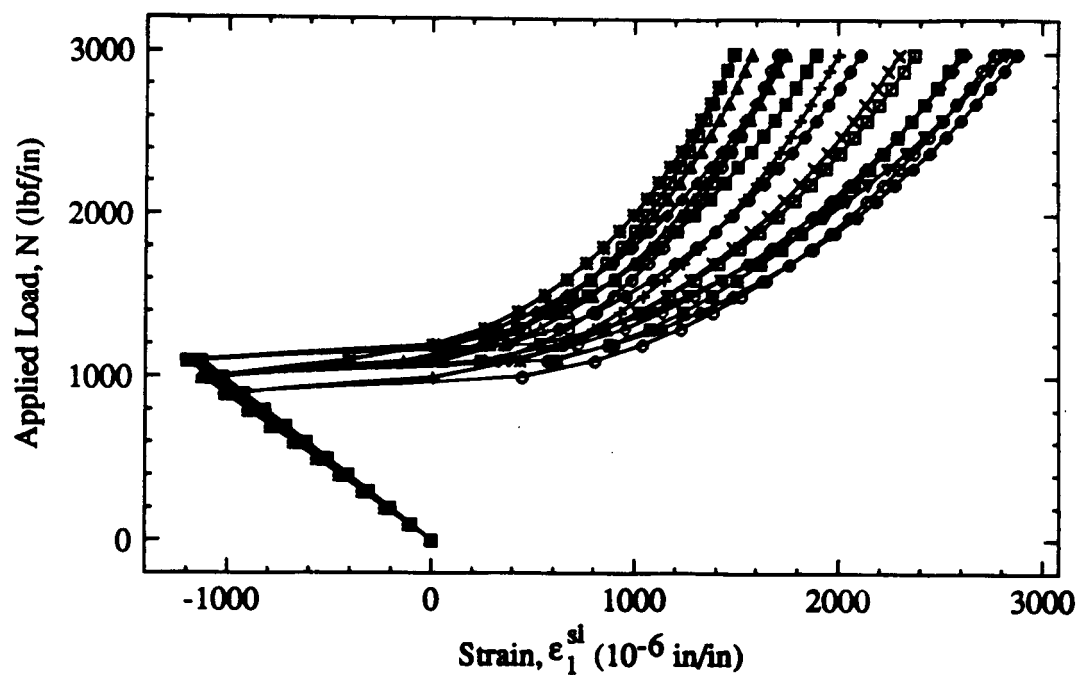


Figure J-2 Uncertainty analysis of Experiment 6-2 prediction. Load versus strain for the sixteen different combinations of input variables.